Technische Universität München

Fakultät für Chemie - Fachgebiet Molekulare Katalyse

# Ruthenium and Gold Complexes as potential Anticancer Drugs targeting selectively Integrin Receptors

**Eva Maria Hahn**

Vollständiger Abdruck der von der Fakultät für Chemie der Technischen Universität München zur Erlangung des akademischen Grades eines

**Doktors der Naturwissenschaften (Dr. rer. nat.)**

genehmigten Dissertation.

| | | |
|---|---|---|
| Vorsitzender: | | Prof. Dr. Lukas Hintermann |
| Prüfer der Dissertation: | 1. | Prof. Dr. Fritz E. Kühn |
| | 2. | Prof. Dr. João D. G. Correia |

Diese Dissertation wurde am 27.07.2016 bei der Technischen Universität München eingereicht und durch die Fakultät für Chemie am 22.09.2016 angenommen.

*„If my mind can conceive it,*

*and my heart can believe it —*

*then I can achieve it.“*

Muhammad Ali

Die vorliegende Arbeit wurde am Lehrstuhl für Anorganische Chemie im Fachgebiet Molekulare Katalyse der Technischen Universität München im Zeitraum von Juli 2013 bis Juni 2016 unter der Betreuung von Professor Dr. Fritz E. Kühn und Professor Angela Casini (Chair of Medicinal and Bioinorganic Chemistry, Cardiff University) angefertigt.

Ganz besonderer Dank gilt meinem Doktorvater

**Prof. Dr. Fritz E. Kühn**

für die herzliche Aufnahme in seine Arbeitsgruppe, für die Schaffung eines positiven Arbeitsumfeldes mit spannenden und vielfältigen Forschungsmöglichkeiten, die herausragende Unterstützung, die Ermöglichung der Kooperation mit Prof. Casini und das entgegengesetzte Vertrauen in meine Arbeit.

My grateful thanks are also dedicated to my second supervisor,

**Prof. Dr. Angela Casini**

for her great supervision and support. Owing to the positive and inspiring attitude she showed in her first seminar at TUM, I decided to get a part of the medicinal chemistry subgroup and thus, I got in touch with this fascinating field of chemistry. Thank you very much for enabling the research project in Lisbon, the introduction into the COST society, the exciting and informative conferences and the ongoing support.

**ACKNOWLEDGEMENTS**

Herzlichen Dank an alle, die an dieser Arbeit beteiligt waren und mir in den letzten drei Jahren zur Seite standen:

**Prof. Dr. João G. Correia**, für die hilfreiche Unterstützung und Betreuung während meiner Zeit in Lissabon.

**Dr. Alexander Pöthig, Dr. Gabriele Raudaschl-Sieber und Dr. Markus Drees** für die gute Zusammenarbeit während den ACII Praktika, die anregenden Unterhaltungen und die Hilfe bei allen Belangen mit der TUM Graduate School.

**Prof. Kessler**, **Tobias Kapp** and **Oleg Maltsev** für die hilfreichen Diskussionen und die tatkräftige Unterstützung bei den Bindungsstudien.

**Meinen Mädels: Andra Schmidt, Julia Rieb, Lavinia Scherf** und **Manuela Hollering** für die Plauderstündchen, das gemeinsame Kaffeetrinken und Sporteln, **Dominik Höhne, Xumin Cai, Michael Wilhelm**, **Michael Anthofer**, für die lustige Zeit mit euch im Labor, **Robert Reich** für die dekorativen Kalender,

und **alle weiteren Kollegen**, meine Zeit an der TUM war einzigartig, vielen Dank für die Hilfe, Ratschläge, gemeinsamen Laufrunden und die lustige Zeit im Kaffeeraum.

Außerdem besten Dank an all meine Forschungspraktikanten und Bacheloranden, die mich bei der Laborarbeit unterstützten. Besonders möchte ich hier **Leon Schuchmann** und **Ben Winkler** erwähnen, mit denen ich tolle Zeiten im AK Hahn verbrachte.

**Jürgen Kudermann** und **Maria Weindl** für die Hilfe bei NMR- oder Charakterisierungs-problemen.
**Irmgard Grötsch**, **Roswitha Kaufmann**, **Renate Schuhbauer-Gerl** und **Ulla Hifinger**, für die Hilfe bei bürokratischen Angelegenheiten.

Dem **Leistungszentrum** und meinen **Boxern** für die mentale Unterstützung, sportliche Förderung und Schlagfertigkeit.

Und schließlich möchte ich noch **meiner Familie** danken, vor allem meinen Eltern und meiner Schwester, die mich seit jeher tatkräftig unterstützen und mir mein Studium ermöglichten und meinem Freund **Max Korehnke**, für die liebevolle Unterstützung, das Vertrauen, die vielen gemeinsamen Stunden, die wir zusammen verbringen konnte und die vielen Abenteuer, die jetzt auf uns warten.

**ABSTRACT**

Nowadays chemotherapies suffer from one severe drawback: the lack of selectivity for cancer cells and the resulting damage of healthy tissue. Therefore, current research focuses on various strategies to solve this problem. One possible approach is based on the attachment of cytotoxic complexes to peptides which are targeting receptors overexpressed at the surface of cancerous cells. One of these targeting peptides is the cyclic pentapeptide cyc(RGDfK) bearing the cyclized amino acid sequence -Arg-Gly-Asp-D-Phe-Lys. This biovector is effectively ligating integrin receptor $\alpha_v\beta_3$, which plays a crucial role in tumor growth and metastasis formation. Hence, this work deals with the synthesis of ruthenium(II) and gold(I) complexes suitable for the conjugation to cyc(RGDfK) as well as for the integration into the pentapeptidic scaffold.

In the first part, different ruthenium(II) complexes are synthesized based on tridentate, bisdentate or monodentate ligands revealing a free carboxylic acid or amine group for coupling to the lysine's amine group of the peptide. After the successful preparation of cyc(RGDfK), two 2,2':6',2''-terpyridine (terpy) based ruthenium complexes are synthesized bearing one or two functional groups for the formation of monomeric or dimeric targeting compounds using an improved coupling procedure. These two bioconjugates show high binding affinities in the nanomolar range towards integrin receptor $\alpha_v\beta_3$ while the dimeric bioconjuagte exhibited 20-fold superior values. However, cytotoxicity studies reveal the poor antiproliferative effects of the terpyridine complexes and their bioconjugates against two cancer cell lines. Additionally, two 2,2'-bipyridine (bipy) based Ru(II) complexes and one additional structure bearing terpy, bipy and 4-aminopyridine as ligands are synthesized. All three compounds are characterized with NMR and ESI-MS whereas a crystal structure of the latter complex is obtained.

In the second part, three bis-*N*-heterocyclic carbene (NHC) gold(I) complexes based on the amino acid L-histidine with methyl-, ethyl-, or benzyl groups as *N*-sidechains, are synthesized, the reaction conditions optimized and the products characterized with NMR and ESI-MS. In ongoing studies, these structures will be integrated into the cyclic RGD peptide through exchange of L-lysine or D-phenylalanine and the binding affinities towards the integrin receptors evaluated.

**KURZFASSUNG**

Ein großer Nachteil derzeitiger Chemotherapien ist die fehlende Selektivität für Krebszellen und die damit verbundene Schädigung von gesundem Gewebe. Daher wird aktuell verstärkt nach Möglichkeiten gesucht um dieses Problem zu lösen. Eine denkbare Vorgehen sweise ist die Verknüpfung von zytotoxischen Komplexen mit Peptiden, welche an Rezeptoren binden, die auf Tumorzellen überexprimiert sind. Eines dieser Peptide ist das zyklische Pentapeptid cyc(RGDfK) (mit der zyklischen Aminosäuresequenz -Arg-Gly-Asp-D-Phe-Lys), welches ein hervorragender Ligand für den Integrinrezeptor $\alpha_v\beta_3$ ist. Dieser Rezeptor spiel eine wichtige Rolle für das Wachstum von Tumoren sowie für die Entstehung von Metasthasen. Demzufolge beschäftigt sich diese Arbeit mit der Herstellung von Ruthenium(II)- und Gold(I)-komplexen für die Verknüpfung mit cyc(RGDfK) sowie für den Einbau in die Penta-peptidstruktur.

Im ersten Teil werden mehrere Ruthenium(II)komplexe basierend auf tridentaten, bidentaten oder monodentaten Liganden mit freien Carbonsäure- oder Amin-gruppen für die Kupplung an die Amingruppe des Lysinrestes im Peptid synthetisiert. Nach der erfolgreichen Synthese des Peptides werden zwei Rutheniumkomplexe basierend auf 2,2':6',2''-Terpyridine (terpy) mit einer oder zwei Carbonsäuregruppen hergestellt, um monomere oder dimere Liganden für den Integrinrezeptor zu designen. Dabei werden die Reaktionsbedingungen für die Kupplung der Komplexe an das Peptid optimiert. Beide Biokonjugate weisen hohe Bindungsaffinitäten im nanomolaren Bereich für den Integrinrezeptor $\alpha_v\beta_3$ auf, wobei die Werte des dimeren Konjugates 20-fach höher sind als die des monomeren Produktes. Zytotoxizitätsstudien mit zwei Krebszelllinien zeigen allerdings, dass der antiproliferative Effekt der terpy-Komplexe und ihrer Biokonjugate nur sehr schwach ausgeprägt ist. Des Weiteren werden zwei Ru(II)-Komplexe basierend auf 2,2'-Bipyridine (bipy) und ein Komplex mit terpy, bipy und 4-Aminopyridine als Liganden hergestellt. Diese drei Produkte werden mit NMR und ESI-MS charakterisiert, wobei eine Kristallstruktur des Letzteren erhalten wird.

Im zweiten Teil dieser Arbeit werden drei bis-NHC Gold(I)komplexe basierend auf der Aminosäure L-Histidin synthetisiert, die Reaktionsbedingungen optimiert und die Produkte mit ESI-MS und NMR charakterisiert. In weiterführenden Studien sollen diese Verbindungen in die Struktur des zyklischen RGD-Peptides durch das Ersetzen von L-Lysin oder D-Phenylalanin eingebaut und die Bindungsaffinitäten für die Integrinrezeptoren evaluiert werden.

**ABBREVIATIONS**

| | |
|---|---|
| β-ala | β-alanine |
| BFC | Bifunctional Chelator |
| bipy | 2,2'-bipyridine |
| bipy-AA | (*S*)-3-([2,2'-bipyridin]-5-yl)-2-((*tert*-butoxycarbonyl)-amino)-propanoic acid |
| Boc | *tert*-butyloxycarbonyl |
| BSA | Bovine Serum Albumin |
| Bz | benzyl- |
| CLC-3 | Chloride Channel Proteins |
| Conc. | concentrated |
| CT | Computer Tomography |
| CTX | Chlorotoxin |
| cyc | cyclic |
| DCM | dichloromethane |
| DIPEA | ethyldiisopropylamine |
| DMF | *N,N*-dimethylformamide |
| DMSO | dimethylsulfoxide |
| dppe | 1,2-bis(diphenylphosphino)ethane |
| EMC | Extracellular Matrix |
| en | ethylenediamine |
| eq | equivalents |
| ESI-MS | Electrospray Ionization Mass Spectroscopy |
| Et | ethyl- |
| fampy | 4-aminopyridine |
| FDA | U.S. Food and Drug Administration |
| Fmoc | 9-fluorenylmethoxycarbonyl |
| GRPr | Gastrin Releasing Peptide receptor |
| HATU | *O*-(7-azabenzotriazol-1-yl)-*N,N,N',N'*-tetramethyluronium hexafluorophosphate |
| HBTU | 2-(1H-benzotriazol-1-yl)-1,1,3,3-tetramethyluronium hexa-fluorophosphate |
| HOAt | 1-hydroxy-7-azabenzotriazole |
| HOBt | 1-hydroxybenzotriazole |

| | |
|---|---|
| $IC_{50}$ | half maximal Inhibitory Concentration |
| inico | isonicotinic acid |
| ivDde | 1-(4,4-dimethyl-2,6-dioxocyclohex-1-ylidene)-3-methylbutyl |
| KP1019 | indazolium-*trans*-[tetrachloridobis-(1H-indazole)ruthenate(III)] |
| L | ligand |
| M | Metal |
| Me | methyl- |
| MTT | 3-(4,5-dimethylthiazol-2-yl)-2,5-diphenyltetrazolium bromide |
| NAMI-A | imidazolium-*trans*-tetrachloro(dimethyl-sulfoxide)imidazole-ruthenium(III) |
| NHC | *N*-heterocyclic carbenes |
| NKP-1339 | sodium-*trans*-[tetrachloridobis-(1H-indazole)ruthenate(III)] |
| NMR | Nuclear Magnetic Resonance |
| NSCLC | Non-Small Cell Lung Cancer |
| PACT | Photoactivated Chemotherapy |
| PARP-1 | Poly(adenosine-diphosphate-ribose)polymerase 1 |
| Pbf | 2,2,4,6,7-pentamethyl-2,3-dihydrobenzofuran-5-sulfonyl |
| PBS buffer | Phosphate Buffered Saline buffer |
| PBS-T buffer | Phosphate Buffered Saline – Tween 20 buffer |
| PDT | Photodynamic Therapy |
| PET | Positron Emission Tomography |
| PLGA-PEG | poly(D,L-lactic-co-glycolic acid)-block-polyethylene glycol |
| PS | photosynthesizer |
| PyBop | benzotriazole-1-yl-oxy-tris-pyrrolidino-phosphonium hexa-fluorophosphate |
| PyPrA | 3-(pyridin-4-yl)propanoic acid |
| RGD | Amino acid sequence L-arginyl-glycyl-L-aspartyl- |
| ROS | Reactive Oxygen Species |
| RP-HPLC | Reverse Phase High Performance Liquid Chromatography |
| $R_t$ | Retention time |
| sat. | saturated |
| SC-XRD | Single Crystal X-ray Diffraction |
| SD | Standard Deviation |
| SPECT | Single Photon Emission Computed Tomography |

| | |
|---|---|
| taci | 1,3,5-triamino-1,3,5-trideoxy-*cis*-inositol |
| tacn | 1,4,7-triazacyclononane |
| *t*Bu | *tert*-butyl |
| terpy | 2,2':6',2''-terpyridine |
| TIPS | triisopropylsilane |
| TrxR | Thioredoxin Reductase |
| TS-B buffer | Tris Buffered Saline with BSA |
| ttcn | 1,4,7-trithiacyclononane |
| TTP | Tumor Targeting Peptide |
| VEGF | Vascular Endothelial Growth Factor |

Amino Acids

| | |
|---|---|
| D / Asp | L-Asparagine |
| f / D-Phe | D-Phenylalanine |
| G / Gly | L-Glycine |
| H / His | L-Histidine |
| K / Lys | L-Lysine |
| R / Arg | L-Arginine |
| V / Val | L-Valine |

**CONTENTS**

# I. INTRODUCTION

# 1 Cancer – A short Summary

In February 2015, the WHO reported in the latest cancer factsheet (No. 297) about the appearance of 14 million new cancer cases and about 8.2 million people who died of cancer in 2012. Cancer is one of the leading causes of death worldwide.[1] Therefore a lot of research has to be carried out to diminish these alarming numbers.

In order to fight against cancer, focus should be brought to its development. The human body consists of about $3.72 \cdot 10^{13}$ cells[2] and just one single cell of these is necessary to start cancer growth. If a cell mutates, resulting in a genetic defect, the signal pathways between the cells fail due to an abnormal signaling protein production. Usually, the DNA of the damaged cell can be repaired or the apoptosis is initiated, but if the cells are growing too fast, the repairing mechanisms are too slow to patch the error. So, the mutation can end up in an endless and uncontrolled division of cells and in the formation of a knot in the tissue (see Figure 1).[3]

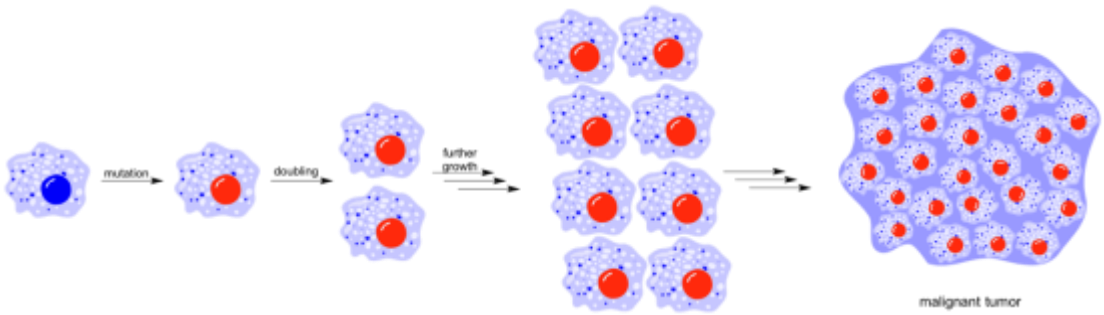


**Figure 1 –** The growing process of tumor tissue.

The mutation of a cell can have many reasons. Either it is caused spontaneously during cell division or by carcinogens. These can be chemicals like asbestos and aflatoxin, biological origins like bacteria and parasites or physical processes like ultraviolet and ionizing radiation. Furthermore, genetic predisposition as well as the age of the patient play a crucial role. Finally, about one third of all cancer death are caused by an unhealthy lifestyle like abuse of tobacco and alcohol, lack of physical activity as well as a high body mass index and lack of vitamins.[1]

Nowadays, there are some strategies to cure cancer patients. In most of the cases they are just promising if the cancer is detected early enough. Surgery for example is the oldest way known to remove cancerous tissue. Herein, the primary tumor has to be located, the malignancy of the tissue checked via biopsy and then the cancer resected from the healthy tissue. Looking at the fact that tumor cells easily detach, metastases are formed in various parts of the body and so, the discovery and surgery of all metastatic lumps is difficult. For some parts of the body like the brain, surgery is not feasible at all due to the severe procedure and enhanced risk of damage of the sensitive healthy tissue.[3]

Another treatment option is the radiation therapy in which the malignant tissue is destroyed by high energetic X-ray radiation. This therapy is one of the procedures mostly used to cure cancer and to slow or stop tumor growth. The malignant tissue can be treated rather local, so the effect of radiation on healthy tissue is particularly low. But still, the drawbacks of this method are obvious due to severe side effects depending on the location of the tumor like skin reactions, fatigue, rectal bleeding, impotence, tooth decay and even the development of new cancerous cells since also the "curing" radiation could lead to DNA damage of healthy cells.[3]

Finally, in chemotherapy anticancer drugs or combinational drugs can be administered in order to stop cancer growth. Usually these drugs destroy all type of cells, but due to the fact that cancer cells divide faster than healthy ones, malignant cells are affected with a higher probability. However, since the healthy tissue is also damaged by the drug, the side effects of this therapy are severe leading to hair loss, nerve damage, digestion and stomach problems, blood disorders, mouth and throat sores and pain in all parts of the body.[3] In the following, focus will be brought to metal-based anticancer agents which promise high potential for curing cancer and even for the selective targeting of cancer cells without affecting healthy tissue

.

# 2 Transition Metals as Anticancer Agents

## 2.1 Platinum Drugs

One of the most potent chemotherapeutic agents used nowadays is cisplatin (see Figure 2). Since its discovery by Rosenberg in the 1960s[4] platinum drugs gained a lot of attention as anticancer agents, especially for solid tumors like colorectal, genitourinary and lung cancer. Today, there are four platinum based anticancer drugs on the market: cisplatin, carboplatin, oxaliplatin and nedaplatin (see Figure 2). Hitherto, their mode of action is not fully understood since they bind to a variety of cellular targets.[5]

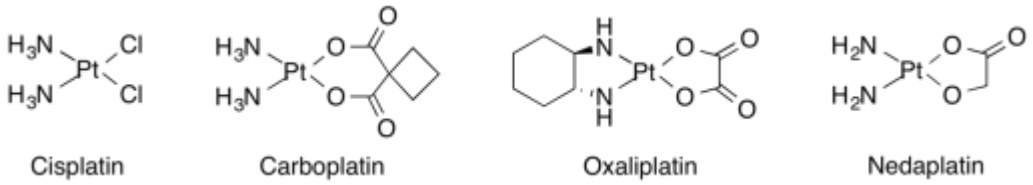


**Figure 2 -** Platinum based anticancer agents available on the market.[5]

However, the main effects result from the interaction with the DNA. After entering the cell, the chloride ligands detach and thus an activated platinum-aqua species is formed, which results in DNA adducts, modifies its helical structure (see Figure 3) and hence, cell division is stopped.[5] In case of early detection of testicular cancer, cure rates of up to 100% are performed which show the great potential of these platinum drugs.[6] However, side effects like the high toxicity for nerve system, liver and kidneys as well as the acquirement of resistances limit the effectiveness of these anticancer agents. Therefore, research started to focus on anticancer agents based on complexes with other transition metals.

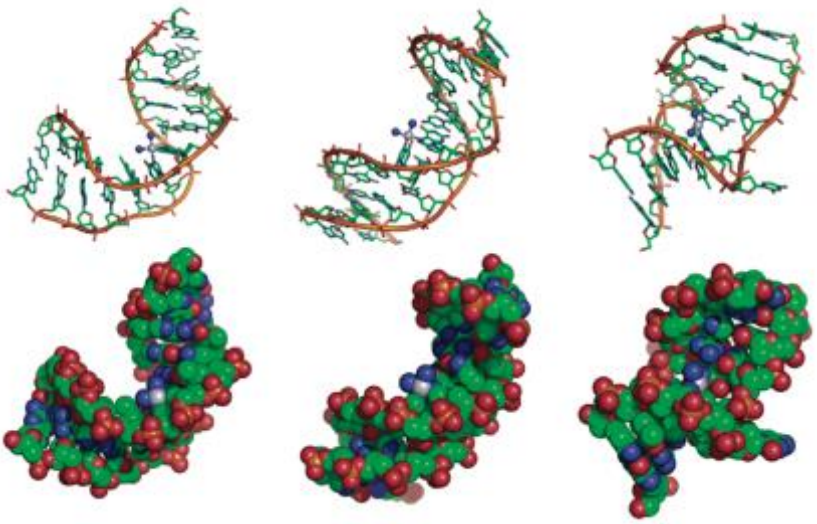

**Figure 3 -** Deformation of the DNA helix by development of Pt-crosslinks in the DNA.[5] Reprinted by permission from American Chemical Society: Chem. Rev. 2007, 107, 1387-1407, Copyright 2007.

## 2.2 Gold Drugs

In 1985 the rheumatoid arthritis drug auranofin (see Figure 4) received FDA approval since it was found to be cytotoxic against cancer cell lines which were resistant to cisplatin.[7, 8] Subsequently, research started to focus on anticancer compounds based on Au(I) and likewise Au(III) complexes.

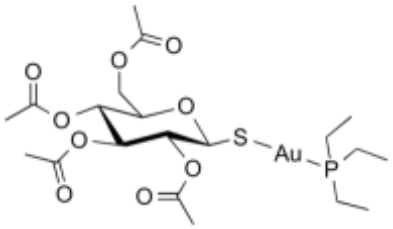


**Figure 4 -** Au(I) complex ligated by triethylphosphine and a thiosugar: Auranofin.

Since the discovery of Auranofin, various similar Au(I) phosphine complexes were screened for their anticancer potential.[9] The gold(I) phosphine complexes can be divided in two classes: the neutral, linear coordinated $[AuL_2]$ complexes (L = ligand) and the cationic $[AuL_2]^+$ complexes with tetrahedral coordination of two bisdentate chelating diphosphine ligands like the 1,2-bis(diphenylphosphino)ethane (dppe) complex $[Au(dppe)_2]^+$.[10] The P-substituents as well as the linker size between the phosphorus atoms play important roles on the cytotoxicity of the complexes showing that sterical and electronical effects must be taken into account for the design of novel gold-based anticancer agents.

In recent publications, *N*-heterocyclic carbenes (NHC) gained a lot of attention due to their high stabilization potential of the Au(I) species.[9, 11] Besides potent single NHC complexes coordinated with additional halogen, phosphine or thiol ligand (examples synthesized by Liu and co-workers[12] see Figure 5, **A**-**C**), also various bis-carbene complexes were prepared.[11] The complex $[Au(caffein\text{-}2\text{-}ylidene)_2][BF_4]$ (see Figure 5, **D**) for example, discovered by Casini *et al.*, exhibits good selectivity for human ovarian cancer cell lines and ligates efficiently the G-quadruplex DNA and slightly the poly(adenosine-diphosphate-ribose)polymerase 1 (PARP-1) enzyme.[13] The high water- and air-stability of these complexes, the facile electronical and sterical tuning of the ligands as well as their σ-donor abilities show the great potential for ongoing studies of gold-NHC compounds as anticancer agents.

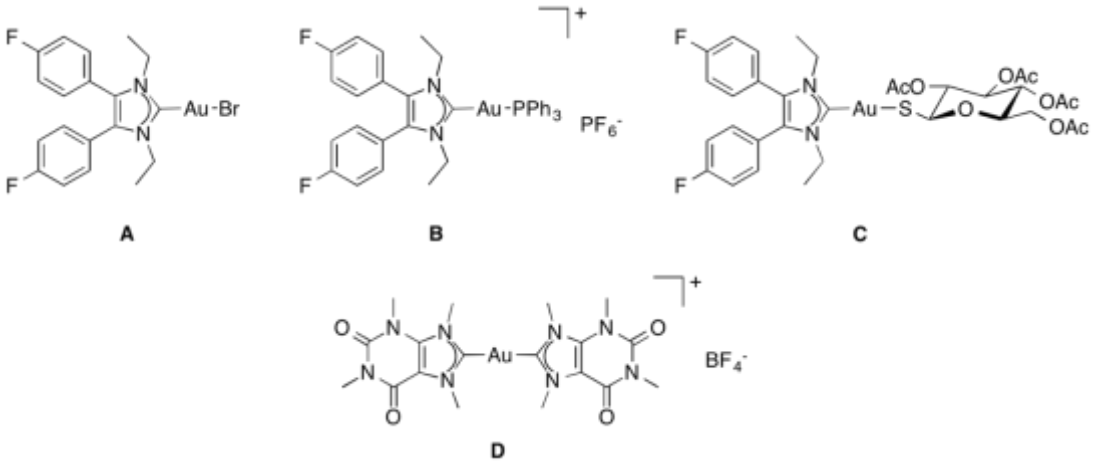


**Figure 5 -** Halogen (**A**), phosphine (**B**), thiol (**C**) NHC-Au(I) complexes[12] and caffeine-based bis-NHC Au(I) complex **D**.[13]

The studies about Au(III) complexes described in literature are rare compared to the ones of Au(I). Like the isoelectronic platinum(II), gold(III) forms square planar complexes. Therefore, similar biological properties of complexes with these two metals were predicted.[14] However, Au(III) complexes suffer of poor stability in solution and of inactivation due to reduction to Au(I) in the body. So, ligands for stabilization of the Au(III) oxidation state are necessary.[9, 13] Besides *N*-heterocyclic carbenes[11], pyridine derivatives can be used to achieve the required stability.[15] One remarkable example of stable dinuclear cyclometalated Au(III)-phosphine complexes (see Figure 6) was published by Che *et al.* which showed *in vitro* apoptosis in hepatocellular cancer cell lines in submicromolar range whereas the analogue Pt(II) complex displayed a poorer cytotoxicity.[14, 16] The potential of reducing the tumor size in mice was found to be higher for the Au(III) complex than for cisplatin or doxorubicin, a cytostatic drug. But unfortunately, also Au(III) complexes suffer form side effects already known from cisplatin: development of drug resistances, lack of selectivity for cancer cells and high systemic toxicity.[9]

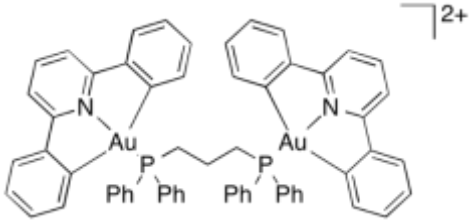


**Figure 6 -** Dinuclear gold(III) complex published by Che and co-workers.[16]

Unlike Pt(II) anticancer agents which are generally targeting the DNA, gold drugs were mainly located in mitochondria and found to inhibit selenoenzymes like the thioredoxin reductase (TrxR) which is involved in tumor development.[11, 13] But still, the exact mechanism of cancer cell apoptosis induced by gold compounds is not fully understood yet since, for example, no correlation between the cytotoxicity and TrxR inhibition was found. Another target for gold complexes bearing phosphine or bipyridinyl ligands was identified by Casini *et al.* as the zincfinger enzyme PARP-1.[17, 18] These enzymes are important for the DNA repair mechanism and are implicated in the development of cancer resistances of chemotherapeutics. The inhibition of purified PARP-1 from cancer cell extracts by dinuclear Au(I) complexes was effectively proofed in certain human cancer cell lines.

### 2.3 Ruthenium Drugs

Moreover, research was focused on further metal complexes with lower systematic toxicity than platinum. Ruthenium is one of these candidates and due to its octahedral coordination, a very variable ligand design for targeting special binding sites is possible.[19] Due to the chemical similarity of iron and ruthenium, Ru complexes are prone to bind to the iron-binding pocket in transferrin which enables the uptake into the cell.[20, 21]

## 2.3.1 Ruthenium Complexes in Clinical Trials

In 1999 the first ruthenium complex, NAMI-A (imidazolium-*trans*-tetrachloro(dimethyl-sulfoxide)imidazole-ruthenium(III)), see Figure 7) was tested on humans.[14] Unfortunately, in 2014 Phase I/II studies with Non-Small Cell Lung Cancer (NSCLC) patients showed just a moderately toleration of NAMI-A in combination with gemcitabine and even a lower anticancer activity than induced by taking gemcitabine alone.[22]

But besides NAMI-A, two other Ru(III) compounds, KP1019 (indazolium-*trans*-[tetrachloridobis-(1H-indazole)ruthenate(III)]),) and its sodium salt NKP-1339 (sodium-*trans*-[tetrachloridobis-(1H-indazole)ruthenate(III)]) discovered by Keppler *et al*.[23], promise high potential as novel antitumor agent. KP1019 was tested on rat colon cancer and showed remarkable results: The tumor volume decreased up to 95% whereas none of the rats died or showed significant body weight loss. These outcomes were better than the results obtained with 5-fluorouracil, the standard drug against colorectal cancer.[24] However, the enhanced water solubility and easy handling of NKP-1339 made this compound proceed for clinical development. In Phase I studies, NKP-1339 showed high potency against NSCLC and in contrast to NAMI-A, no painful blisters formation at hands, fingers and toes was observed.[20]

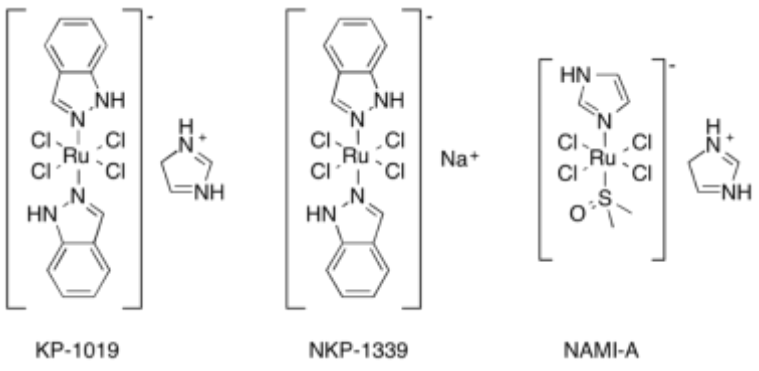


**Figure 7 -** Ruthenium based anticancer agents in clinical trials.

### 2.3.2 Theories of Activation

The anticancer activity of Ru(III) compounds like NAMI-A and NKP-1339 probably arises through the "activation-by-reduction" theory which was published by Clarke.[21] This hypothesis states that Ru(III) is just a prodrug which is reduced in the low-oxygen environment of cancer tissue to Ru(II). In this oxidation state, ligand exchange as well as binding to potential target molecules is enhanced.[21, 23] Besides this intracellular activation, the reduction can be initiated by external triggers like the irradiation of light. Two methods are known in this field: The photodynamic therapy (PDT) and the photoactivated chemotherapy (PACT) which are explained in the following.[25]

#### 2.3.2.1 Photodynamic Therapy (PDT)

First, in PDT a photosynthesizer (PS) which is accumulating in cancer cells, is administered to the patient. After irradiation with light, reactive oxygen species (ROS) are produced directly at the tumor tissue. The oxidative stress causes the cell death and reduction of cancer size. This approach provides a great alternative to the standard cure methods like chemotherapy due to low impact on healthy tissue.

There are three requirements for the application of a molecule as PS-based antitumor agent:[26]

1) Cancer cells as main target
2) Strong phototoxicity but no toxicity without irradiation of light
3) Excitation wavelength > 600 nm for a high penetration depth through human tissue

However, PDT causes the cells to develop survival pathways against ROS by modifying the tumor environment and therefore, research is carried out to inhibit the adaptation.[27]

An example of the nowadays approved anticancer agents is Foscan® (see Figure 8 **A**) which is used for neck and head cancer.[28] However, side effects like light sensitivity are observed after administration of this porphyrin-type drug.[25] By introduction of a metal ion into the scaffold, the selective accumulation in cancer tissue as well as the hydrophilicity and therefore the uptake of the drug can be enhanced. Besides some reports about platinum [29], ruthenium(II) complexes started to gain interest for application in PDT. An interesting example of ruthenium-porphyrin conjugates is shown in Figure 8 **B**, demonstrating excellent phototoxicity towards melanoma cells during irradiation with laser light at 652 nm. [30]

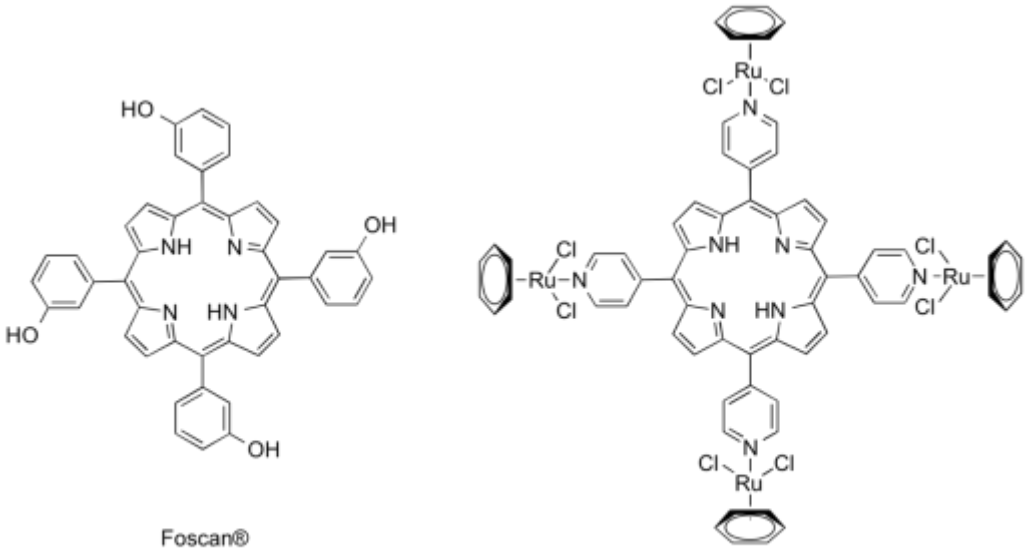


**Figure 8 - A**: Foscan®, a clinically approved PDT-based anticancer agent against head and neck cancer[25] and **B**: ruthenium-porphyrin conjugate applicable in PDT.[30]

### 2.3.2.2 Photoactivated Chemotherapy (PACT)

The second method is called photoactivated chemotherapy, PACT. Herein, the cell death is caused by ligand ejection, DNA crosslinking or caging approaches after light irradiation.[21, 25] Mari and co-workers developed ruthenium polypyridyl complexes coupled to peptides releasing a cytotoxic Ru(II) moiety due to a photolabile linkage (see Figure 9).[25, 31] The peptide attachment results in an enhanced uptake in tumor tissue and during irradiation with light, a cytotoxic species is formed inducing the attack of cancer cells.

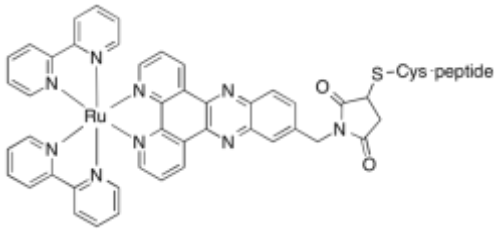


**Figure 9 -** Ru(II) polypyridyl complexes with photocleavable linkage to a peptide.[25]

Mari's work already shows that through the attachment of a bioactive molecule, in this case a bombesin-type peptide which are targeting the human gastrin-releasing peptide receptor (GRPr), the selectivity and uptake of the anticancer agents are enhanced. Further information about the targeting approach will be given in section 3 (The Targeting Approach).

## 2.4 Rhenium and Technetium Radiopharmaceuticals

Early detection is an important factor for a successful tumor therapy. Using radioactive nuclides which are targeting cancer cells, imaging of the malignant tissue is possible. In the recent past, isotopes of the main group elements like $^{11}C$,[32] $^{18}F$,[33] $^{68}Ga$,[34, 35] $^{76}Br$[36] and $^{123}I$[37] as well as the transition metals $^{99m}Tc$, $^{186}Re$ and $^{188}Re$[38-40] were studied for their pharmaceutical use.

Compounds labeled with one of these radionuclides makes it possible to visualize the drug in the body. Two methods can be used for imaging of tumor tissue: Single Photon Emission Computed Tomography (SPECT) and Positron Emission Tomography (PET). SPECT is applied for $\gamma$-emitting nuclides whereas PET needs $\beta^+$-emitters for detection.[40-42]

A prominent example for SPECT imaging is sestamibi, a $^{99m}Tc$ compound available under the trademark Cardiolite®. This lipophilic and cationic Tc(I) complex is stabilized by six isonitril ligands ($[^{99m}Tc(CNR)_6]^+$ (R = $CH_2C(CH_3)_2OCH_3$), see Figure 10) and is applied for early cancer detection and non-invasive monitoring of the tumor multidrug resistance transport function.[43]

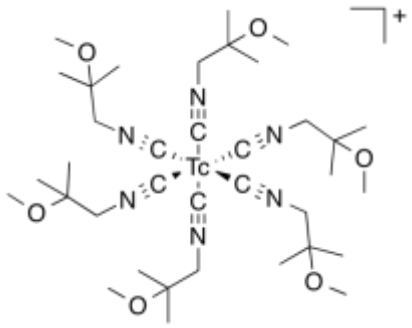

**Figure 10 -** Cardiolite®, a $^{99m}Tc$ based SPECT imaging agent. [43]

On the other hand, PET-CT is an important tool for screening of colorectal cancer. The positron-emitting $^{18}F$-labeled fludeoxyglucose is mainly taken up by cancer cells due to their enhanced energy demand and upregulated glucose uptake. So the radionuclide is accumulating in tumorous tissue and can be visualized due to their $\beta^+$-emissions in PET-CT. This method is already used for staging colorectal cancer and is proposed to be applied for automated screening and early detection in order to avoid invasive and painful colonoscopy.[44]

Hereinafter, the transition metal nuclides $^{99m}$Tc, $^{186}$Re and $^{188}$Re are presented as examples for radiopharmaceuticals in this section.

In approximately 80% of all routine nuclear imaging applications, the γ-emitting isotope $^{99m}$Tc is applied whereas the heavier homologues, $^{186}$Re and $^{188}$Re display $\beta^-$-emitters and can be used for systemic radiotherapy due to the destruction of tumor tissue with $\beta^-$-radiation. As mentioned above, the γ-emissions of the $^{99m}$Tc nuclide allow the usage of SPECT for imaging cancer tissue. Its half-life of six hours is very suitable for clinical use and additionally, the facile synthesis of sodium pertechnetate from commercially available $^{99}$Mo/$^{99m}$Tc generators is another reason for the great success of $^{99m}$Tc as nuclear imaging agent. Besides, $^{188}$Re is synthesized by $^{188}$W generators, has a half-life of 17 hours and emits $\beta^-$-radiation. The $\beta^-$ particle emission displays a maximum energy of 2.12 MeV, whereby it penetrates into soft tissue up to 10.4 mm, revealing the application of $^{188}$Re as therapeutic nuclide. On the other hand, $^{186}$Re has a half-life of 3.7 days and emits γ as well as $\beta^-$-radiation whereas the maximum energy is about 1.02 MeV leading to only 5 mm penetration into tissue. [45]

In recent studies, radiopharmaceuticals have been designed as Bifunctional Chelators (BFC, see Figure 11) in which a metal-chelate complex is connected via a linker to a bioactive molecule.

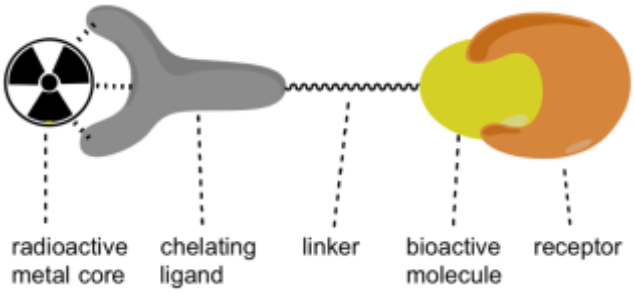


**Figure 11 -** Scheme of a Bifunctional Chelator (BFC).[45]

For the rational design of a BFC, some requirements have to be taken into account: First, the bioactive molecules must selectively target receptors overexpressed on cancer cells. Therefore, compounds like peptides, antibodies, oligosaccharides or other small molecules are useful biovectors.[45] Considerable attention has to be given on the choice of chelating ligand due to its important task: It has to shield the radioactive metal core to inhibit redox processes and ligand substitution. Usually, facial coordination of polydentate or macrocyclic ligands are applied since bidentate ligands are too sensitive and prone to undergo ligand

exchange reaction.[46, 47] Concerning the linkage of the bioactive molecule and the chelate-metal complex, manifold varieties are applicable like peptide or thiourea bond formation and also the linker itself can easily be tuned regarding for example length and lipophilicity. [45]

In recent studies, the $[M(CO)_3]^+$ core promised the best performance for radiopharmaceutical applications. One example is shown in Figure 12 published by Paulo and co-workers. They synthesized different rhenium and technetium tricarbonyl complexes stabilized by a cysteamine based (N,S,O) chelator and connected *via* an ether-containing spacer to the pharmacophore 2-(4'-aminophenyl)benzothiazole.[48] This small bioactive molecule is targeting cytochrome P450 1A1, an enzyme which induces the decomposition of toxins but also the biotransformation of polyaromatic carbohydrates to mutagenes.[49] Benzothiazole derivates like applied in this example are known to be activated by cytochrome P450 1A1 to form very electrophilic compounds targeting tumor DNA.[50] Whereas the rhenium derivative of the complex in Figure 12 can be used as cytotoxic, therapeutic anticancer agent, the radioactive technetium derivative might be applied as imaging agent.[48]

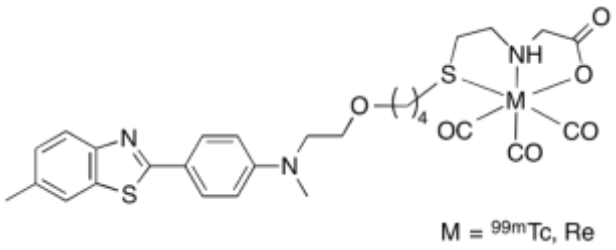


**Figure 12 -** Rhenium or technetium-99m tricarbonyl complex coupled to the pharmacophore 2-(4'-aminophenyl)benzothiazole.[48]

Recently, some attention has been drawn to the $[MO_3]^+$ core with M = Re(VII) or Tc(VII). The relatively small size and the excellent water solubility make these compounds to interesting components for radiopharmaceuticals. Besides, the high oxidation state of the metal prevents oxidation processes in body, so deactivation by the oxygen rich environment in tumor tissue can be excluded.[51, 52] For stabilization of this moiety, numerous cyclic, tridentate ligands were examined to yield in highly stable octahedral complexes. Some examples can be found in Figure 13. Besides cyclononane-based ligands like 1,4,7-triazacyclononane (tacn, **A**) and 1,4,7-trithiacyclononane (ttcn, **B**), there are mixed-donor ligands like 1,3,5-triamino-1,3,5-trideoxy-*cis*-inositol (taci, **C**) or scorpionate based ligands like tris(pyrazolyl)methanes (**D**), which have been already published in literature. They all

built stable octahedral complexes with rhenium or technetium trioxo cores but hitherto, no biological studies or tethering of bioactive molecules were carried out with these compounds. So, the future potential as anticancer agents of these strucutres with radioactive isotopes of technetium and rhenium cannot be evaluated at present.

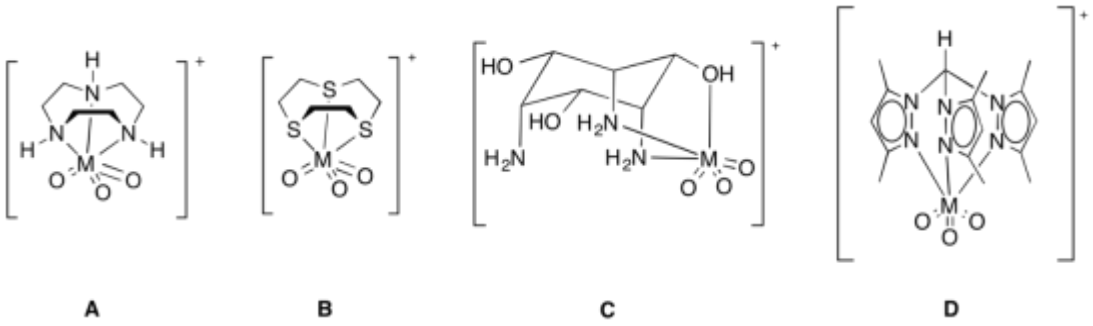


**Figure 13 -** Ligands used for stabilizing the $[MO_3]^+$ core (M = $^{99m}$Tc, Re), **A**: tacn, **B**: ttcn, **C**: taci and **D**: scorpionate ligands.

# 3 The Targeting Approach

As already mentioned, chemotherapy suffers of an intense problem: the damage of healthy tissue. A strategy to solve this drawback is to attach a targeting vector to the cytotoxic species to improve the selectivity for cancer cells. There are different kind of approaches known how to lead the drug directly and with high selectivity towards the cancer cell. Sugars, hormones, amino acids, peptides, small molecules and bisphosphonates act as targeting bioactive molecules due to the ligation of receptors overexpressed at the surface of the malignant cells.[53] The drug is coupled via a spacer or linker to the targeting vector, similar to the structure of a BFC shown in Figure 11, whereas the attachment should have no effect on the bioactivity of the vector as well as on the cytotoxicity of the drug. In the following, some examples of targeting approaches are presented .

## 3.1 Hormones as Targeting Vectors

In breast and ovarian cancer cells, some special kind of estrogen receptors are overexpressed. Generally, the uptake of the lipophilic estrogens takes place due to passive diffusion. Then, in the cytoplasm, they bind to the estrogen receptors and are transferred to the nucleus.[53] The attachment of platinum based anticancer compounds to estrogen showed an increased cellular uptake of the drug and sensitizing of the cancer cells. The complex in Figure 14, synthesized by Croy *et al.*[54] shows [Pt(en)]$Cl_2$ (en = ethylenediamine) attached via carbamate linker to an estrogen. Although this compound exhibits minor binding affinities to the estrogen receptor in contrast to the uncoupled hormone, the activity against some ovarian and breast cancer cell lines is remarkably enhanced in comparison with the Pt species alone. [55],[56]

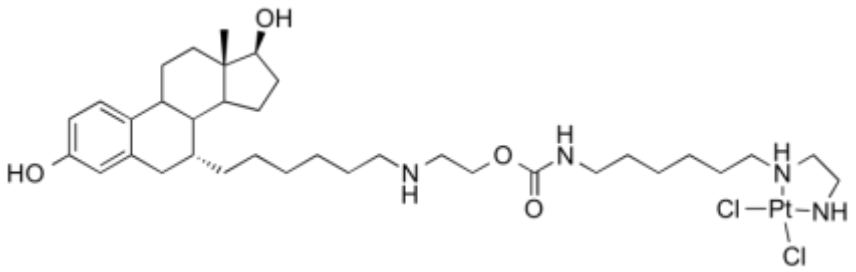


**Figure 14 –** Platinum(II) drug attached to estrogen vector.[54]

## 3.2 Saccharides as Targeting Vectors

Since tumor tissue grows exceptionally fast compared to healthy tissue, cancerous cells have an enhanced energy demand. To meet this demand, receptors for glucose are overexpressed on the surface of cancerous cells.[53] An remarkable example of platinum complex coupled to a monosaccharide moiety is the platinum(II) complex shown in Figure 15 which exhibits lower $IC_{50}$ values than cisplatin in cell studies. It was tested on large cell lung cancer cells and revealed high rates of apoptosis but just low amount of necrosis in healthy cells.[57] Besides this example, the application of polysaccharides like hyaluronic acid and cyclodextrins as targeting vector is described in literature.[53]

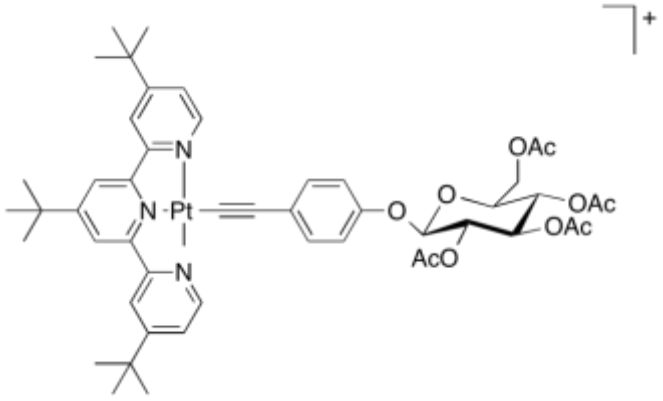


**Figure 15 -** Platinum(II) complex coupled to a monosaccharide moiety for targeting glucose receptors.[57]

## 3.3 Bone-targeting Bisphosphonates

Another targeting approach, particularly applied for bone cancer is based on bisphosphonates. Their ability of chelating calcium ions mainly present in calcified tissue induce a high affinity for bone material and inhibit osteoclastic resorption and tumor growth. An example for a bone-seeking Pt(II) based drug is shown in Figure 16, revealing high cytotoxicity against human osteosarcoma MG-63 cell lines, whereas the reason for the apoptosis is not clear yet, since it is not caused through linkage of the platinum species to the DNA as observed for cisplatin.[58, 59]

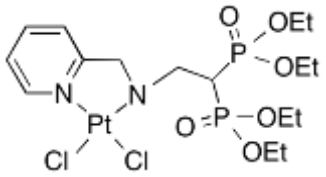


**Figure 16 –** Bone seeking Platinum(II) bisphosphonate complex.[58]

### 3.4 Tumor Targeting Peptides (TTP)

First of all, peptides can be utilized as cage-like drug delivery systems. The iron storage protein apoferritin for example is used as a cage for drugs like cisplatin or carboplatin to transport the cytotoxic agent to ferritin receptors which are mainly expressed in cancer tissue of the brain. In contrast to the common procedure in which the cytotoxic species is coupled to a bioactive molecule, in this approach there is no change in structure necessary for the receptor recognition. The outer shell of the ferritin remains and consequently the affinity for the receptor is not decreased.[60]

Another targeting approach provides the receptor on the tumor surface which stimulates the growth of cancer cells. This human gastrin-releasing peptide receptor (GRPr) is overexpressed at malignant cells of breast, prostatic, pancreatic and small cell lung cancer and selectively ligated by bombesin and gastrin-releasing peptides.[61, 62] Therefore, these peptides can work as a vector to transfer attached anticancer compounds to the tumor tissue. Alberto *et al*. attached for example 1,2-diamino-propionic acid to L-lysine to obtain a tridentate ligand for binding the radiolabeled $[^{99m}Tc(CO)_3]^+$ core (see Figure 17). This ligand was coupled to bombesin to achieve a targeted radiopharmaceutical agent.[63]

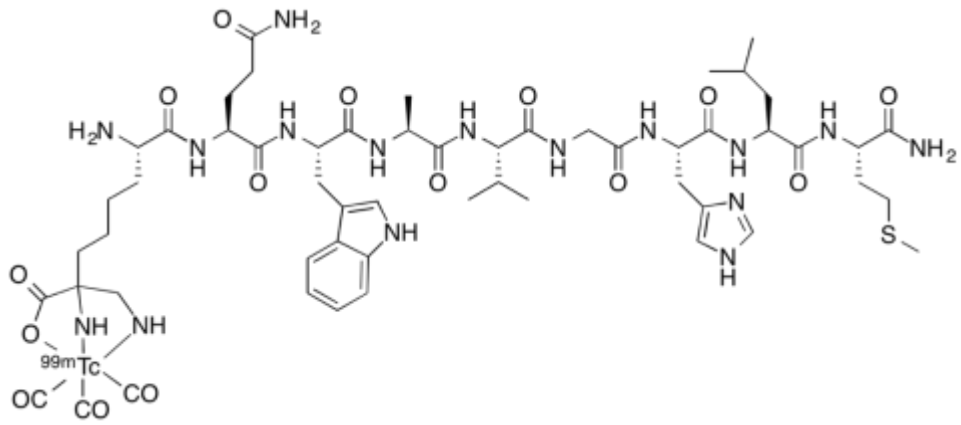

**Figure 17 -** $[^{99m}Tc(CO)_3]^+$ coupled to bombesin for the design of a targeted radiolabeled anticancer agent.[63]

Cancers of the brain, the so-called Gliomas, are characterized by a high expression of chloride channel proteins (CLC-3). Chlorotoxin (CTX), the venom of the deathstalker an extremely poisonous scorpion native in the deserts of Israel, is a 36 amino acid peptide and known to target the CLC-3 protein. Hence, the attachment of Pt(IV) complexes created novel, potential anticancer agents (see Figure 17) revealing a higher cytotoxicity against HeLa cells then of the Pt(IV) precursor or CTX alone. [59, 64]

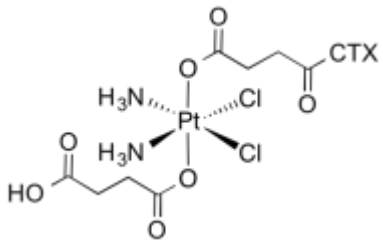

**Figure 17 –** Tethering of CTX to Pt(IV) complexes for targeting CLC-3.[64]

# 4 The Amino Acid Sequence RGD as Targeting Vector

Other receptors which are overexpressed at the surface of malignant cells are the integrins. Since they are the working horses of the studies in this thesis, special attention is given to this family of receptors in the following sections.

## 4.1 The Role of Integrin Receptors in Tumor Angionesis

Angiogenesis means the formation of new blood vessels, a process which is very important in the body considering wound healing, tissue remodeling or the genesis of embryos. However, angiogenesis plays an important role in tumor growth and metastasis formation. Due to the increased metabolisms of tumor tissue, the demand of nutrition and generation of by-products is enhanced and consequently, cancer tissue is growing extremely fast compared to healthy cells. Therefore, the formation of new blood vessels is necessary for the malignant tissue to meet the energy supply. To initiate the angiogenesis, the binding of signaling molecules like the vascular endothelial growth factor (VEGF) to integrin receptors, which are highly overexpressed at the tumor tissue, is necessary. This induces a signal cascade and endothelial cell migration, which is responsible for the formation of metastasis and the growth of new blood vessels.[65, 66] So, by blocking integrin receptor with antagonists, these effects could be prevented. Nowadays, 24 different integrins are known which belong to this receptor family. Besides the tumor related impact, they are important for signaling pathways between cells or between one cell and its surrounding extracellular matrix (EMC).[67, 68] Currently, the integrin receptor $\alpha_v\beta_3$ is extensively studied due to its proven role in tumor growth, metastasis formation and angiogenesis. The expression of this integrin receptor is known to correlate with the progression in some kind of tumors, like melanoma, glioma, breast and ovarian cancer.[68]

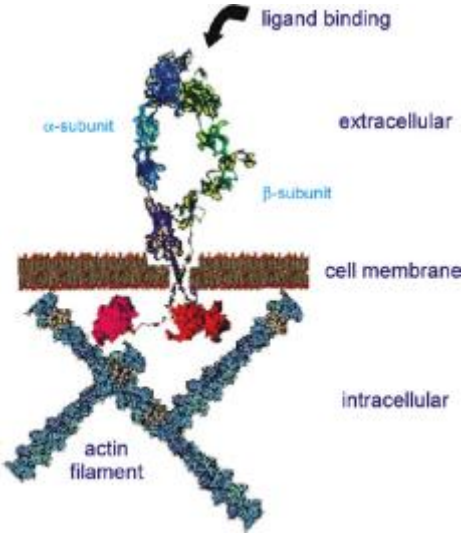


**Figure 18 -** Schematic presentation of integrin $\alpha_v\beta_3$ receptor.[67] Reprinted by permission from American Chemical Society: Acc. Chem. Res. 2009, 42, 969-980, Copyright 2009.

So, in the following, focus is brought to integrin receptor $\alpha_v\beta_3$. As shown in Figure 18,[67] integrin $\alpha_v\beta_3$ consist of two subunits: the α- and the β-part. They are transmembrane proteins and so, within both subunits there is one large extracellular domain and a short cytoplasmic domain, both connected via a transmembrane helix. Between the α- and the β subunit in the extracellular domain, there is the ligand binding site where proteins from the extracellular matrix can ligate the receptor. For integrin $\alpha_v\beta_3$ proteins like vitronectin and fibronectin can bind the pocket.[67] In 1984, Pierschbacher and Ruoslahti found out that in vitronectrin the amino acid sequence L-arginyl-glycyl-L-aspartyl- (RGD) is necessary to bind integrin receptors (see Figure 19, left). Since then, a lot of ligand screenings were carried out to find peptides targeting the different integrin receptors with high selectivity.[69] An increased selectivity for integrin $\alpha_v\beta_3$ was achieved by attaching D-phenylalanine and L-valine to the arginine's N-terminus, followed by the cyclization of the amino acid sequence to give a cyclic pentapeptide, known as cyclo(RGDfV), (cyclic -L-Arg-L-Gly-L-Asp-D-Phe-L-Val-).[65, 70] In 2002, Xiong et al. published the first crystal structure of the binding domain bound to a cyclic pentapeptide with the RGD sequence (see Figure 19, right).[71]

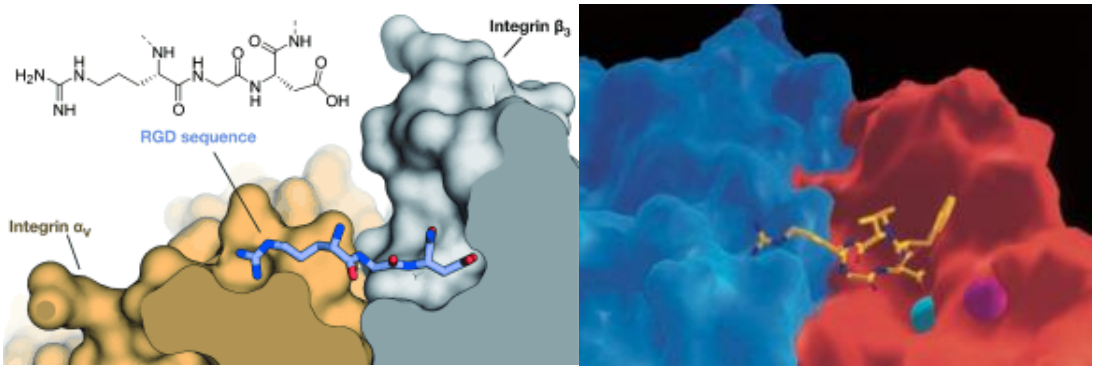


**Figure 19 –** RGD sequence attached to binding pocket of integrin $\alpha_v\beta_3$ (left) and crystal structure of cyclic pentapeptide bound to integrin $\alpha_v\beta_3$ (right).[71, 72] Reprinted by permission from John Wiley and Sons: Angew. Chem. Int. Edit., 2009, 42, 969-980, Copyright 2009, and from the American Association for the Advancement of Science: Science, 2002, 296, 151-155, Copyright 2002.

Herein, the peptide with the sequence Arg-Gly-Asp-{D-Phe}-{*N*-methyl-Val-} (known as Cilengitide) in combination with $Mn^{2+}$ ions was used for the crystallization studies. Since *N*-methyl-valine points outside the binding pocket and is not necessary for ligation of the receptor, this amino acid can be replaced by L-lysine without changing the activity to a high extent. At the free amine group of lysine, attachment of cytotoxic or fluorescent metal complexes is possible to achieve targeted therapeutic or imaging anticancer agents. As mentioned before, the integrin receptor $\alpha_v\beta_3$ is overexpressed on the surface of cancer cells, so the probability that RGD based anticancer agents are directly transferred to tumor tissue is enhanced and the cytotoxic effects on healthy tissue are lowered. So, the chemotherapeutic agent is mainly taken up from the cancer cells and apoptosis is induced. Furthermore, by attachment of fluorescent compounds to cyclic(RGDfK), imaging and localization of the cancer tissue is possible.[73] Therefore, the cyclic pentapeptide with the sequence RGDfK (cyclic -L-Arg-L-Gly-L-Asp-D-Phe-L-Lys-) is the main subject of these studies (see Figure 20).

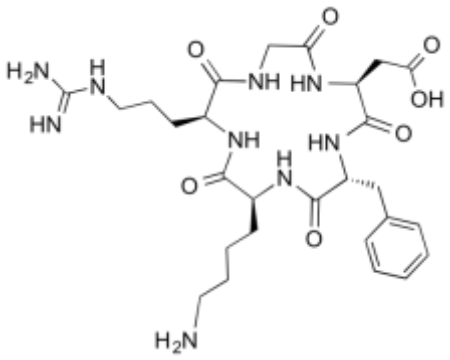

**Figure 20 –** The subject of the following studies: the pentapeptide cyc(RGDfK).

## 4.2 Design of Tumor Targeting Metal Complexes tethered to RGD Peptides

In literature there are already several studies about coupling constructs of RGD peptides and metal-based anticancer agents. First of all, focus is brought to cytotoxic platinum complexes tethered to the RGD sequence. Yuan and co-workers report for example of a cisplatin-based Pt(IV) prodrug which is coupled on the one hand to cyc(RGDfK) and on the other hand to a tetraphenylsilole fluorophore, used as apoptosis sensor molecule.[74] They found out, that in the cell the RGD sequence leads the compound to the cancer tissue where the prodrug is reduced to Pt(II). Cell death is monitored *via* the release of the fluorescent apoptosis sensor. Similar experiments were performed by Massaguer *et al.*[75] Besides the design of a monomeric Pt(IV)-cyc(RGDfK) coupling product, they also reported about the synthesis of a Pt(IV) complex attached to four cyc(RGDfK) peptides (see Figure 21). This tetrameric compound showed remarkable high values for internalization and cytotoxicity compared to the monomeric compound or the Pt(VI) drug without peptide. These results underline the improvement of selectivity and potency of a drug by multiplying the targeting moiety.

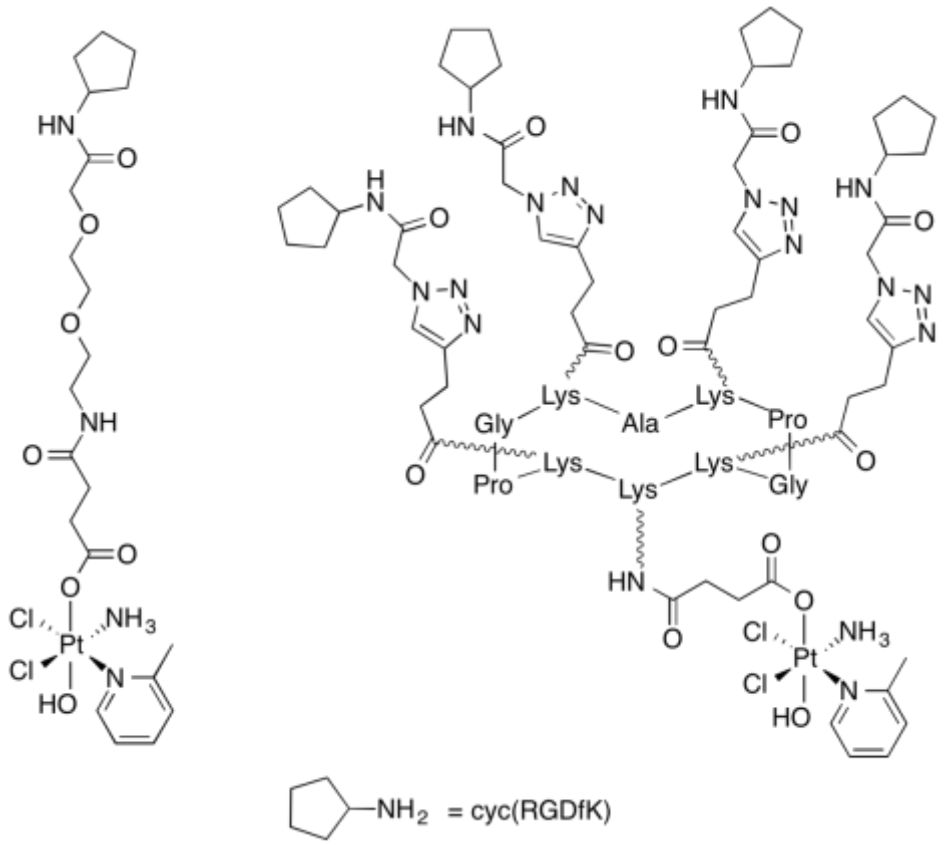


**Figure 21 -** Monomeric and tetrameric RGD – Pt(IV) complexes.[75]

A similar Pt(IV) complex was used by Lippard *et al.* which was encapsulated into poly(D,L-lactic-co-glycolic acid)-block-polyethylene glycol (PLGA-PEG) nano-particles with cyc(RGDfK) attached to the surface. The *in vitro* cytotoxicity against MCF-7 breast cancer cell lines was sixfold higher than for cisplatin and moreover, tumor growth inhibition of 56% was obtained at *in vivo* studies in A2780 xenografts.[76]

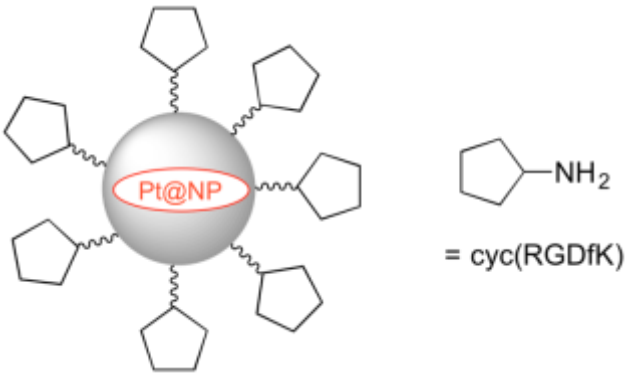


**Figure 22 –** Platinum nanoparticles functionalized with cyc(RGDfK).[76]

Additionally, RGD-functionalized micelles are applied as carrier molecules for platinum based anticancer drugs like *cis*-diaqua(*cis*-1,2-diaminocyclohexane)-platinum(II).[77] As a result of the RGD-functionalization, high accumulation of the drug was observed in glioblastoma cells.

Looking at other metal compounds, gold is widely used as nanoparticle based delivery system for other cytotoxic agents since they are inert, biocompatible, nontoxic and easy to prepare or functionalize.[53] The attachment of RGD peptides at the surface leads to high selectivity for cancerous cells.[78-80] For example, Arosio and co-workers reported of RGD and fluorescein functionalized gold nanoparticles which were able to stain prostate cancer cells *in vitro*.

Finally, there are just few reports about RGD peptides coupled to ruthenium complexes in literature. In 2011, Barragán and co-workers synthesized Ru(II) arene complexes attached to the tripeptide RGD (see Figure 23, **A**).[81] Induced by the irradiation with visible light (420 nm), the ruthenium(II) species dissociated from the peptide and the active aqua species (**B**) was formed. The incubation with DNA lead to formation of monofunctional adducts (**C**) whereas a specificity for guanine bases as ligands was observed.

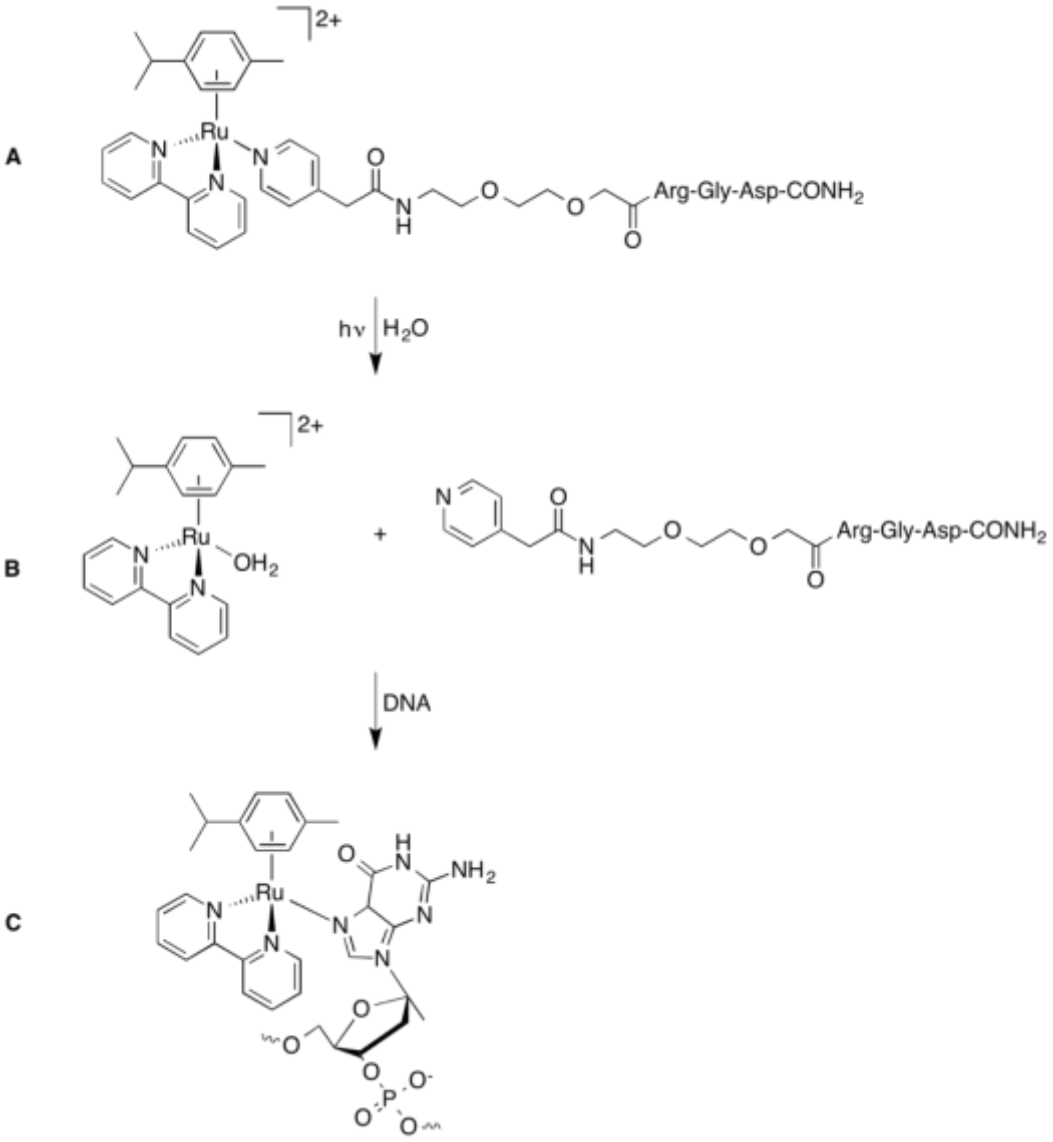


**Figure 23 -** Photocleavable Ru(II) arene complexes of Barragan and co-workers, **A**: Ru(II) peptide conjugate, **B**: formation of activated Ru(II) aqua species, and **C**: formation of DNA adducts.[81]

The Ru(II) polypyridyl-RGD complexes shown in Figure 24 display a high affinity and specificity for integrin $\alpha_{IIv}\beta_3$.[82] In live cell studies with confocal microscopy, the selective binding of the compounds to the integrin receptor was confirmed. These complexes were designed for studying conformational changes of integrin $\alpha_{IIv}\beta_3$ induced by the RGD binding, cytotoxicity studies were not carried out in this approach.

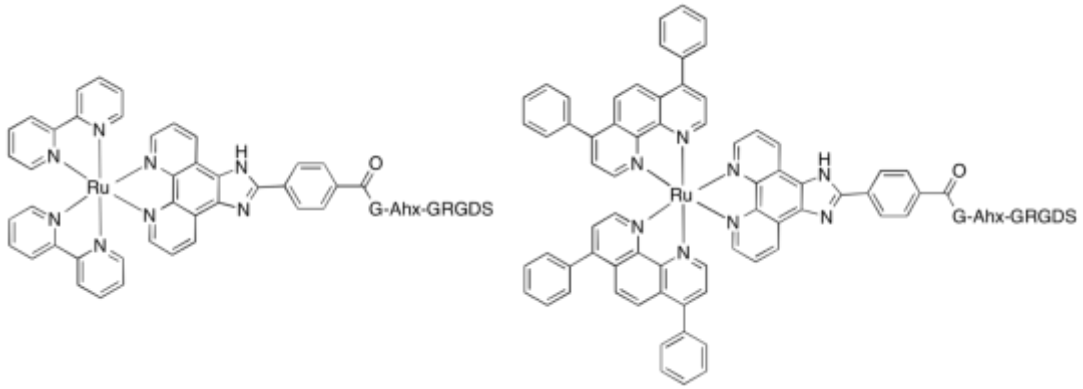


**Figure 24 -** Ru(II) polypyridyl-RGD complexes for studying conformational changes of integrin $\alpha_{IIv}\beta_3$.[82]

Additionally, polypyridyl complexes gained interest since imaging studies for cell uptake and localization of the drug inside the cells are possible. By attaching fluorescent Ru(II) complexes to mesoporous silica nanoparticles functionalized with RGD peptides on the surface, increased selectivity for cancerous cells was induced. After internalization of the nanoparticle, the ruthenium species was released into the cytoplasm where changes of the phosphorylation pathways for some protein kinases induced the cell death. [83]

Besides these publications, no further studies of attaching RGD peptides to ruthenium complexes were carried out until now, although the selectivity and cytotoxicity of coupling products promise great perspectives.

# II. OBJECTIVES

# 5 Design of Ruthenium-RGD-Conjugates as Targeting Anticancer Agents

Nowadays, many anticancer agents suffer of server side effects caused by a high systemic toxicity, the development tumor resistances, and mainly the lack of selectivity towards tumor cells. Patients experience strong pain, digestion and stomach problems, mouth and throat sores, hair loss and nerve damages due to the strong cytotoxic effects on healthy tissue. Therefore, the first part of this work aims in enhancing the selectivity of ruthenium(II) polypyridyl complexes toward cancer cells by attachment of a targeting biomolecule (see Figure 25). This vector is embodied by cyc(RGDfK), a cyclic pentapeptide which is directing the cytotoxic species towards the integrin $\alpha_v\beta_3$ receptor overexpressed at the surface of tumor tissue. Consequently, the cytotoxic metal complex is expected to attach to tumor cell with a higher probability, to accumulate in cancerous tissue and to result to its destruction.

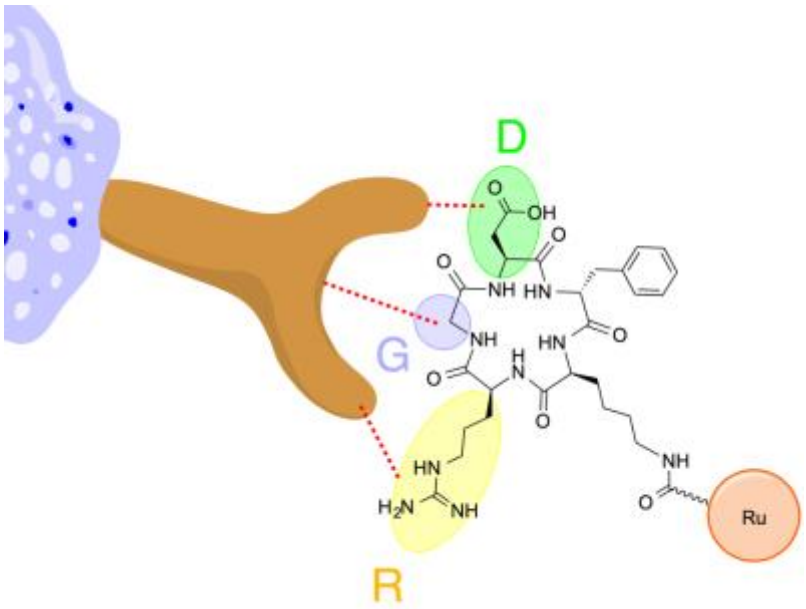


**Figure 25 –** Design of ruthenium cyc(RGDfK) conjugates for targeting integrin $\alpha_v\beta_3$.

For this purpose, different ruthenium(II) polypyridyl complexes are synthesized whereas the functional group for potential coupling to cyc(RGDfK) is attached either to tridentate, bisdentate or monodentate pyridine-based ligands. Two terpyridine-based complexes are

coupled to the peptide leading to a monomeric and a dimeric Ru-RGD-bioconjugate. These compounds are used to investigate the binding affinities to integrin $\alpha_v\beta_3$ and $\alpha_5\beta_1$, as well as the cytotoxicity against human A549 and SKOV-3 cell lines. Finally, the differences between the monomeric and dimeric compound is evaluated.

# 6 Design of Histidine-based Au(I)-NHC Complexes with Potential for Coupling to Peptides

The second part of this work focuses on novel gold(I) complexes based on a *N*-heterocydic carbene derived from the amino acid L-histidine. The extraordinary characteristics of the NHC ligand leading to highly water- and air stable cationic Au(I) complexes allows the rational design of cytotoxic anticancer agents. Hence, the attachment of different *N*-substituents, namely methyl- (Me), ethyl- (Et) and benzyl- (Bz) derivatives, at the imidazolium ring of the amino acid sidechain was carried out to achieve different steric demands at the carbene ligands. The synthesis of the bis-NHC gold(I) complexes was accomplished *via* the formation of silver NHC intermediates *in situ*. Finally, after detachment of the protection group at the amino acid's carboxylate group, the tethering of peptides or even the incorporation of the amino acid into the cyclic RGD pentapeptide is feasible to achieve targeted cytotoxic anticancer agents.

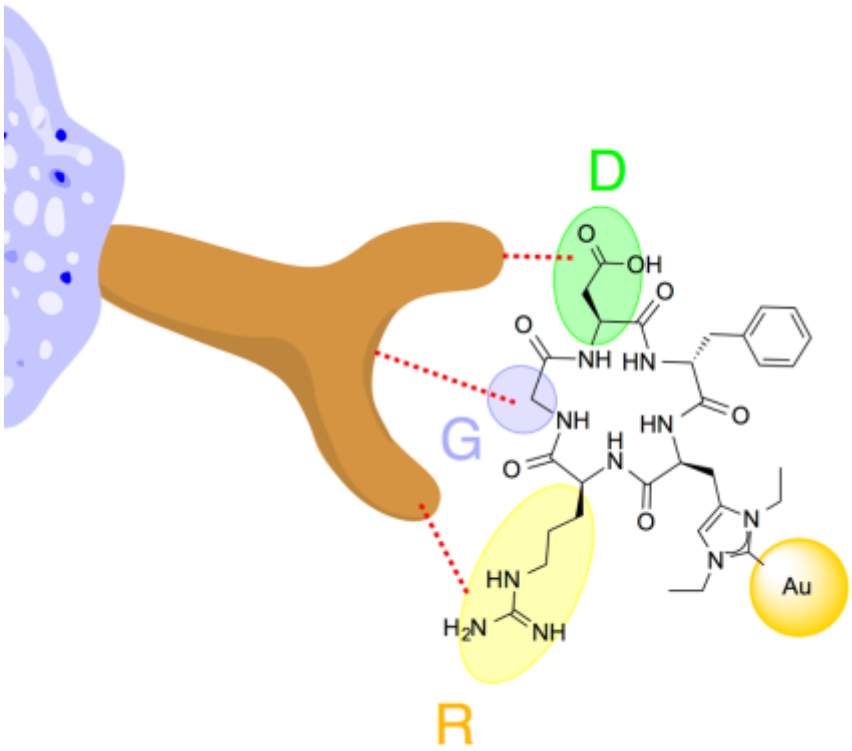


**Figure 26 –** Design of gold(I) bis-NHC complexes for potential incorporation into the peptide strucutre.

# III. RESULTS AND DISCUSSION

# 7 Design of Ruthenium-RGD-Conjugates as Targeting Anticancer Agents

The high selectivity for tumor cells without damaging healthy cells is one of the main challenging tasks in anticancer agent design. Herein, Ru(II) complexes are coupled to a cyclic RGD peptide targeting integrin receptors which are overexpressed on cancer cells to improve the distinction between healthy and abnormal tissue.

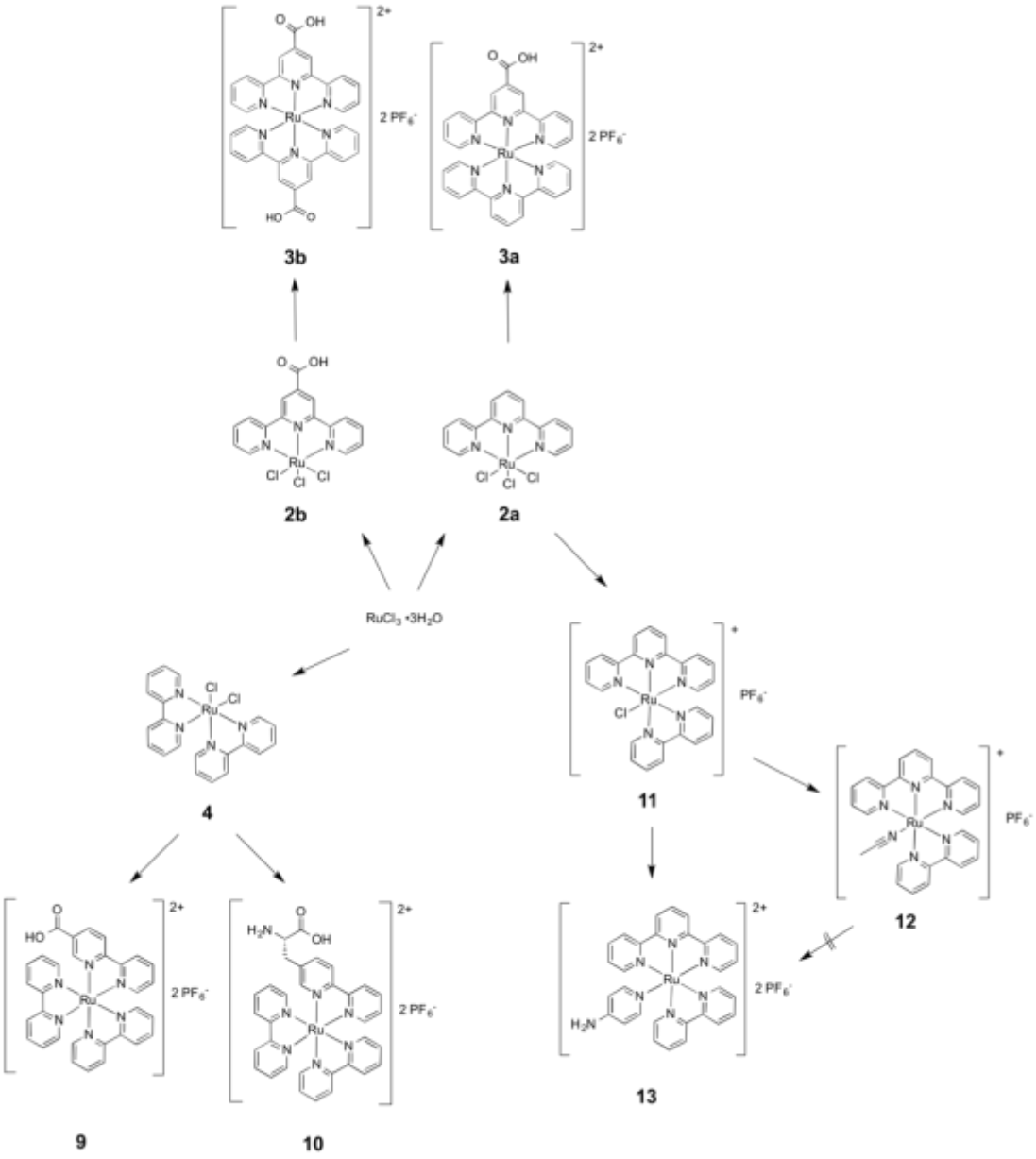


**Scheme 1 –** Overview of the synthesized complexes with functional groups attached to a tridentate, bisdentate or monodentate ligand.

To begin with, synthesis of Ru(II) complexes are biovectors cyclic RGD peptide. Different type of Ru(II) polypyridyl complexes were designed in this work, depending on the location of functional group used for the peptide coupling reaction. Either the group is attached to a tridentate, a bidentate or a monodentate ligand which are in the next step used for the synthesis of the complexes. An overview of the synthesized compounds is shown in Scheme 1.

## 7.1 Tridentate Ligands

First of all, complexes containing two tridentate ligands based on 2,2':6',2''-terpyridine (**1a**, terpy) were synthesized. The benefits of these structures are their high stability on air and in solution induced by the two chelating ligands. Furthermore, the terpy ligand is easy to functionalize at the 4' position and the introduction of a carboxylic acid group required for the coupling procedure is possible. This two-step procedure has been published in literature.[84] First, furfural and 2-acetylpyridine were dissolved in ethanol under basic conditions to obtain 4'-(furan-2-yl)-terpyridine. This intermediate product was then oxidized with $KMnO_4$ to yield in the desired compound, [2,2':6',2''-terpyridine]-4'-carboxylic acid (**1b**, terpy*) (see Scheme 2).

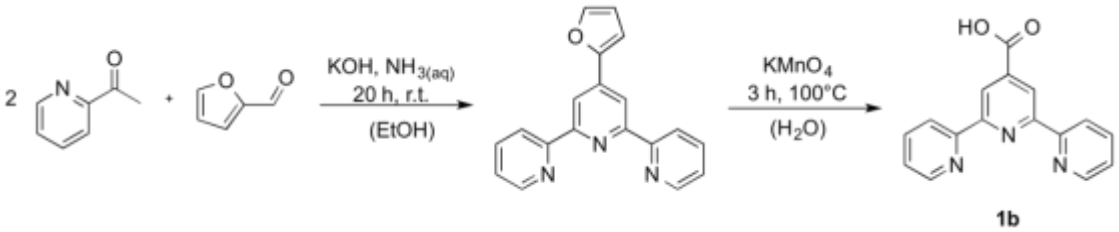


**Scheme 2 -** Synthesis of ligand **1b**, [2,2':6',2''-terpyridine]-4'-carboxylic acid (terpy*).

A novel synthetic route based on literature procedures[85] was carried out for complexes **3a** and **3b**, shown in Scheme 3. The ligands **1a** or **1b** were heated with $RuCl_3 \cdot 3H_2O$ in dry ethanol resulting in the dark brown complexes **2a** and **2b**. In the next step, triethylamine and LiCl (for chloride abstraction) were added to the compounds in ethanol and heated to reflux. During this reaction the reduction of Ru(III) to Ru(II) takes place and so, the resulting Ru(II) complexes [Ru(terpy)(terpy*)]$(PF_6)_2$ (**3a**) and [Ru(terpy*)$_2$]$(PF_6)_2$ (**3b**) were formed providing

one (**3a**) or two (**3b**) carboxylic acid groups, respectively.

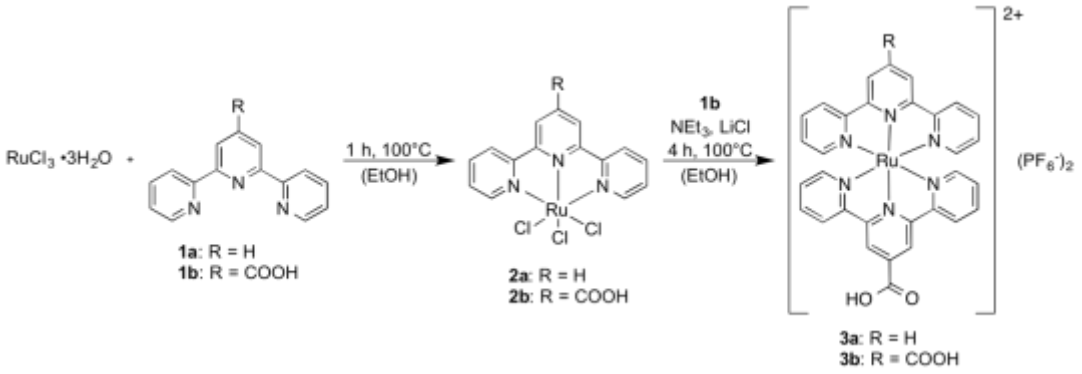


**Scheme 3 -** Two step procedure for the synthesis of [Ru(terpy)(terpy*)]$(PF_6)_2$] (**3a**) and [Ru(terpy*)$_2$]$(PF_6)_2$] (**3b**).

The ligands and ruthenium complexes were analyzed with $^1$H, $^{13}$C and $^{31}$P NMR spectroscopy. However, no NMR spectra for complexes **2a** and **2b** were recorded due to the paramagnetic characteristic of these Ru(III) compounds.

The $^1$H NMR spectra of ligand **1b** and complexes **3a** and **3b** are shown in Figure 27. Comparing the spectra of **1b** and **3a**, several signal shifts are observed due to complex formation. The signals of $H^{3',5'}$ and $H^{3,3''}$ are shifted downfield around Δδ = +0.61 or +0.49 ppm. In contrast, the signal of $H^{4,4''}$ remains and the signals of $H^{6,6''}$ and $H^{5,5''}$ display a strong upfield shift about Δδ = −1.25 or −0.28 ppm. Similar values are observed with **3b** (coordinated by two ligands **1b**). The downfield shift of $H^{3',5'}$ and $H^{3,3''}$ is about Δδ = +0.62 or +0.47 ppm, whereas the signal of $H^{4,4''}$ remains and the signals of $H^{6,6''}$ and $H^{5,5''}$ are shifted upfield about Δδ = −1.20 or −0.26 ppm. For these observations, two effects have to be taken into account: First, the deshielding effect of the carboxylic acid groups and second, the increase of electron density in the aromatic system through coordination of ruthenium. The presence of the $PF_6^-$ counterions in complexes **3a** and **3b** was verified through the characteristic septet in the $^{31}$P NMR spectra. Additionally, in $^{13}$C NMR the carbon atoms of the carboxyl groups of **3a** and **3b** are identified due to the high downfield shift to 165.79 or 165.63 ppm.

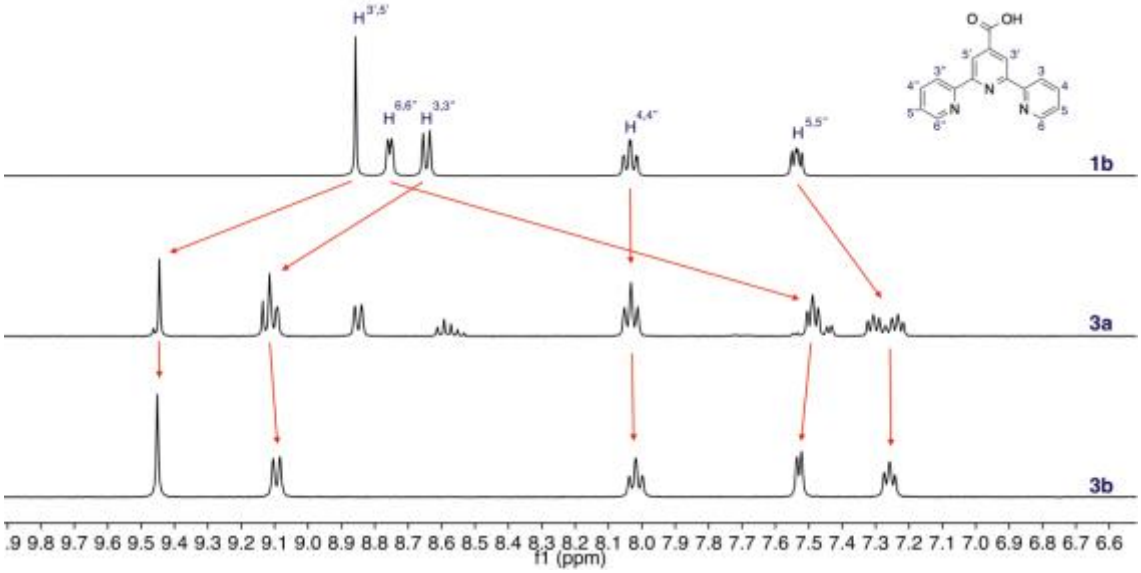


**Figure 27 -** Comparison of $^{1}$H NMR of ligand **1b** and complexes **3a** and **3b**.

The formation of complexes was verified by ESI-MS whereas the characteristic isotopic patterns of the main signals were compared with the calculated ones. The complexes show signals at 757.05 and 306.04 m/z for **3a** (see Figure 28) and 801.04 and 328.04 m/z for **3b** (see Figure 30), in each case indicating the loss of one or two $PF_6^-$ anions leading to a single or double positive charged complex. The characteristic isotopic patterns of the signals match perfectly with the calculated ones, as depicted in Figures 29 (for **3a**) and 31 (for **3b**).

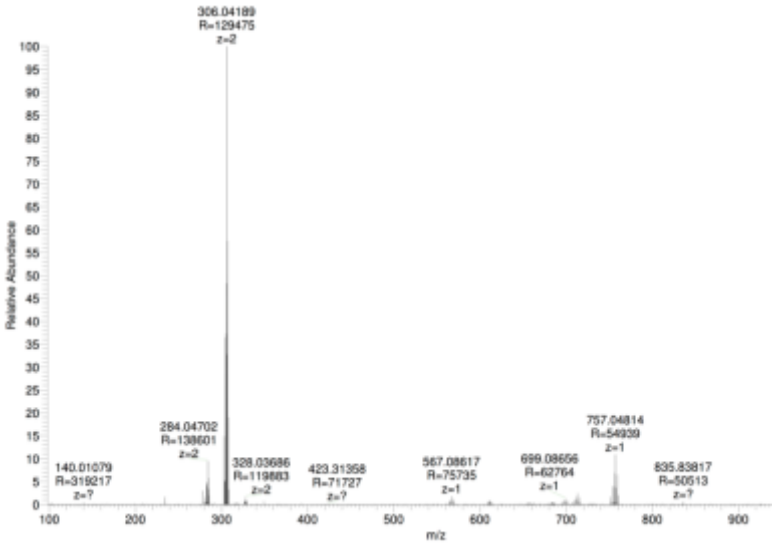


**Figure 28 –** ESI-MS of complex **3a**.

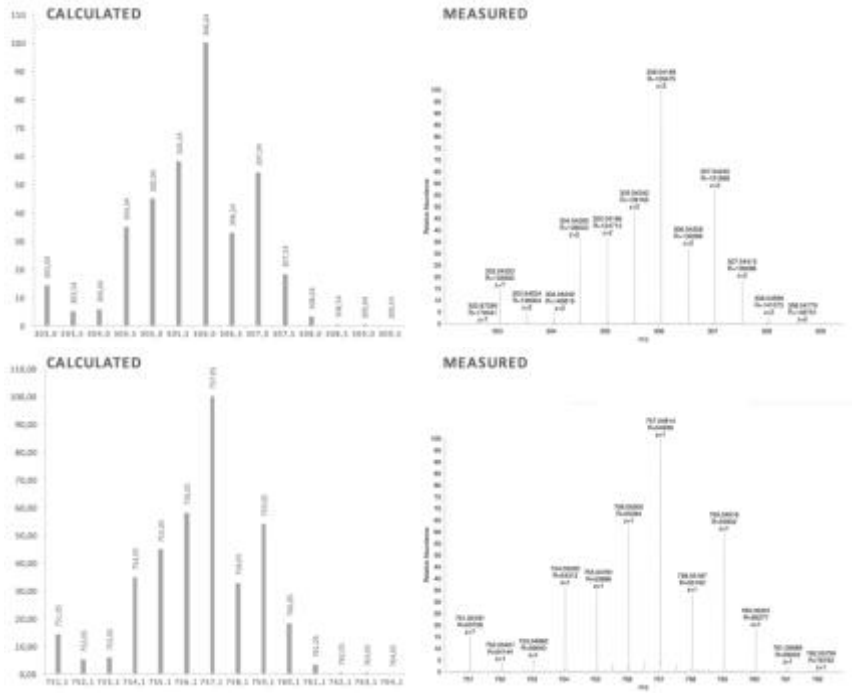


**Figure 29 -** Comparison of calculated and measured isotopic patterns of **3a** in ESI-MS.

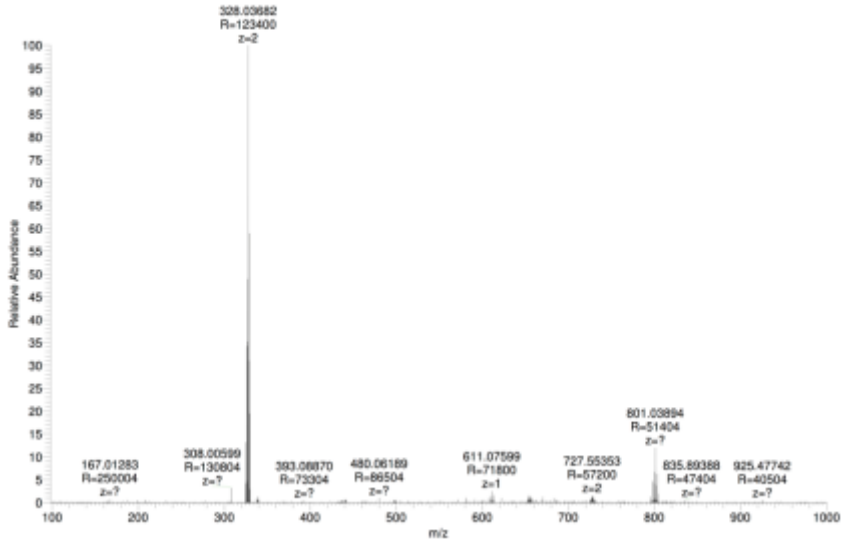


**Figure 28 –** ESI-MS of complex **3b**.

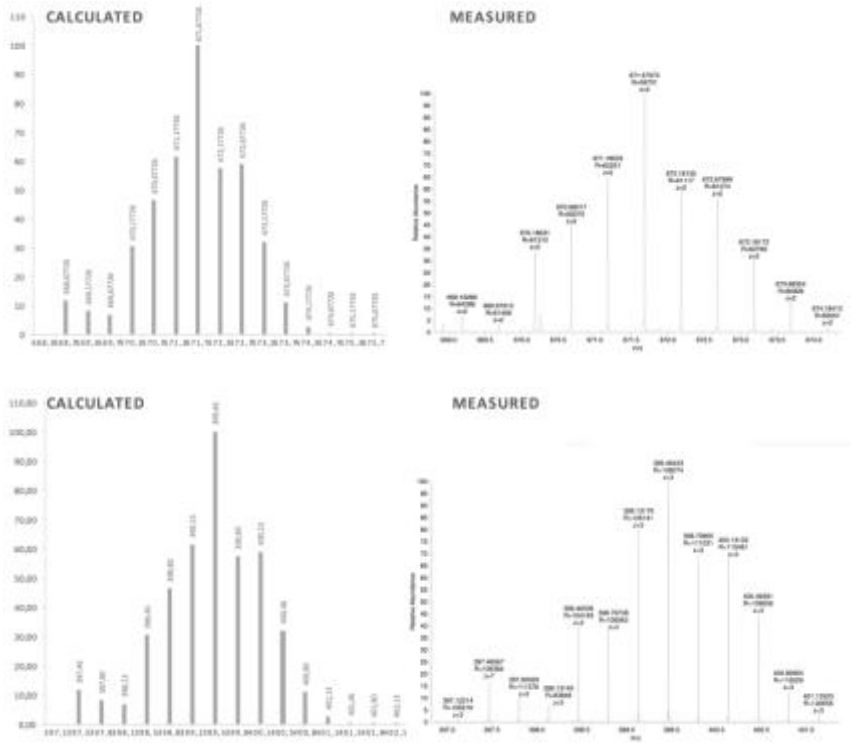


**Figure 29 -** Comparison of calculated and measured isotopic patterns of **3b** in ESI-MS.

Due to their easy synthesis and high stability, the two synthesized complexes **3a** and **3b** are suitable compounds for tethering the cyclic pentapeptide leading hopefully to stable, water soluble and cytotoxic compounds mainly targeting the $\alpha_v\beta_3$ integrin receptor.

## 7.2 Bisdentate Ligands

The second type of ruthenium complexes synthesized in this work are the bisdentate, 2,2'-bipyridine (bipy) based systems. These complexes are known to show high fluorescence properties[86], a feature which is essential for studying the uptake of a drug by fluorescence microscopy. As precursor complex, $[Ru(bipy)_2Cl_2]$ was synthesized using Schlenk techniques through the reaction of $RuCl_3 \cdot 3H_2O$ and two equivalents of 2,2'-bipyridine (see Scheme 4). The neutral compound was precipitated by addition of acetone and isolated *via* filtration.

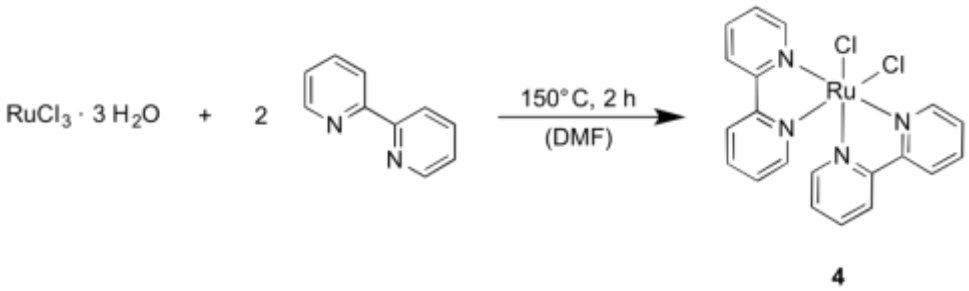


**Scheme 4 –** Synthesis of bipyridine-based Ru(II) precursor **4**.

In analogy to the functionalized terpy ligand **1b**, a 2,2'-bipyridine ligand is designed likewise bearing a carboxylic acid moiety for coupling. Unfortunately, the synthesis of bipyridine functionalized systems is more complex than for terpyridines. Therefore, an elaborate four-step procedure shown in Scheme 5 was applied for the synthesis of a functionalized bipyridine ligand, bearing a carboxyl group at $C^5$: 5-carboxy-2,2'-bipyridine.[87]

First of all, path **A** of Scheme 5 is clarified. 2-Amino-5-methylpyridine is commercially available and a rather cost-effective starting material. For using this compound in the intended palladium-catalyzed Negishi crosscoupling reaction, the amino group has to be converted into a triflate leaving group in a two-step procedure. First, 2-amino-5-methylpyridine was mixed with concentrated $H_2SO_4$ and $NaNO_2$ inducing a diazotization and the subsequent hydrolyzation to yield in 2-hydroxy-5-methylpyrdine (**5**). In the second step, this compound was dissolved in pyridine and mixed with 1.20 equivalents of trifluoromethanesulfonic anhydride. The product was purified *via* distillation under reduced pressure to yield in 5-methylpyridin-2-yl trifluoromethanesulfonate (**6**) as colorless liquid.

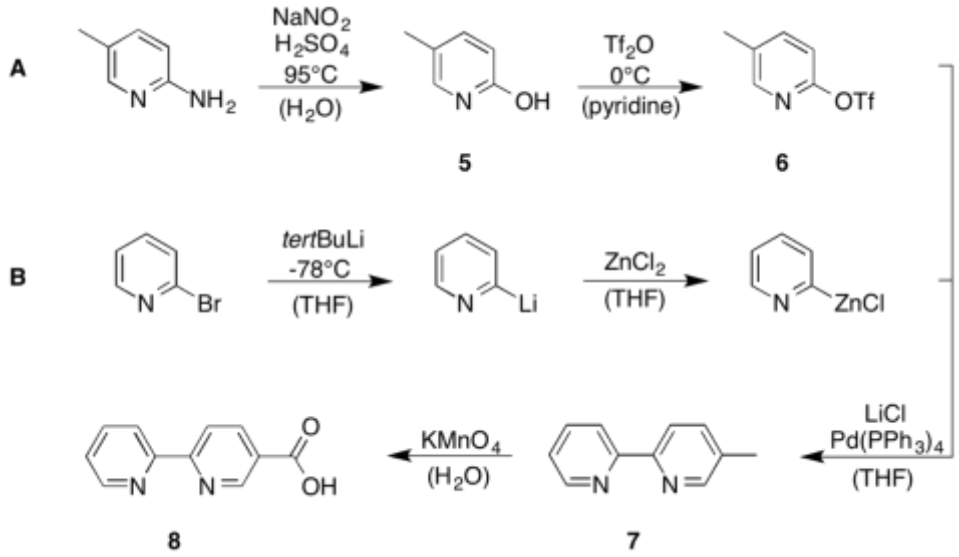


**Scheme 5 –** Four step procedure for the synthesis of 5-carboxy-2,2'-bipyridine (**8**); path **A**: synthesis of 5-methylpyridin-2-yl trifluoromethanesulfonate (**6**) and path **B**: synthesis of pyridin-2-ylzinc(II) chloride.

Considering path **B** of Scheme 5, in the first step 2-bromopyridine was converted *in situ via* metal-halogen exchange into 2-pyridinyllithium using *tert*-butyllithium at -78°C. The zinc compound necessary for the Negishi crosscoupling was generated through the addition of $ZnCl_2$ solution in diethylether. Pyridin-2-ylzinc(II) chloride is not further purified but rather the solution used immediately for the crosscoupling reaction. The addition of 5-methylpyridin-2-yl trifluoromethanesulfonate produced in path **A**, LiCl and $Pd(PPh_3)_4$ as catalyst induced the coupling reaction to yield in the penultimate product 5-methyl-2,2'-bipyridine (**7**). The methyl group was easily oxidized by addition of $KMnO_4$ in aqueous solution. The reaction solution was filtered over celite to remove the side product $MnO_2$ and 5-carboxy-2,2'-bipyridine (bipy*, **8**) was obtained as white solid. Since as the Negishi cross coupling and the oxidation with $KMnO_4$ suffered of inefficiency, the yield is just about 23% or rather 7%. Consequently, an overall yield of just 1% was achieved.

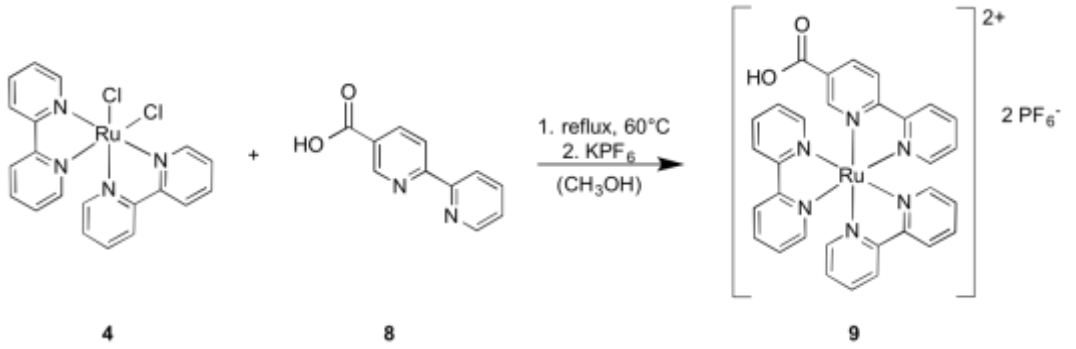


4 8 9

**Scheme 6 –** Synthesic procedure for bipyridine based ruthenium complex **9**.

**8** was reacted with the Ru(II) precursor $[Ru(bipy)_2Cl_2]$ (**4**) in dry methanol under inert atmosphere (see Scheme 6). After 5 hours at 60°C the dark violet product, $[Ru(bipy)_2(bipy^*)_2](PF_6)_2$ (**9**) was precipitated by addition of aqueous 1 M $KPF_6$ solution and isolated *via* filtration. Unfortunately, the yield of this complex was unusually low regarding the fact that bipyridines are excellent bidentate ligands for ruthenium(II) complexes. However, the unsuccessful chloride abstraction or side reactions induced by the carboxy group could be the reason for this outcome. The product was characterized with NMR as well as with ESI-MS.

The $^1$H NMR of **4**, **8** and **9** are depicted in the following Figure 30. The proton of the carboxylic acid group of **9** shows up at 13.93 ppm. The broad signal at 9.67 ppm results from the proton of the carboxylic acid group of **8** (at $C^5$). The other signals can barely be assigned. Comparing the $^1$H NMR of the starting materials **4** and **8** with the product **9**, some shifts into the deep field and upfield can be observed by complex formation. The ESI-MS signals at $m/z$ = 758.87 for the single positive charged complex $[M\text{-}PF_6]^+$ and 307.15 for the double positive charged complex $[M\text{-}2PF_6]^{2+}$ proof the formation of the desired product.

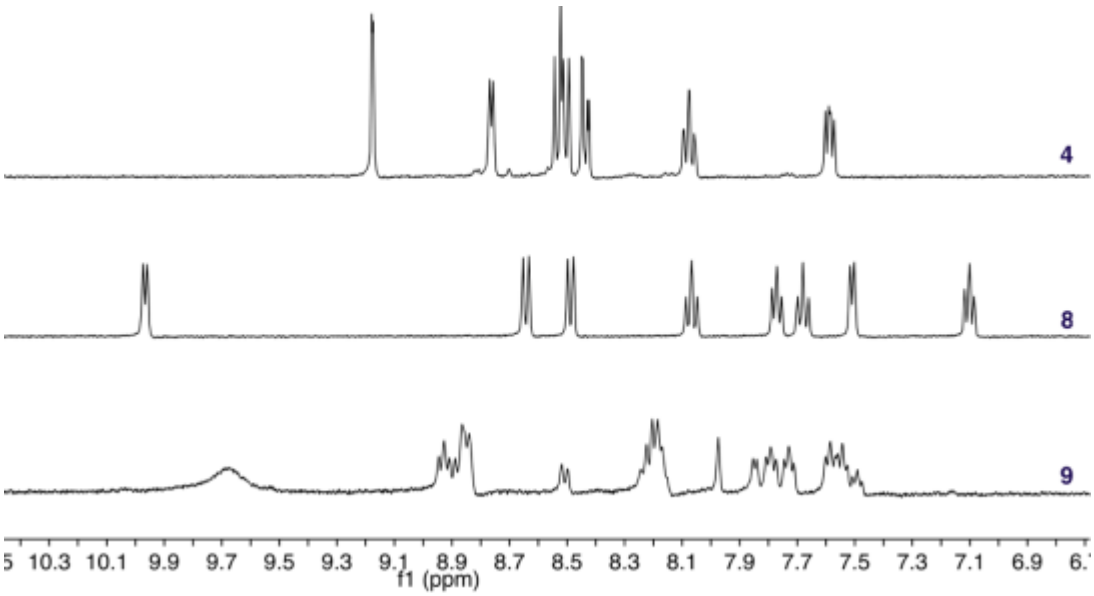


**Figure 30 –** $^{1}$H NMR of precursor complex **4**, ligand **8** and the **9**

Besides the carboxylate bearing ligand **8**, an unnatural, Boc-protected (Boc = *tert*-butyloxycarbonyl) amino acid, namely (*S*)-3-([2,2'-bipyridin]-5-yl)-2-((*tert*-butoxycarbonyl)-amino)propanoic acid (Boc-bipy-AA) provided by Prof. João D. G. Correia from the Técnico Lisboa was reacted with $[Ru(bipy)_2Cl_2]$ in a J.Young tube in $CD_3OD$ at 60°C (see Scheme 7). The reaction was monitored *via* $^{1}$H NMR, whereas due to the low amount of Boc-bipy-AA the signals were just poorly dissolved. After 6 hours, some new signals in the aromatic region were observed and the reaction was stopped by addition of aqueous 1 M $KPF_6$ to precipitate the product (**10**) as dark yellow solid. Also in this synthetic approach the yield of product was just 1.0 mg, so ongoing attachment to peptides were not feasible.

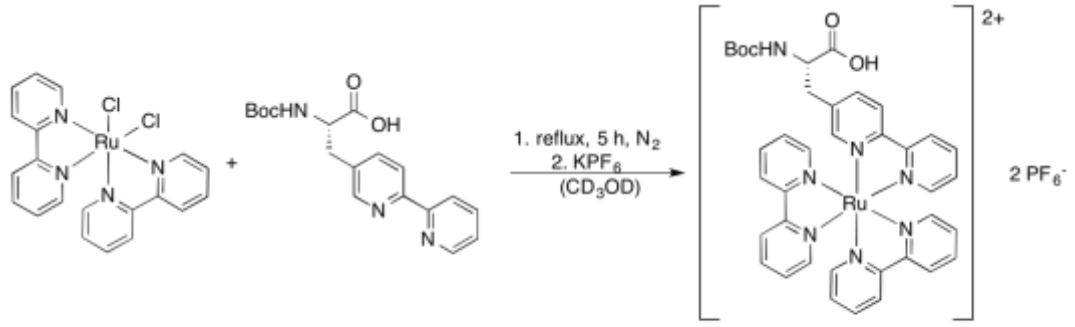


**4** **10**

**Scheme 7 –** Synthesis of Ru(II) complex **10** bearing the unnatural amino acid Boc-bipy-AA.

The ESI-MS in Figure 31 confirms the formation of the desired product complex **10**. The signal

at 901.75 m/z originates from the single positive charged complex due to the loss of one $PF_6^-$, whereas the signal at 378.35 m/z matches to the double positive charged complex without any anion.

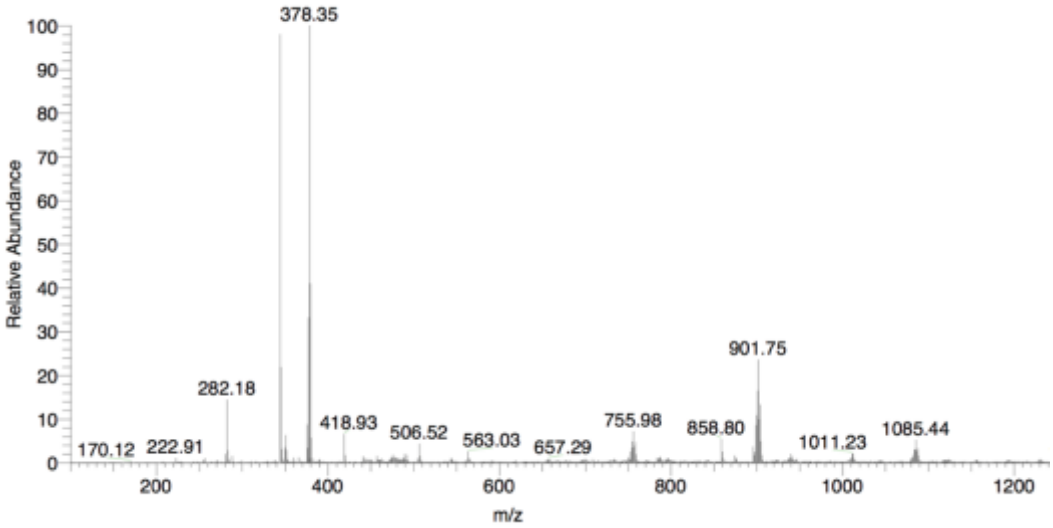


**Figure 31 –** ESI-MS of **10**, showing the formation of the desired product at m/z = 901.75 and 378.35.

Consequently, the two bipyridine based ruthenium(II) complexes **9** and **10** were successfully synthesized and their formation verified with NMR or rather ESI-MS. Due to the low reaction yields, no tethering of cyc(RGDfK) was possible. However, considering the outstanding fluorescent characteristics of these ruthenium complexes,[86] after coupling to the peptide they can be used as fluorescent probes to observe the uptake of the compound *in vivo* by fluorescence microscopy.

## 7.3 Monodentate Ligands

Finally, a monodentate ligand is attached to the ruthenium complex bearing a second functional group for coupling to peptides. In order to complete the octahedral coordination sphere of the $Ru^{2+}$ cation, one terpyridine and one bipyridine ligand were attached to the metal. Based on the precursor [Ru(terpy)$Cl_3$] (synthesis described in section 7.1) the complex [Ru(terpy)(bipy)Cl]$PF_6$ (**11**) was prepared as shown in Scheme 8. Lithium chloride was added for chloride abstraction and besides, through the reaction in ethanol, the reduction of Ru(III) to Ru(II) takes place. The resulting chloro complex was precipitated with $KPF_6$ to yield in the dark red product complex **11**.

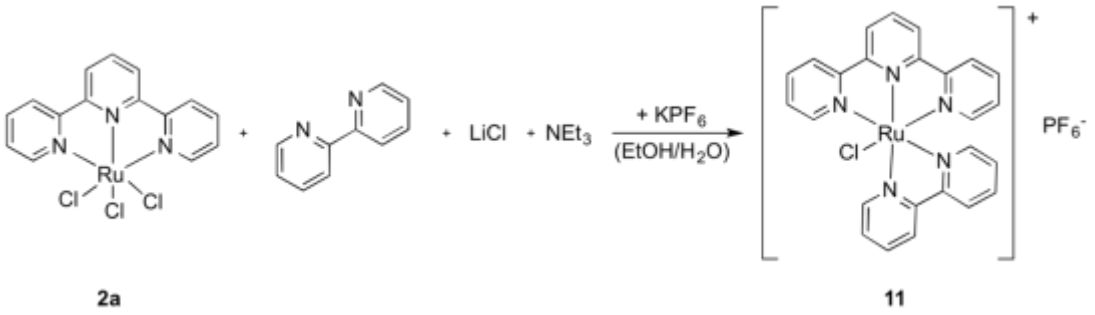


**Scheme 8 –** Synthesis of [Ru(terpy)(bipy)Cl]$PF_6$ (**11**).

Based on **11**, the acetonitrile complex [Ru(terpy)(bipy)($CH_3CN$)]$(PF_6)_2$ (**12**) was synthesized as shown in Scheme 9 and was considered as the best precursor complex for ligand exchange reactions since the acetonitrile solvent ligand can easily diffuse from the complex. Therefore, in the following, ligand exchange with the bifunctional molecules depicted in Figure 32 were performed. N-donor ligands like ethylenediamine (en, **A**), 4-aminopyridine (fampy, **B**) bearing a free amine for coupling as well as β-alanine (β-ala, **C**), isonicotinic acid (inico, **D**) and 3-(pyridin-4-yl)propanoic acid (PyPrA, **E**) containing a carboxylic acid function for coupling were chosen.

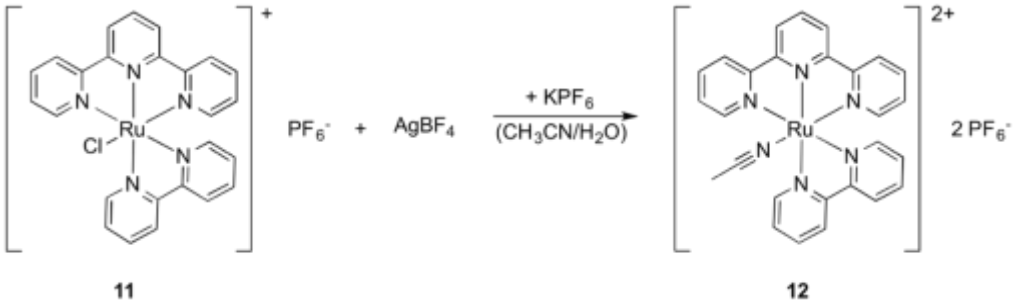


**Scheme 9 –** Synthetic procedure for the formation of the acetonitrile complex **12**.

However, ligand exchange reactions in acetonitrile lead to incomplete conversion or degeneration and reformation of complex **11**, **12** or actually the aqua complex $[Ru(terpy)(bipy)(H_2O)](PF_6)_2$. Even the application of dimethylsulfoxide (DMSO) as solvent and heating up above the boiling point of acetonitrile, complete formation of product was not observed. Additionally, during purification, decomposition of the product and formation of the aqua complex was observed. For the isolation of the product from the crude reaction mixture, column chromatography with silica and a mixture of $CH_3CN$, $H_2O$ and $KNO_{3,sat}$ was used as eluent. Therefore, decomposition could potentially be caused by the acidic solid phase or the water content of the mobile phase. Another potential reason could be the low stability of the product complexes at light and on air, however, application of Schlenk techniques, dry solvents and light-protected reaction flasks, could not improve the result of the reaction. Nevertheless, if these complexes miss stability on air or in water, application as anticancer agent is excluded since these features are essential for medicinal usage.

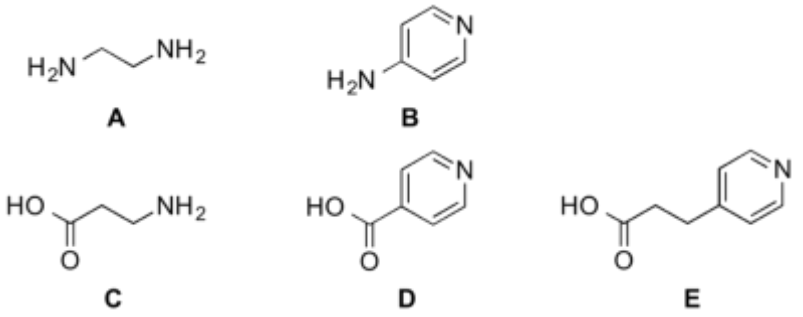


**Figure 32 –** Substrates applied in ligand exchange reactions with **11** or **12**, **A**: ethylenediamine (en), **B**: 4-aminopyridine (fampy), **C**: β-alanine (β-ala), **D**: isonicotinic acid (inico) and **E**: 3-(pyridin-4-yl)propanoic acid (PyPrAE).

However, the previous complex **11** was found to be a better starting material for ligand

exchange reactions since the chloro ligand can be easily abstracted for example by addition of silver ions. Likewise, through the addition of $AgPF_6$ no further precipitation with $PF_6^-$ ions after the reaction is necessary to isolate the complexes. Using this procedure, complex **11** was reacted with fampy in a mixture of acetone and water at 70°C to yield the pure product after precipitation with diethylether (see Scheme 10).

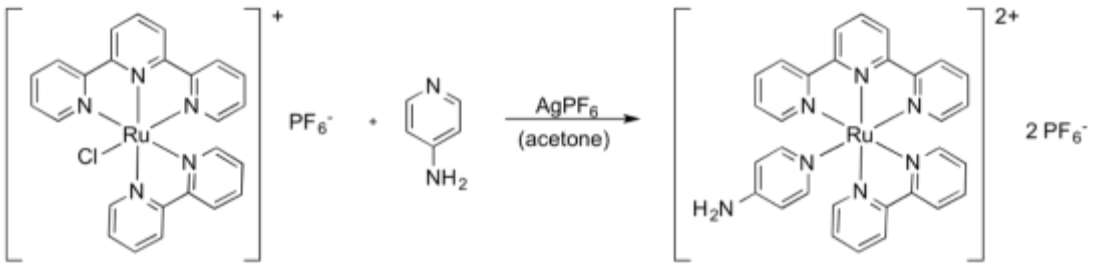


**11** **13**

**Scheme 10 –** Synthetic procedure for ligand exchange reaction spplying complex **11** as starting material.

The product was characterized by elemental analysis, $^1H$ and $^{13}C$ NMR, ESI-MS, single crystal X-ray diffraction (SC-XRD) and UV/Vis spectroscopy and furthermore, the stability in water was evaluated.

First of all, the $^1H$ NMR spectra of complexes **11** and **13**, shown in Figure 33 demonstrate the impact on the shifts by addition of fampy. The aromatic protons of the new ligand can easily be located at 7.2 and 6.5 ppm (see blue labels) as well as its amine group at 6.3 ppm (green label). These signals appear quite high field shifted compared to the signals of the remaining polypyridyl protons which were not assigned in detail. Interestingly, the signal of complex **11** at 10.4 ppm, located furthest in the deep field, is remarkably shifted into the high field through ligand exchange (see red labels). This observation indicates, that this proton is probably $H^{6'}$ of the bipyridine ligand pointing towards the chloride ligand. The high electronegativity of the chloride atom presumably influences this spatially close located proton through space and induces a shift into the deep flied. After chloride abstraction and attachment of fampy, this shift is annulated and the proton signal switches to the higher field.

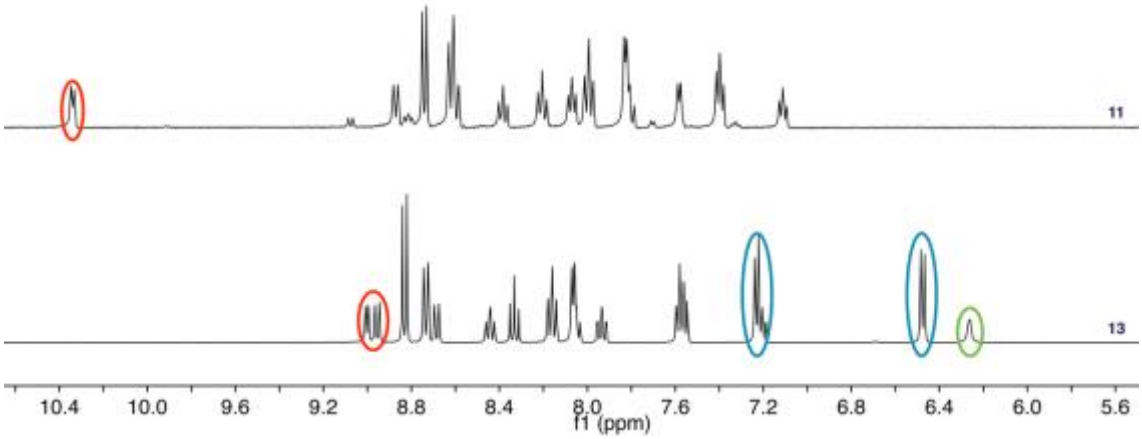


**Figure 33 –** Comparison of $^{1}$H NMR spectra of ruthenium complexes **11** and **13**.

ESI-MS analysis reveals signals at m/z = 292.45 for $[M\text{-}2PF_6]^{2+}$ and 729.92 $[M\text{-}PF_6]^{+}$ (see Figure 34). Additionally, the characteristic isotopic pattern of the single positive charged ruthenium complex is depicted in the magnification of the signal at 729.92.

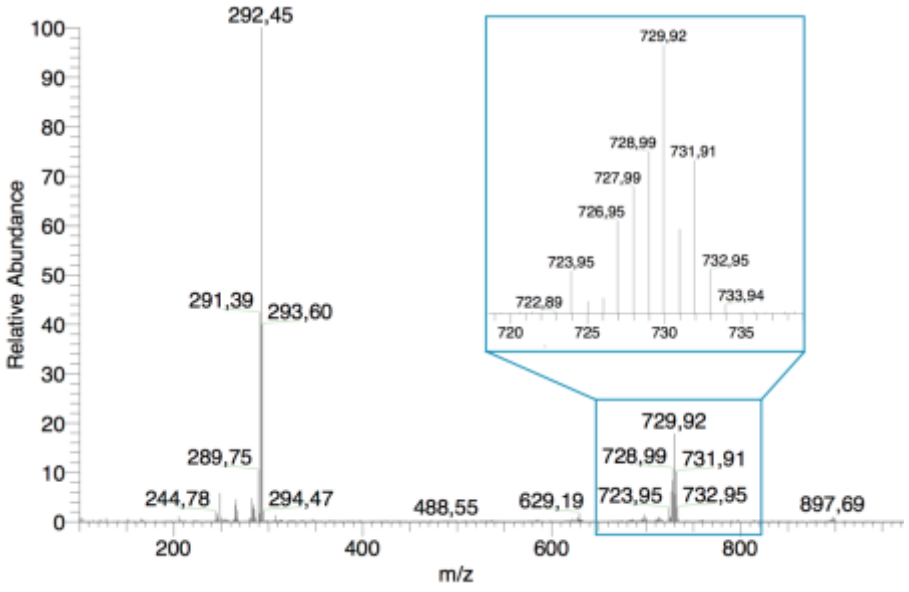


**Figure 34 –** ESI-MS of compound **13** and the characteristic isotopic pattern of the $[M\text{-}PF_6]^{+}$ signal.

Additionally, the solubility of compound **13** in different solvents as well as its stability in water was evaluated. Regarding the solubility, complex **13** is highly soluble in various polar aprotic solvents like DMSO, DMF, and acetone. But unfortunately, NMR studies reveal that

in water or in mixtures of acetone and water (1:1), within 48 hours the fampy ligand is cleaved, water binds the ruthenium metal center and the aqua complex starts to crystallize. This decomposition process is favorable considering the uptake of the drug into the cell, but otherwise should not occur during conjugation to peptides or during transfer towards the cancer cell. Therefore, ongoing studies have to be carried out considering the performance of the compound in living organism.

Subsequently, a solution of **13** in DMSO was tested with UV/Vis spectroscopy. Local maxima are visible at 280 nm, 310 nm and 480 nm, whereas due to the absorption between 400 and 550 nm the complex appears in a dark red-violet color.

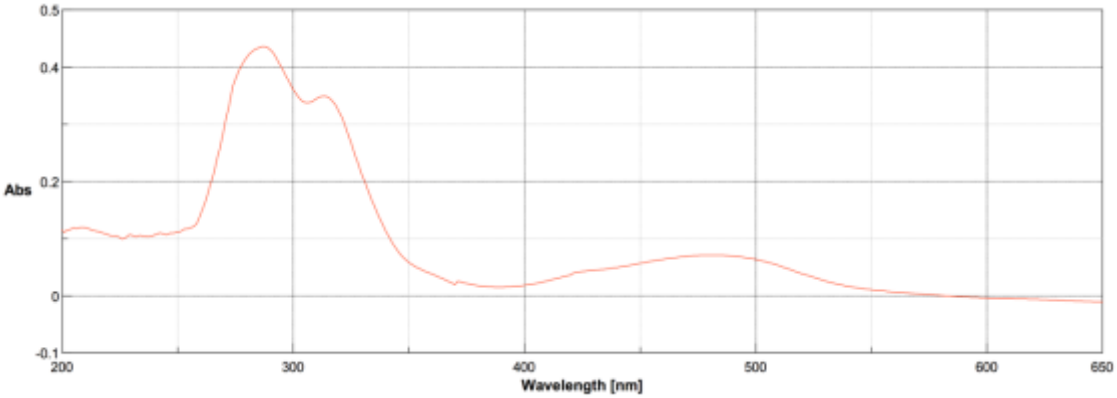


**Figure 35 –** UV/Vis spectrum of **13** in DMSO.

Finally, a single crystal structure of **13** was determined by SC-XRD of a dark red needle-shaped crystal obtained through the addition of diethylether to a solution of **13** in acetone/water (see Figure 36). The compound crystallizes in the P121/c1 space group and reveals a monoclinic crystal system. The bond length between the central metal ruthenium and the N-donor atoms of the ligands range around 2 Å, whereas the bond towards the fampy N-atom reveals the longest (2.122(2) Å) and the bond towards one of thete rpy N-atoms the shortes (1.962(2) Å) connection, most probably due to the chelating effect. Within the terpy ligand, the N1-Ru-N2 or N2-Ru-N3 angles enclose about 79.7°, likewise the N4-Ru1-N5 angle of the bipy ligand displays values of 78.2 or rather 78.9°. A comparison of the angles between the three ligands indicates that fampy is located approximately perpendicular to the terpy ligand, since all angles display values around 90° (N1-Ru1-N6 = 90.9°, N3-Ru1-N6 = 89.1°, N2-Ru1-N6 = 89.6°). The plane of the bipy ligands deviates about 5° from the ideal perpendicular towards the terpy ligand, as assigned by the angles N5-Ru1-N1 = 96.5°, N5-Ru1-N2 = 95.2°, and N5-Ru1-N3 = 85.2°. Finally, the crystal structure refer to the observations

of the $^{1}$H NMR, since the proton H$^{6'}$ (at C16 in Figure 36) points clearly towards the fampy ligand but is not affected throuh space as observed in complex **11** by the extremely electronegative chlorido ligand.

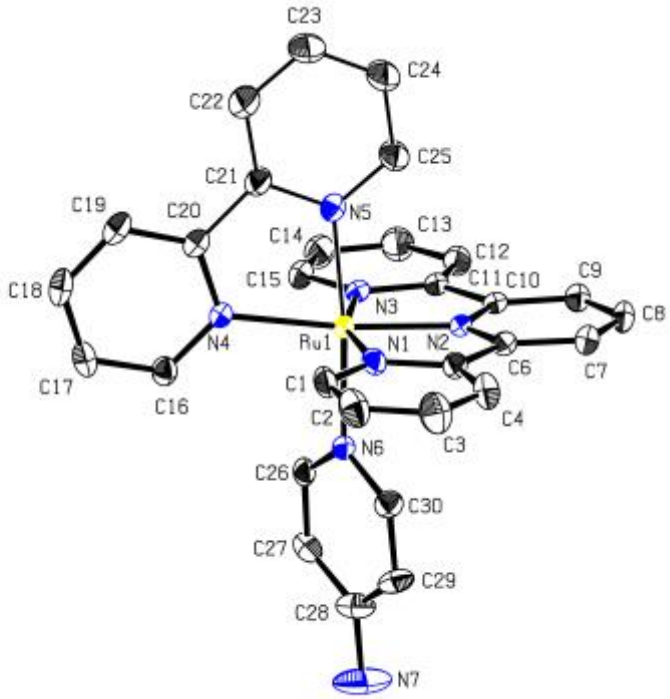


**Figure 36 -** ORTEP style drawing of **13** in the solid state. Thermal ellipsoids are drawn at the 50% probability level. Selected bond lengths [Å] and bond angles [°]: Ru1–N1 2.071(2), Ru1–N2 1.962(2), Ru1–N4 2.086(2), Ru1–N6 2.122(2), N1–Ru1–N6 90.90(9), N1–Ru1–N4 98.75(9), N4–Ru1–N6 97.17(9).

## 7.4 Synthesis of the Peptides

The peptide cyc(RGDfK) is known to target $\alpha_v\beta_3$ integrin receptors overexpressed on the surface of cancer cells. More exceptionally, the free amino group of L-lysine points out of the binding pocket of the receptor. This provides space as well as potential for the attachment of cytotoxic complexes and the design of targeted therapeutic anticancer agents.

Since cyc(RGDfK) is just a small pentapeptide, it was synthesized manually by solid phase peptide synthesis applying Fmoc (9-fluorenylmethoxycarbonyl) strategy, 2-chlorotritylchloride as resin, and the following protected amino acids: 2,2,4,6,7-pentamethyl-2,3-dihydrobenzofuran-5-sulfonyl (Pbf) protected arginine, *tert*-butyl (*t*Bu) protected aspartic acid and 1-(4,4-dimethyl-2,6-dioxocyclohex-1-ylidene)-3-methylbutyl (ivDde) protected lysine. An overview of the synthesis is presented in Scheme 11.

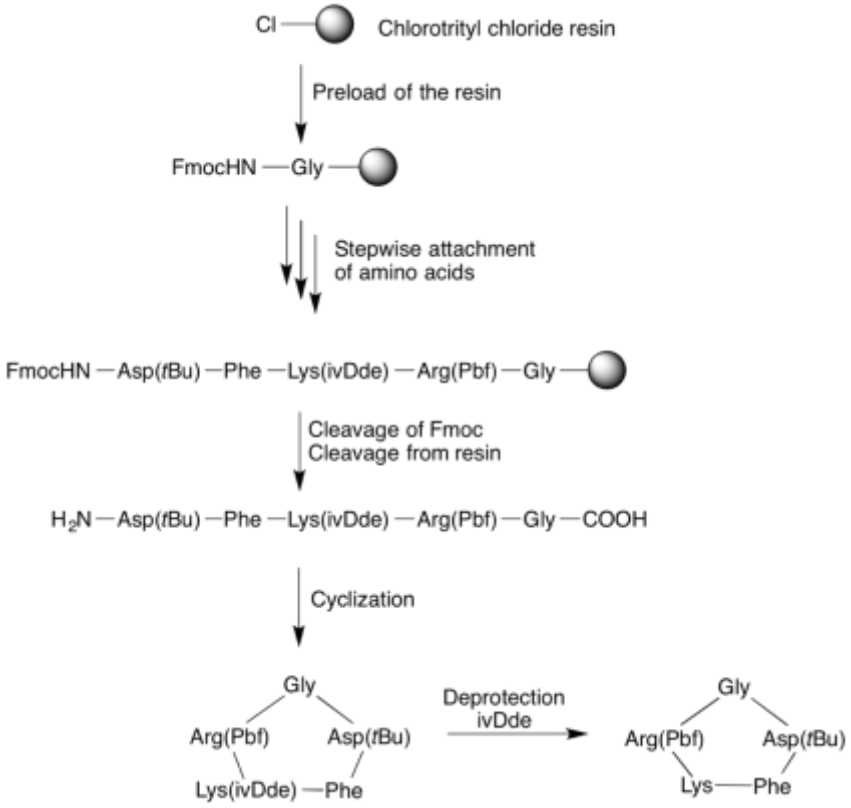


**Scheme 11 –** Procedure for solid phase peptide synthesis of cyc(R(Pbf)GD(tBu)fK).

To begin with, the synthesis was performed using 2-Chlorotrityl chloride resin which was preloaded with the first amino acid (Fmoc-Gly-OH) prior to use. The detailed preloading

procedure is shown in Scheme 12.

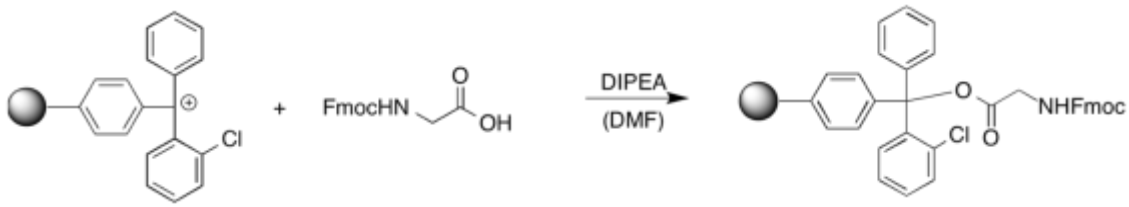


**Scheme 12 -** Preloading procedure of 2-chlorotrityl resin with Fmoc-Gly-OH.

In order to avoid that non-preloaded resin undergoes reactions with the next amino acids added and thus resulting in unwanted amino acid sequences, the resin was treated with a combination of methanol and DIPEA (ethyldiisopropylamine). So, the unreacted resin is capped with a methoxy group and no further amino acid can be coupled. Then, the amino acid sequence was built up step by step by addition of next amino acid together with the coupling agents benzotriazole-1-yl-oxy-tris-pyrrolidino-phosphonium hexafluorophosphate (PyBop) and 1-hydroxybenzotriazole (HOBt) as well as DIPEA as base whereas double coupling of each amino acid was performed to ensure full conversion. After cleavage of the capping Fmoc protection group with 20% piperidine in DMF, the next amino acid is added until the pentapeptide structure is completed. Then the produced amino acid sequence $H_2N$-Asp(*t*Bu)-D-Phe-Lys(ivDde)-Arg(Pbf)-Gly-OH is split from the resin and cyclized through amino acid bond formation between Gly-OH and Asp-$NH_2$ using PyBop and HOBt for activation (see Scheme 13). The protection groups at the lysine, aspartic acid and arginine prevent the occurrence of unwanted reactions within the side chains. To eliminate the risk of polymerization, a very diluted solution of the peptide was added to a solution of DIPEA. The cyclization was monitored with RP-HPLC, exhibiting a change in retention time from 20.6 min to 10.4 min (see Figure 37). Some amount of this cyclization product, cyc(R(Pbf)GD(*t*Bu)fK(ivDde)) was provided by the group of Prof. Kessler (Institute of Advanced Studies, Technical University Munich).

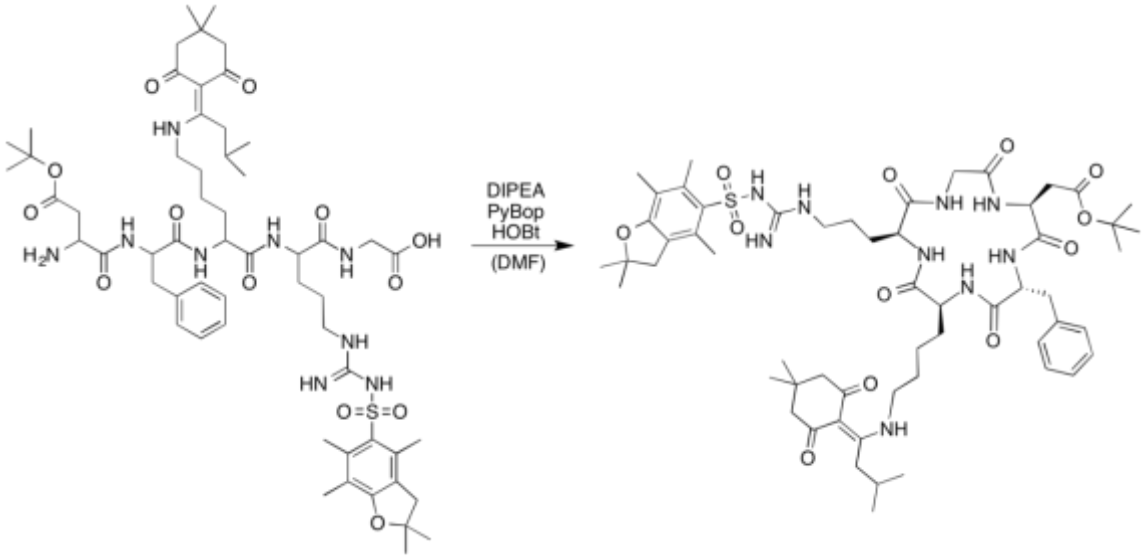


**Scheme 13 –** Cyclization of the linear peptide to yield the protected pentapeptide cyc(R(Pbf)GD(*t*Bu)fK(ivDde)).

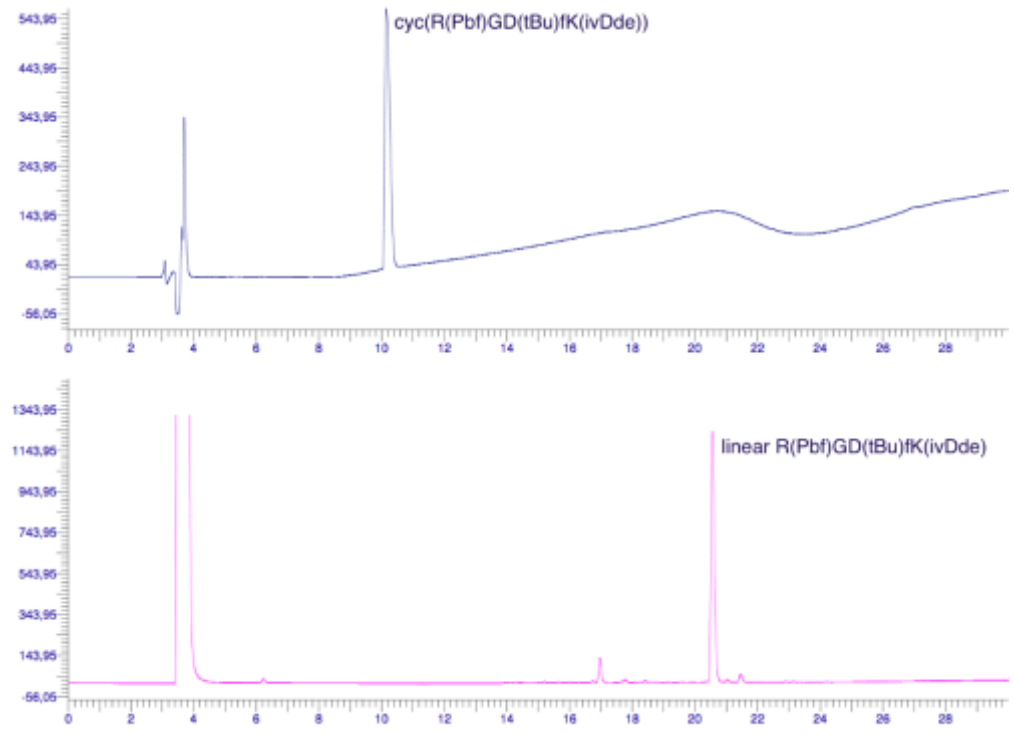


**Figure 37 –** Comparison of analytical RP-HPLC chromatograms of cyc(R(Pbf)GD(*t*Bu)fK(ivDde)) (top) and linear $H_2N$-R(Pbf)GD(*t*Bu)fK(ivDde)-OH (bottom) using method A.

Prior to use for conjugation reactions, the ivDde protection group was cleaved by treatment with 2% hydrazine in DMF yielding in cyc(R(Pbf)GD(*t*Bu)fK). Additionally, an aliquot of peptide was mixed with a deprotection cocktail (80% TFA, 5% triisopropylsilane (TIPS), 5% $H_2O$, 10% DCM) to cleave the Pbf- and *t*Bu-protection groups. The two resulting peptides cyc(R(Pbf)GD(*t*Bu)fK) and cyc(RGDfK), see Figure 38, were used for the following coupling studies.

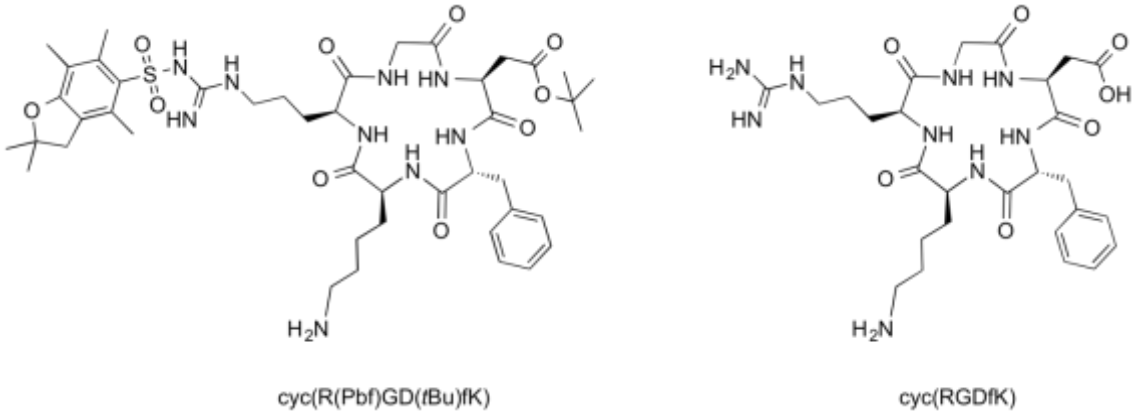


**Figure 38 –** Cyclic pentapeptides used for coupling reactions. Left: cyc(R(Pbf)GD(*t*Bu)fK) and right: cyc(RGDfK).

## 7.5 Coupling reactions

In the first attempts, cyc(RGDfK) was used as starting material for the coupling reactions. Moreover, just the ligand was attached to the peptide and the complex formation with ruthenium was carried out in the second step.

### 7.5.1 Conjugation of Fmoc-bipy-AA

First, the unnatural, Fmoc-protected amino acid bipy-AA is coupled to cyc(RGDfK) using 2-(1H-benzotriazol-1-yl)-1,1,3,3-tetramethyluronium hexafluorophosphate (HBTU) as coupling agent. This uronium salt is well established in solid phase peptide synthesis and known for couplings under mild conditions.[88] Indeed, HBTU forms an activated ester with the free carboxylic acid group of bipy-AA which facilitates the formation of the amide bond. The coupling product cyc(RGDfK(bipy-AA)) (**14**) can be identified with ESI-MS due to the signals at 1051.4 $[M+H]^+$, 526.4 $[M+2H]^{2+}$ (see Figure 39).

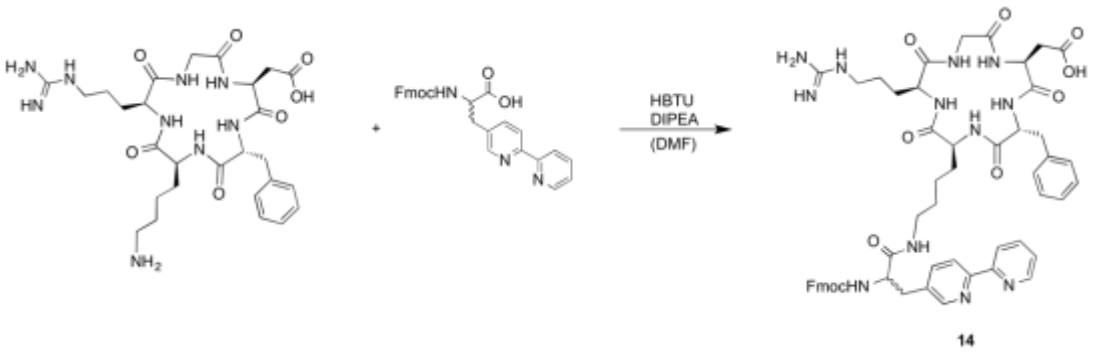


**Scheme 14 –** Conjugation of Fmoc-bipy-AA to cyc(RGDfK) yielding in coupling product **14**.

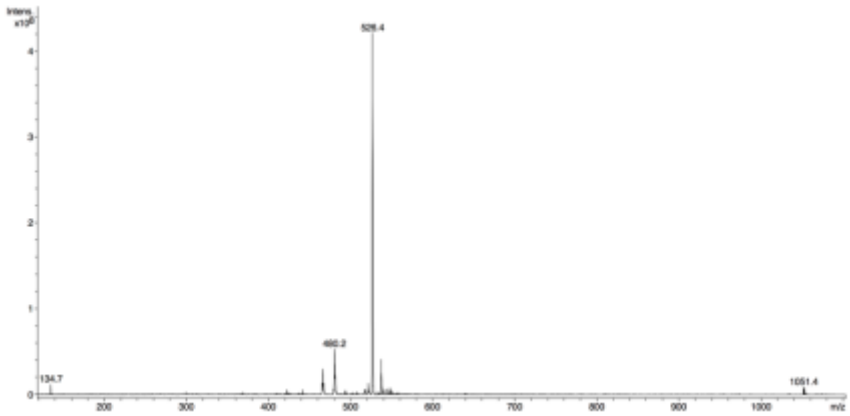


**Figure 39 -** ESI-MS of conjugation product **14**.

Right after the successful coupling, the complex synthesis with conjugate **14** is carried out using **4** as ruthenium precursor. Usually, the formation of the analogues complex **10** (see Scheme 7) takes place in methanol at elevated temperatures (60°C) and within five hours. However, peptides cannot stand these high temperatures since denaturation occurs typically above 40°C. Therefore, the complex formation had to be carried out at room temperature and the reaction was monitored by RP-HPLC. Considering the chromatograms in Figure 40, the development of a new product is observed after two hours at $R_t$ = 22.1 min. Additionally, the signal of the peptide vanishes, and likewise the amount of the ruthenium precursor **4** diminishes.

The expected product signal should appear in ESI-MS at m/z = 732.8 $[M\text{-}2PF_6]^{2+}$ or 488.5 $[M+H\text{-}2PF_6]^{3+}$. However, none of these signals is visible. Instead, there are not assignable signals at m/z = 413.3, 527.2 and 638.1 displaying ruthenium containing isotopic patterns, but not the desired product. In conclusion, using this synthetic strategy, the desired ruthenium peptide conjugate could not be obtained.

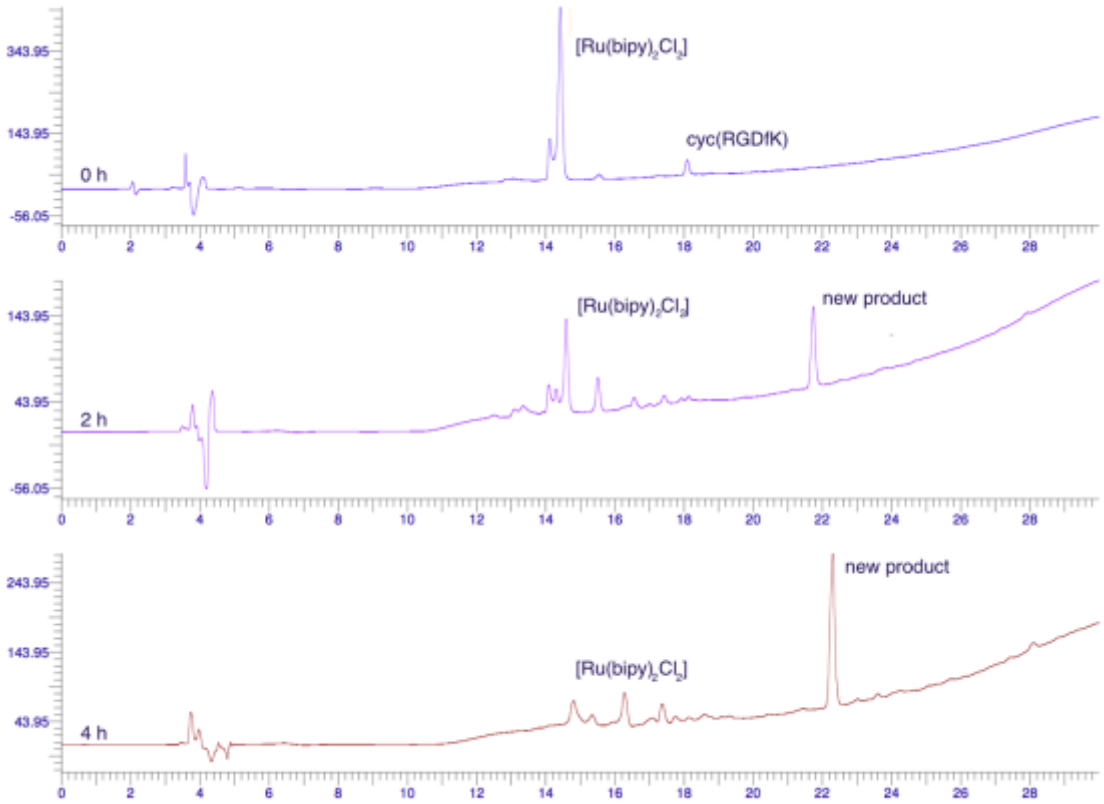


**Figure 40 –** Chromatograms during the complex synthesis of $[Ru(bipy)_2Cl_2]$ with **14** after 0 hours (top), 2 hours (middle) and 4 hours (bottom).

### 7.5.2 Conjugation of 1b

The next coupling was carried out under the same conditions as described before in section 7.5.1, but this time tethering ligand **1b** to cyc(RGDfK). The reaction was monitored with RP-HPLC, whereas the development of a new product was observed after 2 hours. Indeed, ESI-MS analysis of the new product at $R_t$ = 13.5 min (analytical column) shows the presence of the desired coupling product cyc(RGDfK(bipy*)), **15**, at m/z = 863.07 but also reveals a signal at 845 m/z (see Figure 42). This signal can be interpreted as intramolecular cyclization product of compound **15**. Through the formation of an amide bond - for example between the side chains' function groups of aspartic acid and arginine - and the resulting release of one water molecule, the occurrence of this signal could be explained. However, the spatial feasibility of this prediction stays uncertain. Another signal visible in ESI-MS at 887.4 m/z is probably dedicated to three cyc(RGDfK) peptides hydrolyzed together *via* the unprotected amine and carboxylic acid groups. These two observations imply that in the following

experiments, the functional groups at the side chains of aspartic acid and arginine must be protected during coupling reactions to prevent side reactions.

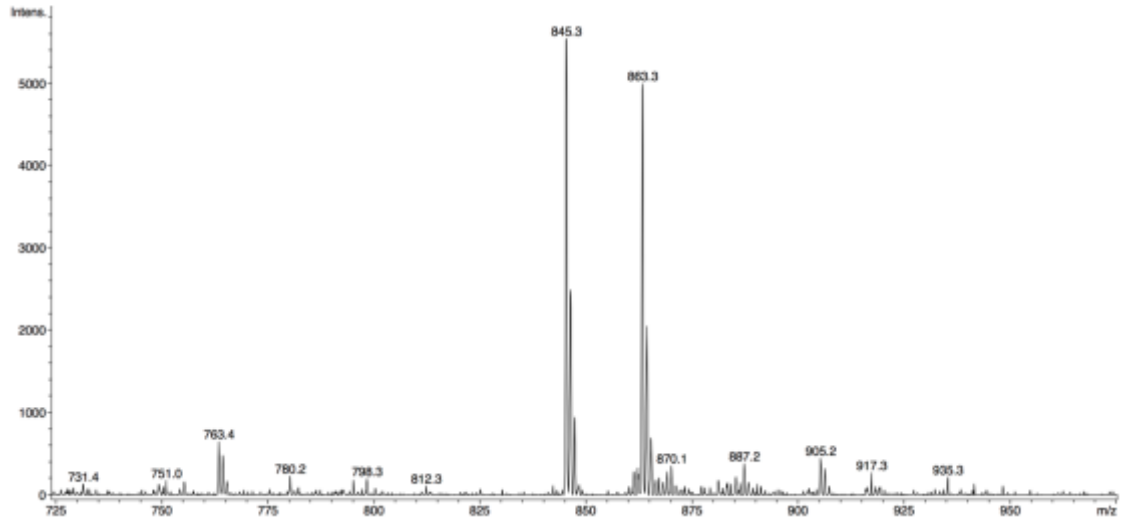


**Figure 41 –** ESI-MS of compound **15**, showing the product at m/z = 863.3 and side products at m/z = 845.3 and 887.2.

Consequently, the partially protected peptide cyc(R(Pbf)GD(*t*Bu)fK) is applied as starting material for the ongoing conjugations. Additionally, the low yields for **14** and **15** indicate that a change of coupling agents to more active substances is required. Particularly the carboxyl group of ligand **1b** is quite unreactive due to the extensive $\pi$ electron system of the polypyridyl moiety right next to this functional group. Therefore, more suitable activation agents have to be found for the coupling reactions whereas the strong activating agents 1-hydroxy-7-azabenzotriazole (HOAt) and *O*-(7-azabenzo-triazol-1-yl)-*N,N,N',N'*-tetramethyluronium hexafluorophosphate (HATU) are assessed to solve the activation problem. Finally, on the basis of the unsuccessful complex formation with bioconjugate **14** reported in section 7.5.2, the synthetic strategy is changed. First, the complexes are prepared and purified and then, in the second step, the conjugation to the peptide takes place.

### 7.5.3 Conjugation of 3a and 3b

The complexes **3a** and **3b** based on a terpyridine ligand system were linked to the cyclic peptide cyc[R(Pbf)GD(*t*Bu)fK] through amide bond formation between the complexes' free carboxylic acid groups and the primary amine at the lysine side chain using a 1:1 mixture of HATU and HOAt as activating agents (see Scheme 15). The success of the bioconjugation reaction was confirmed considering the signals of the intermediate products at m/z = 752.78 for $[Ru(terpy)(terpy\text{-}cyc(R(Pbf)GD(tBu)fK))]^{2+}$ and 1221.58 for $[Ru(terpy\text{-}cyc(R(Pbf)GD(tBu)fK])_2]^{2+}$ in ESI-MS. In the next step, the remaining protection groups (*t*Bu and Pbf) were cleaved using a standard cleavage cocktail. The purification procedure with semi-preparative RP-HPLC failed due to the formation of non-assignable side products. Therefore, the purification of the crude product was carried out with Sephadex® G-15 in PBS buffer (pH = 7.4). Precipitation of the final products was achieved by addition of solid $KPF_6$ to give $[Ru(terpy)(terpy\text{-}cyc(RGDfK))](PF_6)_2$ **16a** and $[Ru(terpy\text{-}cyc(RGDfK)_2)](PF_6)_2$ **16b** as dark red solids.

The coupling products **16a** and **16b** were characterized with ESI-MS, also considering their characteristic isotopic patterns matching with the calculated ones. For both complexes, the loss of $PF_6^-$ anions is detected in ESI-MS, and additionally due to the high basicity of the arginine side chain, the attachment of protons is observed within the ionization process, leading to a higher positive charge of the complexes. Hence, for **16a** signals at 671.68 and 399.46 m/z are observed indicating the loss of one anion and addition of one proton or rather the loss of both anions and addition of one proton. Due to the dimeric character of species **16b**, signals at 609.23 and 457.17 m/z are observed, indicating the loss of both $PF_6^-$ anions and the addition of one or two protons. Also a signal at 913.34 m/z was found indicating the double positive charged complex without any anion or proton attached. The characteristic isotopic patterns of the signals match entirely with the calculated ones, which can be seen in the Figures 42 and 43.

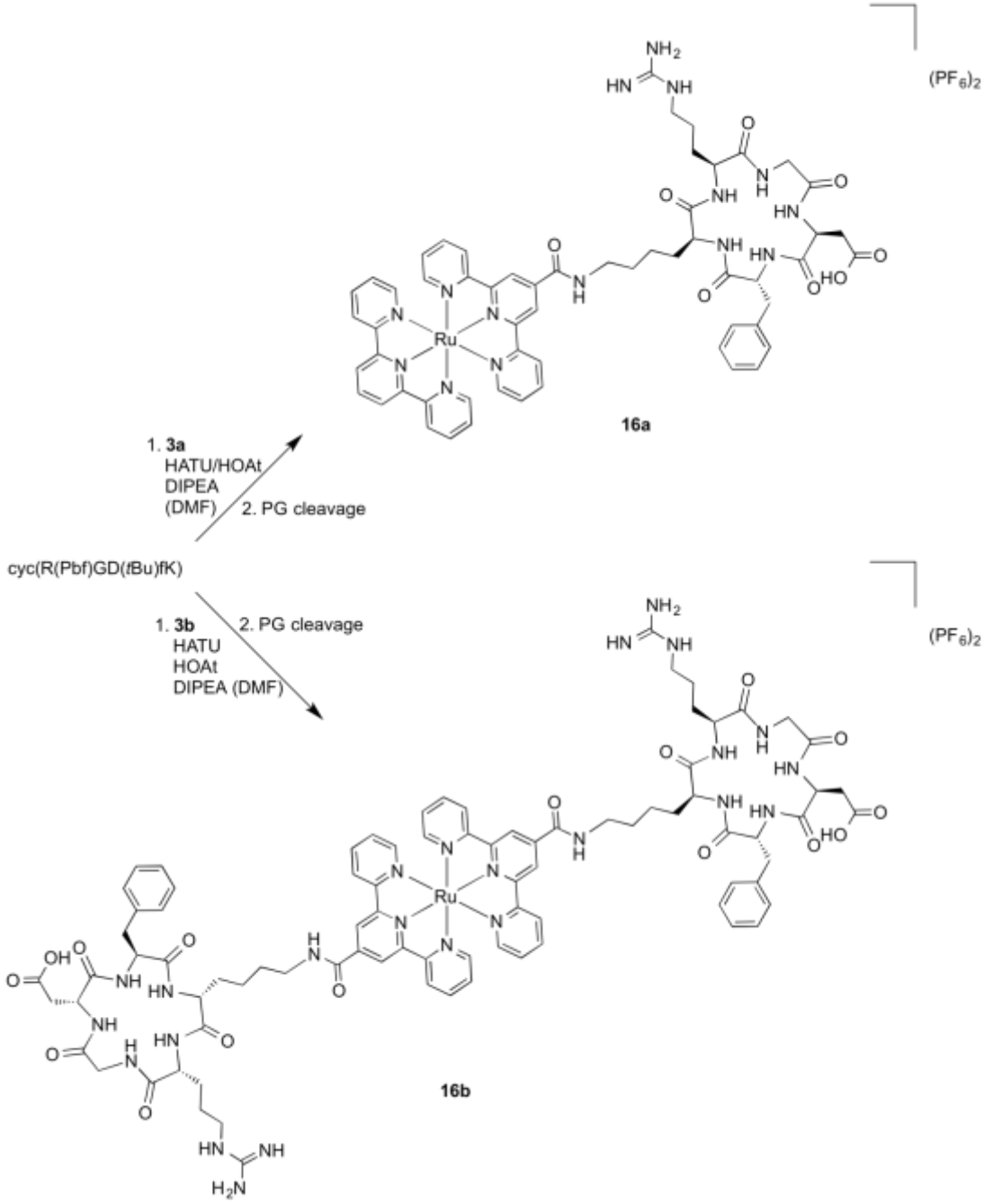


**Scheme 15 -** Synthesis of the coupling products **16a** and **16b**.

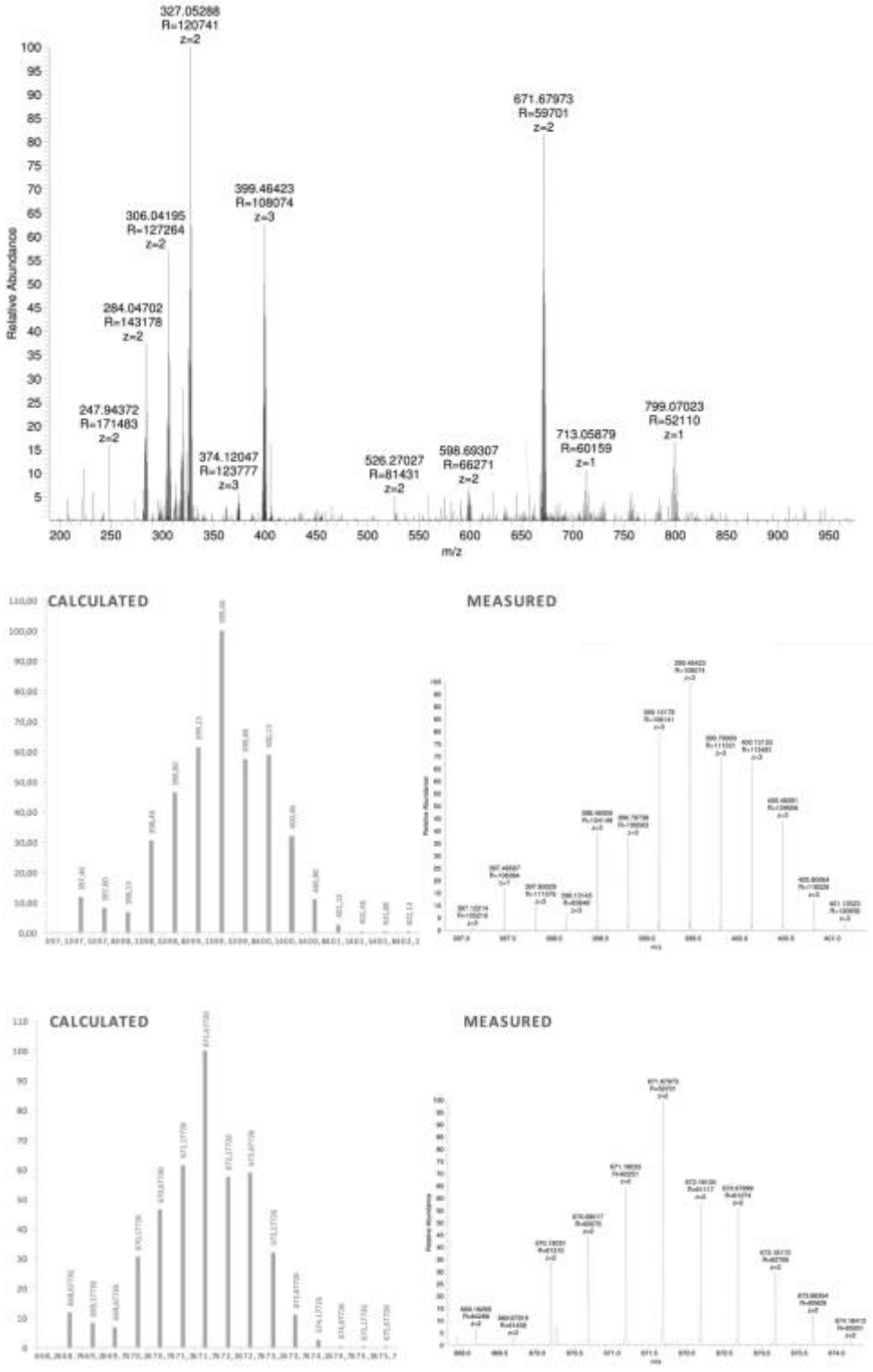


**Figure 42 –** ESI-MS of conjugate **16a** and the measured vs. calculated isotopic patterns.

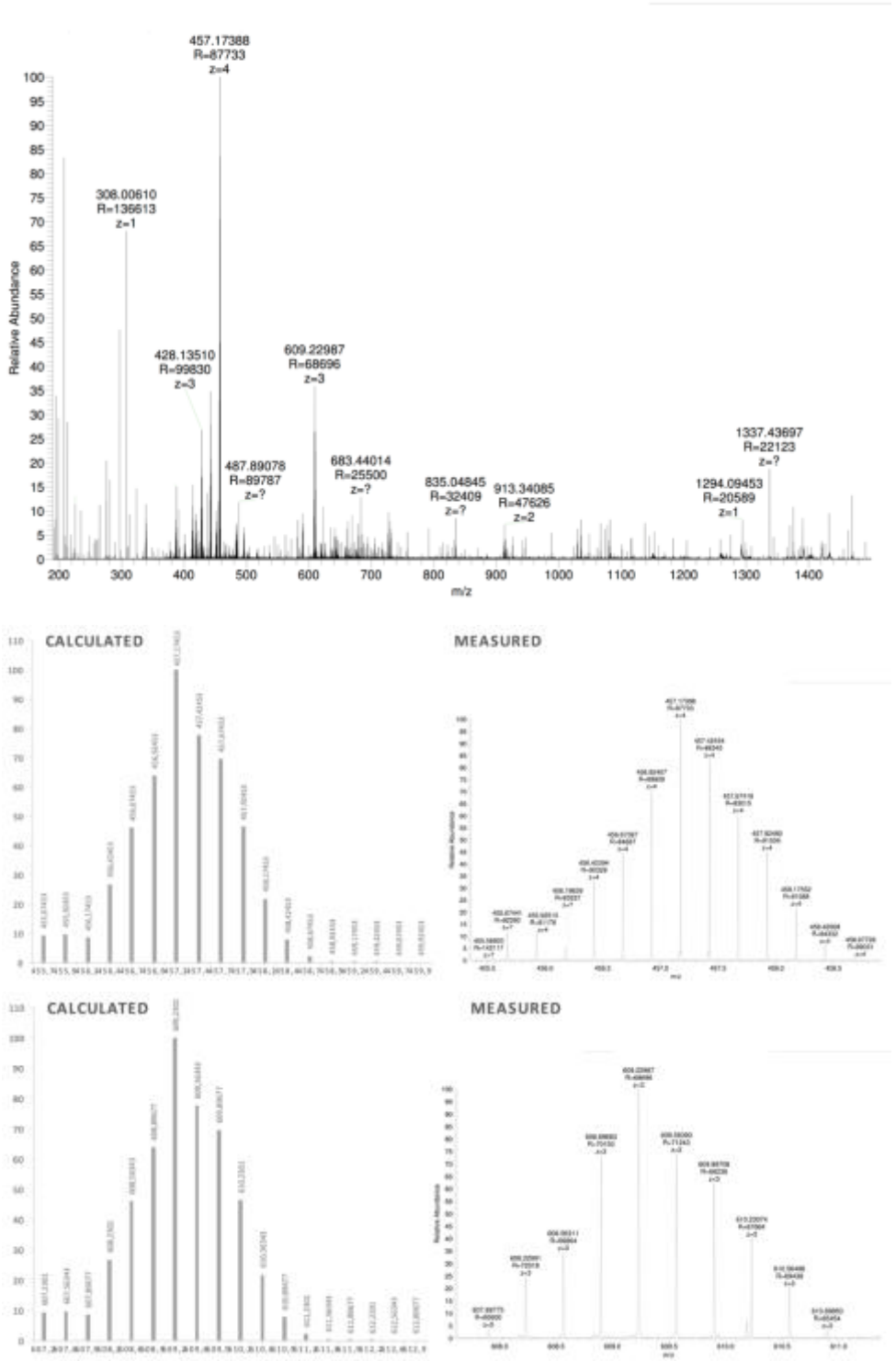


**Figure 43 -** ESI-MS of conjugate **16b** and the measured vs. calculated isotopic patterns.

In the following, the binding affinities of both bionconjugates for the integrin receptors $\alpha_v\beta_3$ and $\alpha_5\beta_1$ were evaluated and compared with the standard Cilengitide (see Table 1).

**16a** exhibits an affinity of 49 ± 4.3 nM, a hundred times higher $IC_{50}$ than observed for Cilengitide (0.54 ± 0.06 nM), whereas the selectivity of **16a** for $\alpha_v\beta_3$ is rather high considering the fact that $\alpha_5\beta_1$ is not ligated at all ($IC_{50}$ >1000 nM), whereas Cilengitide reflects affinities of 15.4 ± 0.2 nM. For the other bioconjugate **16b** an enhanced binding affinity is expected due to the dimeric character of the compound. Indeed, the binding affinity for integrin $\alpha_v\beta_3$ exhibits affinities of 2.5 ± 0.3 nM, indicating a more than 20-fold higher affinity than for the monomeric product. For $\alpha_5\beta_1$, the binding affinity of **16b** is negligible (595 ± 67 nM), therefore a high selectivity for the $\alpha_v\beta_3$ receptor can be attributed.

**Table 1 -** Results of integrin binding assays for the bioconjugates **16a** and **16b**, in comparison to the benchmark cilengitide.[89]

| | **$IC_{50}$ [nM]** | |
|---|---|---|
| | $\alpha_v\beta_3$ | $\alpha_5\beta_1$ |
| **Cilengitide**[89] | 0.54 ± 0.06 | 15.4 ± 0.2 |
| **16a** | 49 ± 4.3 | >1000 |
| **16b** | 2.5 ± 0.3 | 595 ± 67 |

Furthermore, the antiproliferative properties of the two ruthenium compounds **3a** and **3b** and their respective bioconjugates **16a** and **16b** were tested on two human cancer cell lines expressing integrins in a low (A549) or moderate amount (SKOV-3) (Table 2). But unfortunately, the ruthenium polypyridyl complexes **3a** and **3b** as well as their targeted bioconjugates showed only slight cytotoxic effects on both cell lines, irrelevant if a targeting peptide is attached or not. These observations probably result from the crucial low anticancer effects of the chosen ruthenium derivatives or the low uptake of the compounds.

Presumably, the compounds attach the cell through the ligation of the integrin receptor but the uptake into the cell cannot take place due to the big size or high stability of the tridentate ligands of the compounds. Therefore, ongoing research has to focus on the design of a different ligand set exhibiting stabilities high enough to be transferred to the cell without changing the structure but also low enough to cleave ligands for the uptake.

**Table 2 -** $IC_{50}$ values of complexes **3a** and **3b** and the bioconjugates **16a** and **16b** against human A549 and SKOV-3 cell lines.

| | **$IC_{50}$ (µM)[a]** | |
|---|---|---|
| **Compound** | **A549** | **SKOV-3** |

| | | |
|---|---|---|
| **3a** | 70.3 ± 9.8 | 74.5 ± 13.7 |
| **16a** | 87.7 ± 5.4 | 85.2 ± 18.7 |
| **3b** | >100 | >100 |
| **16b** | >100 | >100 |

[a] The reported values are the mean ± SD of at least three determinations

# 8 Histidine-based NHC-gold(I) complexes

In earlier days, gold drugs were mainly used for the therapy of rheumatoid arthritis until hypotheses of the connection between the biochemical pathways for anticancer and rheumatoid drugs were established. Hence, the rheumatoid arthritis drug Auranofin was adopted as anticancer agent.[11] In contrast to phosphine ligands like applied in Auranofin, *N*-heterocyclic carbenes provide many advantages for the design of gold(I)-based anticancer drugs. Besides the strong σ-donor abilities leading to air- and water stable, but water soluble cationic complexes, NHCs are renowned for their highly variable design due to the easy functionalization of the *N*-side chains. Hence, first studies for the rational design of novel gold(I) anticancer agents based on the amino acid Boc-L-Histidine is reported in this section.

## 8.1 Synthesis of the Ligands

The synthesis of the ligands was carried out based on a published procedure.[90] Boc-protected L-histidine was used as starting material to prevent side reactions at the amine group. To introduce *N*-substituents at the imidazolyl side chain and in the same step protect the carboxylic acid function, the amino acid was dissolved in acetonitrile, base ($NaHCO_3$) was added and then, the suspension mixed with different alkyl halides (R-X, see Scheme 16) and refluxed for 16 hours. Methyl- and ethyl iodide as well as benzyl bromide were successfully reacted with the amino acid to yield in the corresponding methyl- (Me), ethyl- (Et) or benzyl- (Bz) imidazolium salts which were finally dissolved in water and precipitated by addition of solid $KPF_6$ to yield in the respective $PF_6^-$ salt Boc-His-Me (**17a**), Boc-His-Et (**17b**), Boc-His-Bz (**17c**). Actually, through the addition of five equivalents of alkyl halide, the carboxylic acid protection and both *N*-substitutions proceed in one step and so the imidazolium salts are ready for use in the complex synthesis.

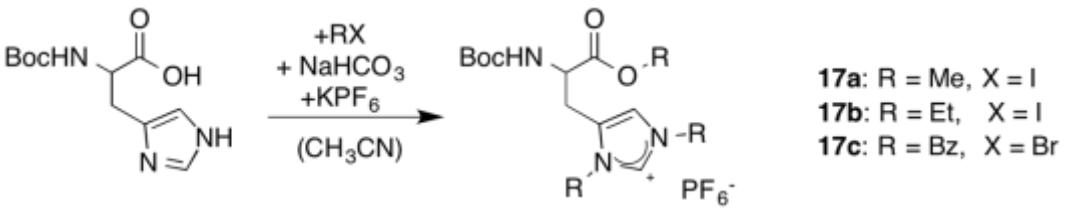


**Scheme 16 –** Procedure for the synthesis of histidine-based imidazolium salts **17a**-**c**.

## 8.2 Synthesis of the Complexes

The complex syntheses using the imidazolium salts **17a**-**c** were carried out in $CH_2Cl_2$ with $Ag_2O$ as internal base leading to silver(I) biscarbene complexes as intermediate. The purification of these Ag(I) complexes was not carried out due to their instability at light and on air. Consequently, the reaction flask was covered with alumina foil during the reaction to prevent the decomposition of the intermediate. The addition of the gold(I) precursor chloro(dimethylsulfide)gold(I) to the silver bis-NHC solution led to *in situ* transmetalation, as shown in Scheme 17, to the precipitation of silver chloride generating the driving force of the reaction and additionally to the desired gold complexes $[Au(Boc\text{-}His\text{-}Me)_2]PF_6$ (**18a**), $[Au(Boc\text{-}His\text{-}Et)_2]PF_6$ (**18b**) and $[Au(Boc\text{-}His\text{-}Bz)_2]PF_6$ (**18c**).

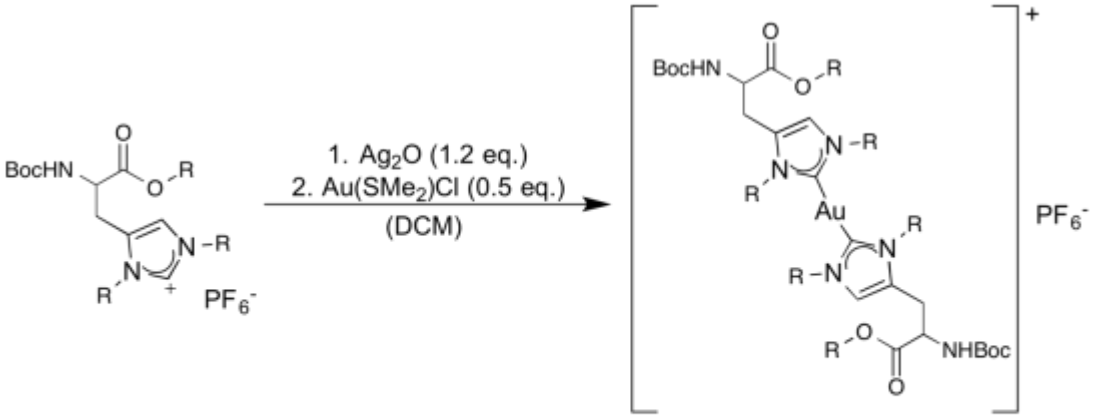


**Scheme 17 –** Procedure for the one-pot synthesis of the bis-NHC complexes **18a**, **b** and **c**.

## 8.3 Characterization of Ligands and Complexes

The three novel histidine-based ligands synthesized in this work (**17a**–**c**) were characterized with ESI-MS showing the single positive charged imidazolium cations at the corresponding m/z values: 298.04 (**17a**), 340.13 (**17b**) and 526.27 (**17c**) (see Figure 44).

**17a**

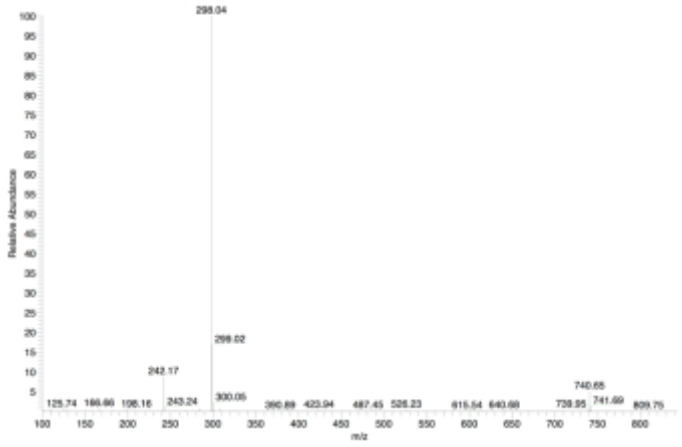


**17b**

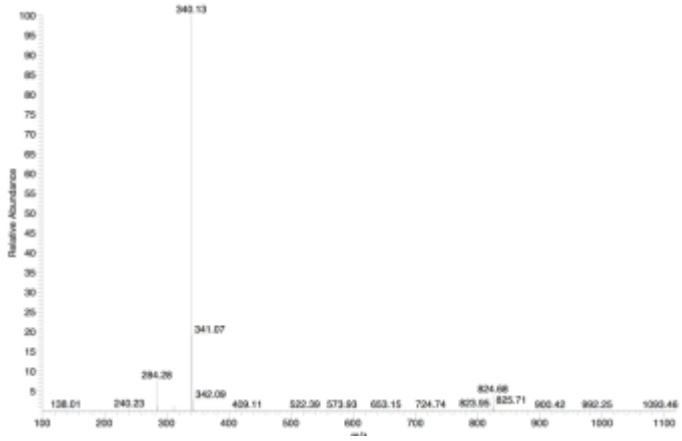


**17c**

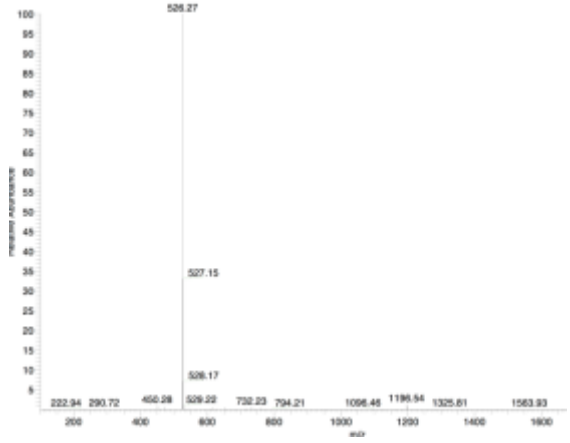


**Figure 44 –** ESI-MS spectra of the ligands **17a**, **b** and **c**.

The structure and purity of the alkyl substituted ligand **17a-c** is verified with $^{1}$H NMR (see Figures 45-47). The imidazolium protons at $C^{2}$ show the strongest downfield shift (**17a**: 8.30 ppm, **17b**: 8.41 ppm, **17c**: 8.46 ppm) reflecting the high acidity of these protons and their easy cleavage by base, essential for the formation of the carbene-metal bond. Besides, the protons of the imidazolium backbones are located further upfield (**17a**: 7.13 ppm, **17b**: 7.21 ppm, **17c**: 7.18 ppm).

The protons of the introduced substituents attached during ligand synthesis show slight different shifts depending on the neighboring heteroatom (N or O). For **17a**, the -$CH_3$ groups are observed as three singlets with integral of three protons at 3.77, 3.73 and 3.72 ppm. Regarding the higher electronegativity of the oxygen atom, the signal at 3.77 ppm is supposed to feature the methoxy group, whereas the other two singlets are determined as -$NCH_3$ groups. Looking at ethyl substituted complex **17b** and the benzyl substituted complex **17c**, similar observations are detectable in $^1$H NMR spectra.

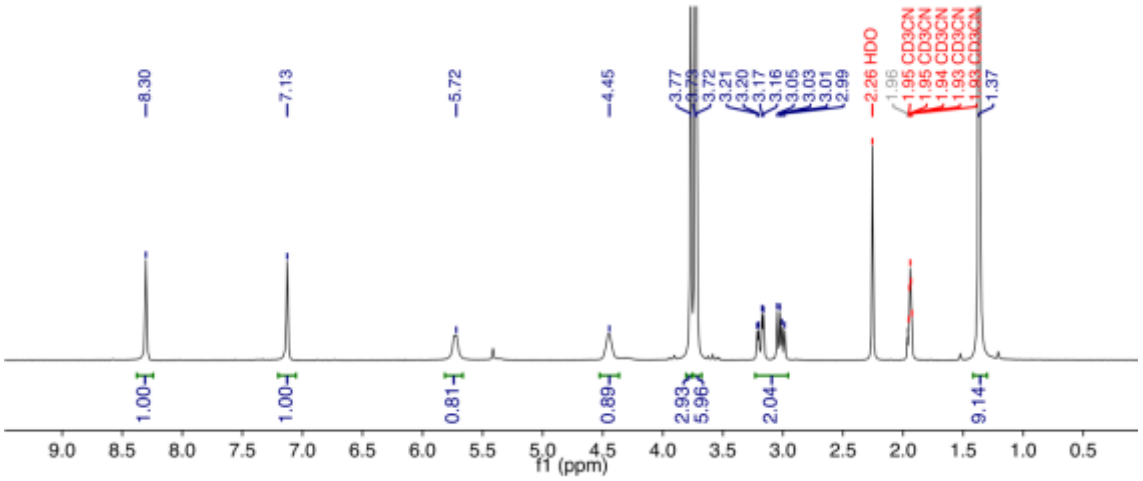


**Figure 45 –** $^1$H NMR of the methyl substituted ligand **17a** in $CD_3CN$.

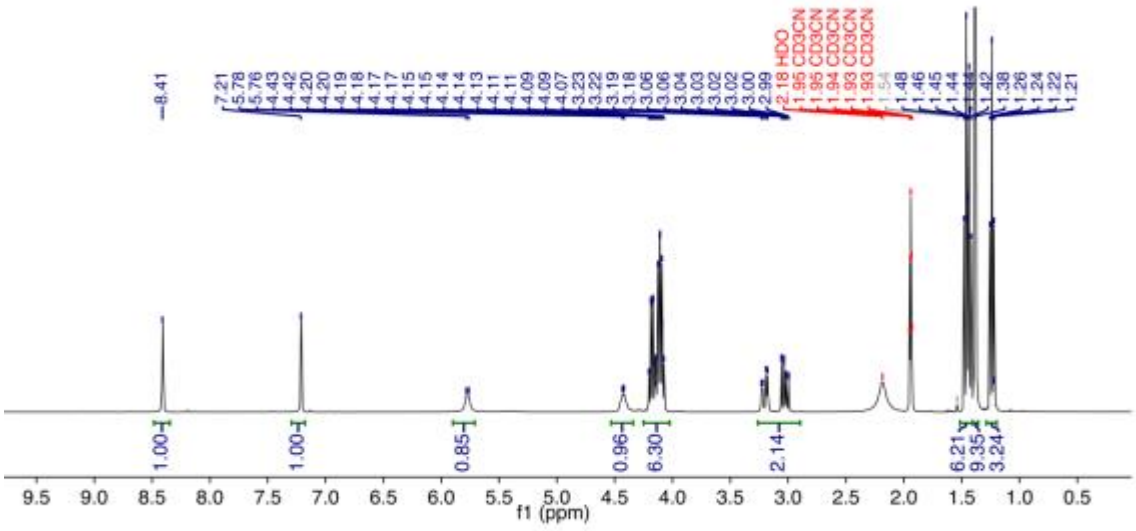


**Figure 46 -** $^1$H NMR of the ethyl substituted ligand **17b** in $CD_3CN$.

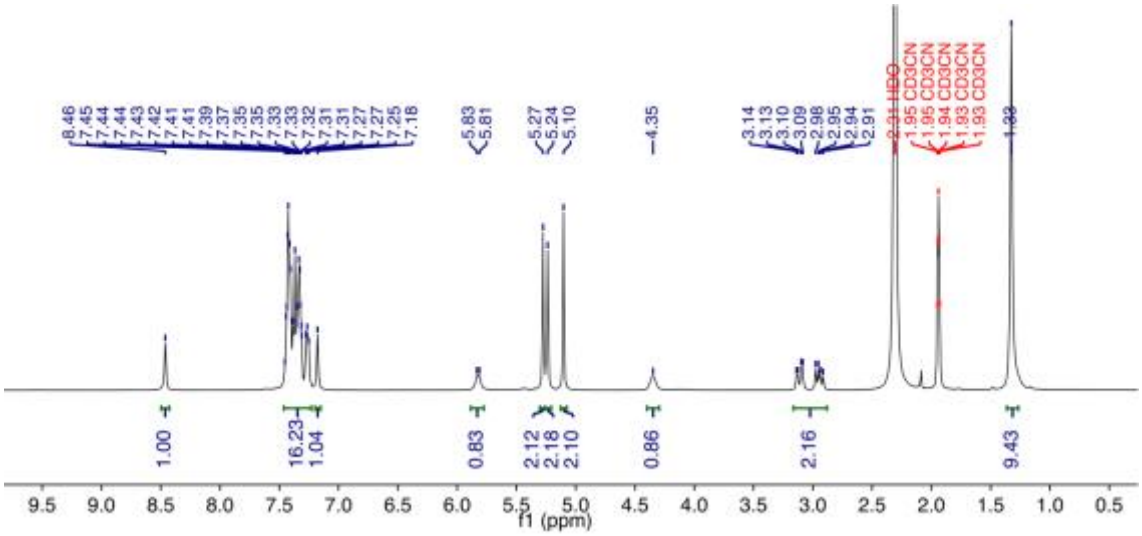


**Figure 47 -** $^{1}$H NMR of the benzyl substituted ligand **17c** in $CD_3CN$.

In the next step, the ligands were reacted in a one-pot complex synthesis which was monitored with ESI-MS to observe the progress of the complex formation. In the following, the synthesis of the benzyl substituted complex **18c** is explained in detail.

Indeed, the reaction of **17c** (= L) with silver oxide leads to the formation of the silver biscarbene complex $[AgL_2]^+$, observed in ESI-MS at m/z = 1159.23 (see Figure 48) and showing the characteristic isotopic pattern for silver complexes. Unfortunately, the spectrum showed continuously unreacted ligand at m/z = 526.27. However, this observation probably results of the ionization process during the measurement but also of incomplete conversion during the reaction. Conversely, increased reaction time up to seven days or the addition of further 1.6 equivalents of $Ag_2O$ did not improve the conversion. Therefore, the reaction was carried out for 72 hours with 1.6 equivalents of silver oxide in total before adding the gold precursor. The transmetalation from silver to gold proceeds in 25 hours leading to pure complex **18c**.

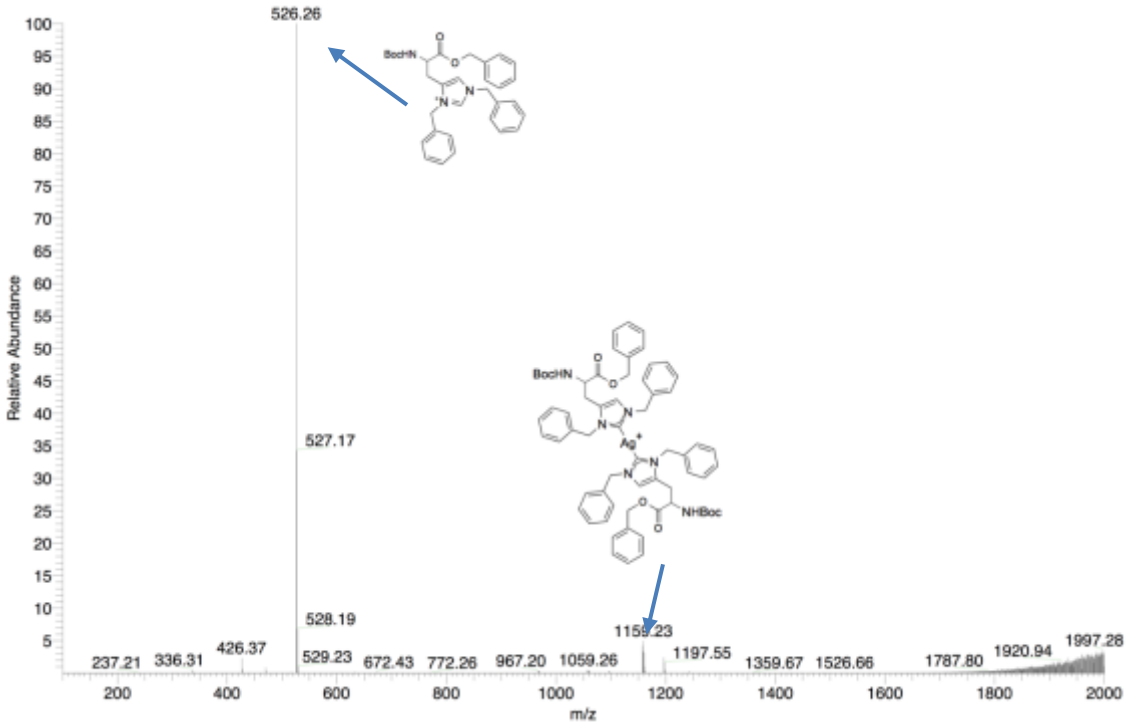


**Figure 48 –** ESI-MS of the reaction solution for the synthesis of complex **18c** showing the intermediate silver bis-NHC complex.

Comparing $^{1}H$ NMR in $CD_2Cl_2$ of the benzyl substituted ligand **17c** and its gold complex **18c** (see Figure 49), obvious proton shifts are detected due to complex formation. The imidazolium proton of ligand **17c** visible at 10.8 ppm is abstracted during the reaction by the internal base, resulting in the formation of the carbene-metal bond and to the disappearance of the signal in the $^{1}H$ NMR spectrum of **18c**. Through metal coordination, the electron density in the imidazolyl ring system is slightly enhanced causing the upfield shift of the imidazolium backbone proton of about 0.3 ppm.

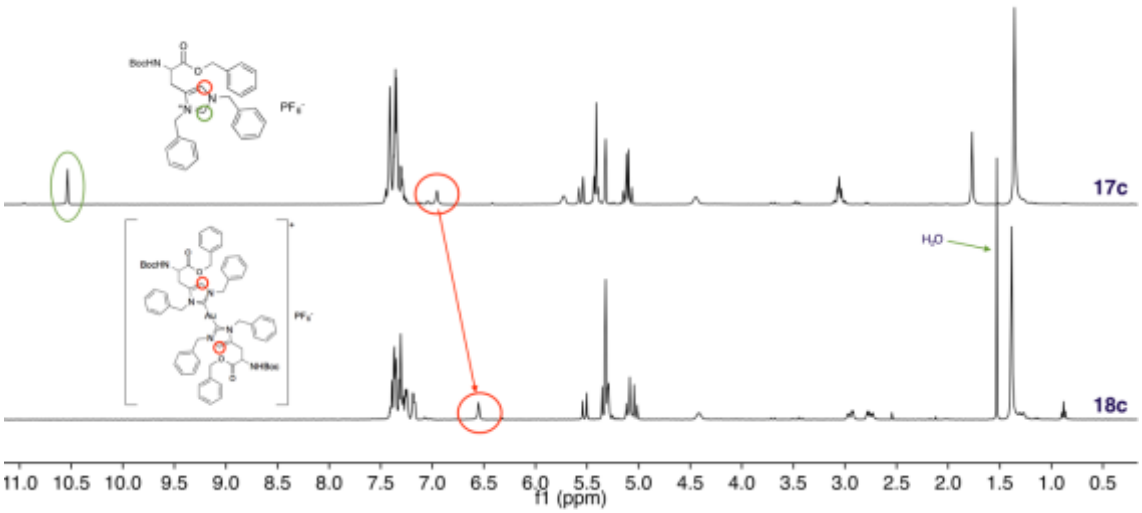


**Figure 49 -** $^{1}$H NMR in $CD_2Cl_2$ of the benzyl substituted compounds **17c** and **18c**.

ESI-MS analysis proofs the formation of the complex considering the signal at m/z = 1247.43 (see Figure 50) which displays the positive charged complex by loss of the $PF_6^-$ anion.

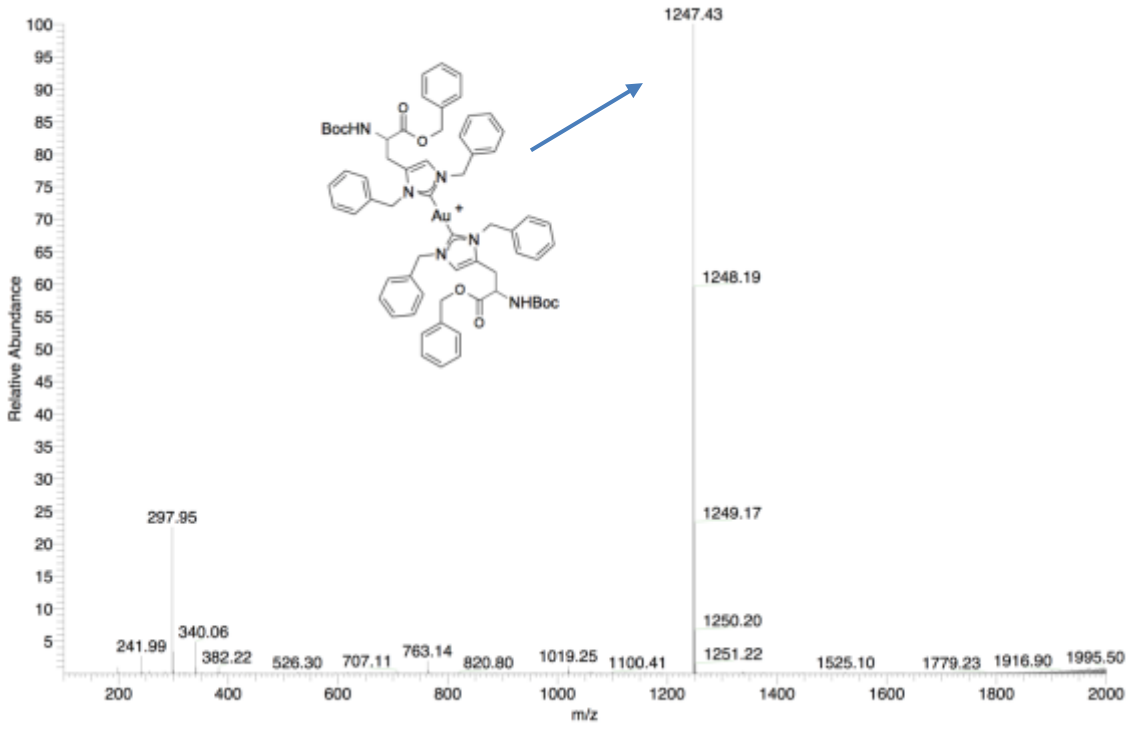


**Figure 50 –** ESI-MS of the histidine-based gold(I) bis-NHC complex **18c**.

In the following, the complex formation with the ethyl substituted ligand **17b** is investigated. As expected, the reaction proceeds in analogy to the benzyl-substituted complex, first forming *in situ* the silver bis-NHC complex, monitored *via* ESI-MS by means of the signal at m/z = 785.2. After addition of the gold precursor, the desired product, visible at m/z = 875.29 (see Figure 51) is obtained.

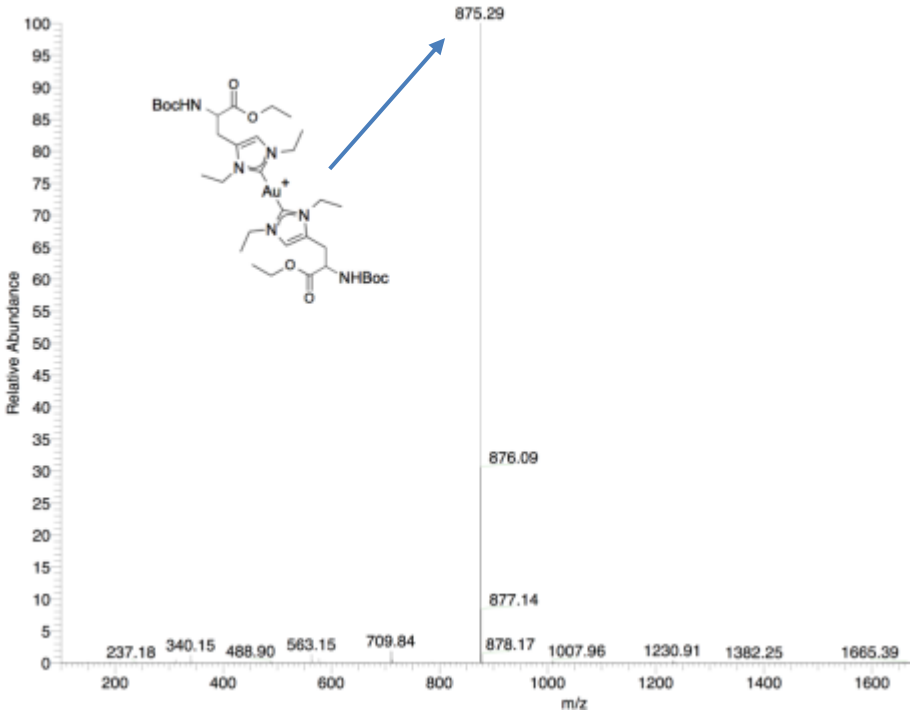


**Figure 51 -** ESI-MS of histidine-based gold(I) complex **18b**.

The $^{1}$H NMR (see Figure 52) is illustrated in two parts and additionally, two signals of remaining diethylether are resected to refine the product signals in the quite diluted spectrum. First of all, some side products at 7.6 and 5.4 ppm are evident in the spectrum. The C$^{2}$-imidazolium proton is not observed any more due to the abstraction with silver oxide and carbene bond formation. The spectrum shows all expected product signal, however some integrals are not matching perfectly. Anyway, the $^{1}$H NMR spectrum as well as the ESI-MS are consistent with the formation of the desired complex **17b**.

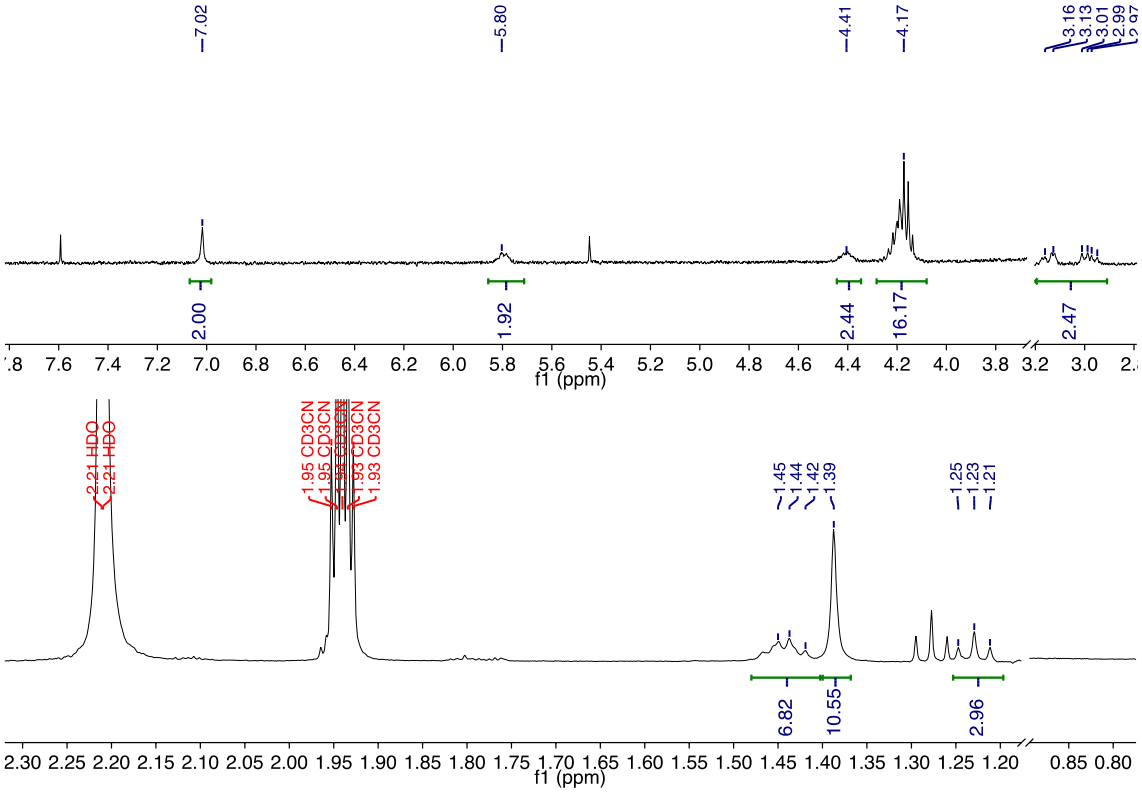


**Figure 52:** $^{1}$H NMR of gold(I) complex **18b** (solvent signals of diethylether between 3.70 -3.20 ppm and 1.15 – 0.90 ppm are resected).

Finally, the analytical data of the methyl substituted complex **18a** is investigated. The same features described above apply for this $^{1}$H NMR spectrum, too (see Figure 53). The proton attached to $C^{2}$ vanishes due to complex formation whereas the other signals rather remain in the same region of the spectrum. The successful synthesis of the complex was confirmed with ESI-MS (see Figure 54), regarding the signal at m/z = 791.15.

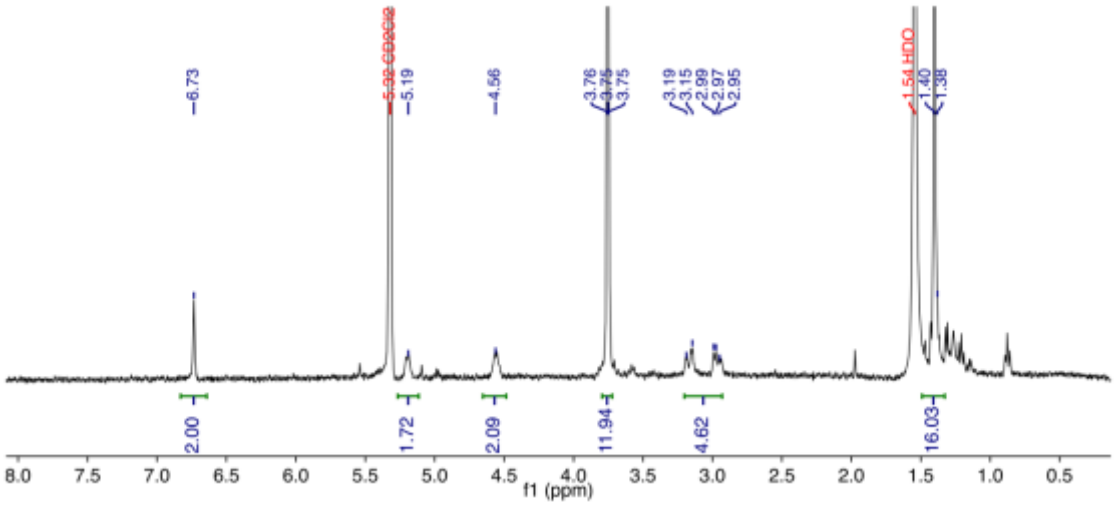


**Figure 53** - $^{1}$H NMR of histidine-based gold(I) complex **18a**.

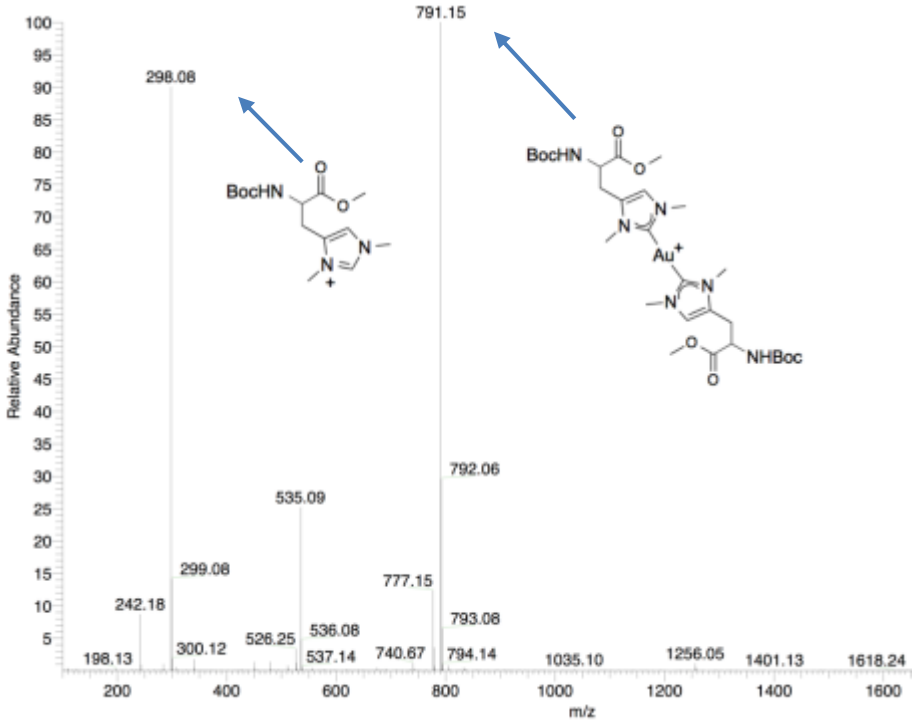


**Figure 54 -** ESI-MS of the gold(I) complex **18a**.

Finally, for all compounds, $^{31}P$ NMR spectra were measured to proof the existence of the $PF_6^-$ counterions.

In conclusion, all three ligands **17a-c** and complexes **18a-c** were successfully synthesized and characterized. As solid, the complexes are stable on air, however, some decomposition was observed during crystallization procedures, possibly caused by missing stability in solution or at room temperature. Therefore, low temperature crystallization experiments have to be performed to obtain single crystals for X-ray diffraction.

# IV. CONCLUSION AND OUTLOOK

# 9 Ruthenium Complexes and their RGD-Biconjugates

Nowadays chemotherapies suffer of severe side effects like pain in the hole body, fatigue, diarrhea, vomiting, blood disorders or even nerve damages. Therefore, recent anticancer research has to focus on novel strategies to enhance the selectivity of the anticancer drug towards tumor cells and to protect healthy tissue from damage. Hence, this work deals with the attachment of the tumor targeting peptide cyc(RGDfK) to ruthenium(II) or gold(I) compounds to achieve agents targeting selectively the integrin receptor $\alpha_v\beta_3$, which is overexpressed at the surface of cancer cells. Based on this strategy, an enhanced selectivity for cancer cells should be achieved.

To begin with, the cyclic pentapeptides cyc(R(Pbf)GD(*t*Bu)fK) and cyc(RGDfK) were obtained by solid phase peptide synthesis of the linear amino acid sequence and the following cyclization and deprotection of the respective protection groups. Two couplings were carried out with the unnatural amino acid bipy-AA or 5-carboxy-2,2'-bipyridine (**8**) using HOBT as coupling agent. The two resulting bioconjugates could be obtained in rather low yields and due to the fairly harsh reaction necessary for the ongoing complex formation, the desired products could not be obtained following this route.

Therefore, the procedure was changed starting with the complex syntheses and then, in the second step coupling the purified complexes to the peptide using a mixture of HOAt and HATU as activation agents. Following this approach, two terpyridine based Ru(II) complexes **3a** and **3b** were synthesized, yielding in a monomeric (**16a**) and a dimeric (**16b**) bioconjugate which showed indeed high selectivity for binding the integrin receptor $\alpha_v\beta_3$, but unfortunately revealed poor cytotoxicity on two human cancer cell lines.

Moreover, two bipyridine based complexes with bipy-AA and ligand **8**, useful for coupling reactions were synthesized (**9** and **10**), as well as one complex bearing a free amine group at a monodentate (4-aminopyridine) ligand (**13**). The latter was fully characterized and furthermore, a crystal structure was obtained. Indeed, the monodentate ligand reveals a rather low stability in water, therefore its viability as bioconjugate is doubted.

However, since the terpy based conjugates seem to be too stable and the fampy complex too unstable, bisdentate ligands are predicted to offer best stability for coupling reactions and uptake. Additionally, in ongoing studies, research could be focused on the design of distorted octahedral complexes as photoactivated bioconjugates revealing an enhanced selectivity for tumor tissue due to the local radiation and photoactivation of the drug leading to cytotoxic moieties directly at the cancer tissue.

# 10 Histidine-based Gold(I) Complexes

In the second part of this work, the natural amino acid L-histidine was used as precursor for synthesizing gold(I) complexes with different sterical demands. Since various gold complexes show cytotoxic characteristics in cisplatin resistant cell lines, they offer promising potential in tumor therapy. Regarding the high selectivity of the cyclic RGD peptide for cancer cells, targeting anticancer agents can be designed by incorporation of histidine based gold(I) complexes. Consequently, three different ligands with methyl-, ethyl- and benzyl-substituents at the imidazoliums' nitrogen atoms were prepared leading to imidazolium salts **17a**-**c** with altered steric demands. These ligands were first reacted with silver oxide resulting *in situ* in the respective silver(I) bis-*N*-heterocyclic carbene complexes, and in the following equipped with the gold(I) precursor chloro(dimethylsulfoxide)gold(I) yielding in the gold(I) bis-NHC complexes **18a**-**c**. These compounds were characterized with NMR and ESI-MS and are promising candidates as antitumor agents.

In future studies, a library of ligands with different sterical and electronical characteristics will be synthesized and used for the complex synthesis. The cytotoxicity of the ligands and complexes should be studied to evaluate their anticancer potential as well as the structure-activity relationship. Finally, after deprotection of the ester group, the complexes might be attached to peptides or even incorporated into the pentapeptide structure, for example by replacement of the D-phenylalanine or L-lysine in order to achieve targeted anticancer agents.

# V. EXPERIMENTAL PART

# 11 General

All synthesis with water- or air sensitive compounds were performed by exclusion of air and moisture using standard Schlenk techniques and argon 6.0 as inert gas. If mentioned, work was carried out in a glovebox of the company MBraun. All chemicals were purchased from commercial sources and used without further purification. Some amount of the peptide cyc(RGDfK) was provided by the group of Prof. H. Kessler, TUM. HPLC grade DMF, acetonitrile and DMSO were used, all other solvents were freshly distilled. Dry solvents were obtained from the MBraun MB SPS 800 purification system and stored over molecular sieves and under argon.

# 12 Analytical Methods

**Nuclear Magnetic Resonance Spectroscopy (NMR)**

NMR spectra were recorded at room temperature on a Bruker Advance DPX 400 or a Bruker DRX 400. The measuring frequencies are 400 MHz (for $^{1}H$), 162 MHz (for $^{31}P$), 101 MHz (for $^{13}C$). $CDCl_3$, $CD_2Cl_2$, $CD_3CN$, acetone-$d_6$ and DMSO-$d_6$ were used as deuterated solvents. The chemical shifts $\delta$ are reported in ppm and refer to the signal of the deuterated solvent used. The following abbreviations are used for the resulting multiplicities: s = singlet, d = doublet, t = triplet, q = quartet, s = septet, m = multiplet.

**Electrospray Ionisation Mass Spectrometry (ESI-MS)**

Electrospray ionization mass spectrometry was carried out on LCQ classic or on a LTQ FT Ultra, both from Thermo Finnigan. Acetonitrile or methanol were used as solvents for sample preparation. All values are given in m/z, the ratio of mass and charge.

**Elemental Analysis**

Elemental Analysis were performed in the microanalytical laboratories of the Technical University Munich.

**UV/VIS**

UV/Vis spectra were measured in DMSO solution in 10 mm cuvettes on an Agilent Cary 60.

**X-ray Single Crystal Diffraction**

Data has been collected on a single crystal X-ray diffractometer equipped with a CCD detector (APEX II, *κ*-CCD), a rotating anode FR591 and a Montel mirror optic using the SMART software package.[91] The measurements were performed with single crystals coated with perfluorinated ether. The crystals were fixed on the top of a microsampler and transferred to the diffractometer. Crystals were frozen under a stream of cold nitrogen. A matrix scan was used to determine the initial lattice parameters. Reflections were merged and corrected for Lorentz and polarization effects, scan speed, and background using SAINT.[92] Absorption corrections, including odd and even ordered spherical harmonics were performed using SADABS.[92] Space group assignments were based upon systematic absences, *E* statistics, and successful refinement of the structures. Structures were solved by direct methods with the aid of successive difference Fourier maps[93], and were refined against all data using the APEX 2 software[91] in conjunction with SHELXL-97 or SHELXL-2014[94] and SHELXLE[95]. Methyl hydrogen atoms were refined as part of rigid rotating groups, with a C–H distance of 0.98 Å and $U_{iso(H)} = 1.5 \cdot U_{eq(C)}$. Other H atoms were placed in calculated positions and refined using a riding model, with methylene and aromatic C–H distances of 0.99 and 0.95 Å, respectively, and $U_{iso(H)} = 1.2 \cdot U_{eq(C)}$. Non-hydrogen atoms were refined with anisotropic displacement parameters. Full-matrix least-squares refinements were carried out by minimizing $\Sigma w(F_o^2 - F_c^2)^2$ with SHELXL-97[94] weighting scheme. Neutral atom scattering factors for all atoms and anomalous dispersion corrections for the non-hydrogen atoms were taken from *International Tables for Crystallography*.[96] Images of the crystal structures were generated by PLATON.[97]

**Table 3:** Crystallographic data for **13**

| | **13** |
|---|---|
| Formular | $C_{36}H_{37}F_{11.92}N_7O_2P_2Ru$ |
| Fw | 989.26 |
| Colour/habit | Clear intense red fragment |
| Crystal system | Monoclinic |
| Space group | P 1 21/c 1 |
| *a*, Å | 11.0225(5) |
| *b*, Å | 13.7463(6) |
| *c*, Å | 29.7938(14) |
| $\alpha$, deg | 90 |
| $\beta$, deg | 98.132(3) |
| $\gamma$, deg | 90 |
| *V*, Å$^3$ | 4468.9(4) |

| | |
|---|---|
| *Z* | 4 |
| *T*, K | 100(2) |
| $D_{calc.}$, g cm$^{-3}$ | 1.470 |
| μ, mm$^{-1}$ | 0.511 |
| *F*(000) | 1997 |
| θ range, deg | 1.63 to 26.02 |
| Index ranges (*h, k, l*) | -13<=*h*<=13, -16<=*k*<=16, -36<=*l*<=36 |
| No. of rflns collected | 72489 |
| No. of independent rflns/$R_{int}$ | 8798[R(int) = 0.0460] |
| Coverage of independent reflections | 100.0% |
| Adsorption correction | Multi-scan |
| Max. and min. transmission | 0.9630 and 0.8040 |
| No. of data/restraints/parameters | 8798 / 377 / 779 |
| $\Delta/\sigma_{max}$ | 0.001 |
| Final R indices | 7372 data; I>2$\sigma$(I): R1 = 0.0388, wR2 = 0.0930<br>All data: R1 = 0.0496, wR2 = 0.0988 |
| Weighting scheme | w=1/[$\sigma^2$($F_O^2$)+ 0.0393P)2+7.7208P]<br>where P= ($F_O^2$+2$F_C^2$)/3 |
| GOF (on $F^2$) | 1.067 |
| Absolute structure parameter | 0.0(0) |
| Largest diff peak and hole (e·Å$^{-3}$) | 1.1560 and -0.515 |
| R.M.S. deviation from mean (e·Å$^{-3}$) | 0.074 |

## Reverse Phase High Performance Liquid Chromatography (RP-HPLC)

Reverse phase HPLC analysis were performed with a Perkin Elmer LC pump. UV detectors of Shimadzu SPD-10AV or Perkin Elmer LC 290 were used. HPLC grade solvents were applied. The bidistilled water was filtered over Millipore 0.22 µm filters prior to use. Analytical measurements were carried out on a Discovery® BIO Wide Pore C18 (Sigma Aldrich, 150 mm x 4.6 mm, 5 µm) with a flow rate of 1 mL/min. Purifications were carried out on a semi-preparative column of Themo Scientific™ (Hypersil™ C18, ODS, 250 x 8 mm, 10 µm) and a precolumn from Hypersil C18 (ODS, 4.6 mm × 25 mm, 10 µm) with a flow of 5.0 mL/min. Linear gradients of solvent A (0.1% TFA in $H_2O$) and solvent B (0.1% TFA in $CH_3CN$) were applied according to the following methods:

**Table 4:** Method A

| Step | Time (min) | % B |
|---|---|---|
| 0 | 5 | 10 |
| 1 | 0 – 3 | 10 |

| | | |
|---|---|---|
| 2 | 3 – 23 | 10 → 100 |
| 3 | 23 – 27 | 100 |
| 4 | 27 – 28 | 100 → 10 |
| 5 | 28 – 30 | 10 |

**Table 5:** Method B

| Step | Time (min) | % B |
|---|---|---|
| 0 | 5 | 30 |
| 1 | 0 – 3 | 30 |
| 2 | 3 – 33 | 30 → 75 |
| 3 | 33 – 37 | 75 |
| 4 | 37 – 38 | 75 → 100 |
| 5 | 38 – 40 | 100 |
| 6 | 40 – 41 | 100 → 30 |
| 7 | 42 - 45 | 30 |

**Integrin Binding Assays**

For the integrin binding assays, the following buffer solutions were used: carbonate buffer (15 mM $Na_2CO_3$, 35 mM $NaHCO_3$, pH 9.6), PBS-T buffer (phosphate-buffered saline/Tween20: 137 mM NaCl, 2.7 mM KCl, 10 mM $Na_2HPO_4$, 0.01% Tween20, pH 7.4) and TS-B buffer (Tris-saline/BSA buffer, 20 mM Tris-HCl, 150 mM NaCl, 1 mM $CaCl_2$, 1 mM $MgCl_2$, 1 mM $MgCl_2$, 1 mM $MnCl_2$, pH 7.5, 1% BSA).

The selectivity of integrin ligand binding was determined by a solid-phase binding assay which was carried out according to the procedure published by Kessler *et al.*[98] As internal standard Cilengitide (cyc(RGDf(*N*Me)V) was used. Flat-bottom 96-well ELISA plates were coated with 100 µL ECM protein (1.0 µg/mL human vitronectin for $\alpha_v\beta_3$ or 0.5 µg/mL human fibronectin for $\alpha_5\beta_1$) in carbonate buffer per well overnight at 4 °C. The wells were washed two times with 200 µL PBS-T buffer and blocked with 150 µL TS-B buffer for 1 h at room temperature. Again, the wells were washed three times with each 200 µL PBS-T. A dilution series of the bioconjugates **16a**, **16b** and cilengitide as internal standard in the range of 20 µM to 6.4 nM in 1:5 dilution steps were prepared and 50 uL of each dilution transferred to the wells B – G. In well A 100 uL of TSB solution as blank and in well H 50 uL of TS-B buffer were added. Then 50 uL of a 2.0 µg/mL solution of human $\alpha_v\beta_3$ integrin (for $\alpha_v\beta_3$) or of human

$\alpha_5\beta_1$ integrin (for $\alpha_5\beta_1$) in TS-B buffer was transferred to wells B to H and incubated at room temperature. After 1 h, the plate was washed three times with PBS-T and 100 µL of a primary antibody (2.0 µg/mL mouse anti-human CD51/61 for $\alpha_v\beta_3$ or 1.0 µg/mL mouse anti-human CD49e for $\alpha_5\beta_1$) were added. After incubation of 1 h at room temperature, the plate was washed three times with PBS-T buffer. 100 µL of the secondary peroxidase-labeled antibody (1.0 µg/mL anti-mouse IgG-POD for $\alpha_v\beta_3$ or 2.0 µg/mL anti-mouse IgG-POD for $\alpha_5\beta_1$) was added to each well. After 1 hour at room temperature, the plate was washed three times with PBS-T buffer and developed by addition of 50 µL SeramunBlau in each well. The plates remained for 5 minutes in the dark, and afterwards the reaction was stopped by addition of 50 µL 3 M $H_2SO_4$ to each well. The absorbance was measured at 450 nm with a plate reader and the resulting inhibition curves analyzed using OriginPro 7.5G software. The inflection point describes the $IC_{50}$ value. All determined $IC_{50}$ were referenced to the activity of the internal standard Cilengitide.

**Cell lines**

A549 (human lung cancer) and SKOV-3 (human ovarian cancer) cell lines were obtained from the European Centre of Cell Cultures ECACC, Salisbury, UK, and cultured in DMEM containing GlutaMax-I supplemented with 10% FBS and 1% penicillin/streptomycin (Invitrogen) at 37°C in a humidified atmosphere (95% of air, 5% $CO_2$; Heraeus, Germany).

**Antiproliferative assays**

In 96-well plates (Costar 3595) cells in an exponential growth rate were seeded (8000 cells per well) and cultivated in complete medium for 24 h. Stock solutions of the ruthenium compounds ($10^{-2}$ M in DMSO) were used to prepare the necessary solution in culture media (max. 0.2% DMSO in the culture medium). Then, the intermediate dilutions of the compounds were added to the wells in order to get final concentrations from 1 to 100 µM. After 72 h, 3-(4,5-dimethylthiazol-2-yl)-2,5-diphenyltetrazolium bromide (MTT) was added to the cells at a final concentration of 0.50 mg/ml in PBS (Phosphate Buffered Saline solution) and the mixture incubated for 2.5 h. In the following, the solution was removed and the formazan crystals were dissolved in DMSO. The optical density of each sample was quantified in quadruplicate at 550 nm by a multi-well plate reader (ThermoMax microplate reader, Molecular devices, US). The ratio of absorbance between treated and untreated cells was

used to calculate the percentage of surviving cells. The $IC_{50}$ value was calculated as the concentration inhibiting the cells growth by 50% and is presented as a mean (± SD) of at least two independent experiments.

# 13 Synthesis of functionalized Ruthenium Complexes

## 13.1 Synthesis of the ligands

***4'-(Furan-2-yl)-2,2':6',2''-terpyridine***

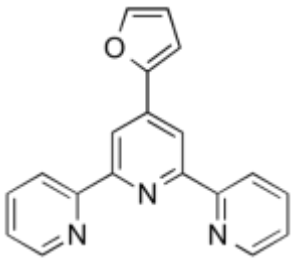


$C_{19}H_{13}N_3O$
299,33 g $mol^{-1}$

The synthesis was carried out as published in literature.[84] 4.50 mL 2-acetylpyridine (4.84 g, 40.0 mmol, 2.00 eq) was dissolved in in 100 mL ethanol. Then 1.70 mL furfural (1.92 g, 20.0 mmol, 1.00 eq) and 3.08 g KOH (55.0 mmol, 2.75 eq) were added and stirred for 20 minutes at room temperature. 58.0 mL ammonia solution (w = 25%) was transferred to the mixture and stirred for further 20 hours. The resulting white solid was filtered, washed five times with cold ethanolic solution (50 Vol.-%) and dried under reduced pressure to give 2.55 g, 43% product.

**$^1$H NMR**: δH [ppm] (400 MHz; $CDCl_3$) 8.74 (d, 2H, $H^{6,6''}$), 8.72 (s, 2H, $H^{3',5'}$), 8.65 (dt, 2H, $H^{3,3''}$), 7.88 (td, 2H, $H^{4,4''}$), 7.59 (d, 1H, $H^{4'''}$), 7.36 (ddd, 2H, $H^{5,5''}$), 7.12 (d, 1H, $H^{5'''}$), 6.57 (dd, 1H, $H^{3'''}$).

***[2,2':6',2''-Terpyridine]-4'-carboxylic acid (1b)***

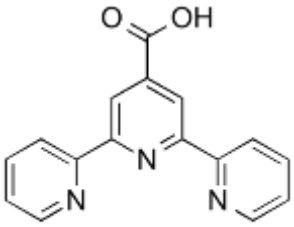

$C_{16}H_{11}N_3O_2$
277,28 g mol$^{-1}$

The synthesis was carried out as published in literature.[84] 2.10 g (7.02 mmol, 1.00 eq) 4'-(Furan-2-yl)-2,2':6',2''-terpyridine were diluted in 110 mL $H_2O$ and by addition of solid KOH the pH was set to 10. $KMnO_4$ (4.43 g, 28.0 mmol, 4.00 eq) was added and the mixture refluxed for three hours. After cooling down to room temperature, manganese dioxide was removed *via* filtration over celite. The filtrate was set to pH 5 with $HCl_{conc.}$ and the resulting white precipitate obtained by filtration. The white powder was washed two times with 20 mL water and dried under reduced pressure to yield 1.58 g, 81% product.

**$^1$H NMR**: δH [ppm] (400 MHz; DMSO-$d_6$) 13.86 (s, 1H, COO*H*), 8.83 (s, 2H, $H^{3',5'}$), 8.73 (d, 2H, $H^{6,6''}$), 8.62 (d, 2H, $H^{3,3''}$), 8.02 (td, 2H, $H^{4,4''}$), 7.52 (dd, 2H, $H^{5,5''}$).

**$^{13}$C NMR**: δC [ppm] (101 MHz; DMSO-$d_6$) 166.10, 156.05, 154.25, 149.54, 140.65, 137.63, 124.87, 120.91, 119.64.

**ESI-MS**: *m*/*z* 278.30 $[M+H]^+$.

***2-Hydroxy-5-methylpyridine (5)***

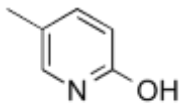


$C_6H_7NO$
109,13 g mol-1

The synthesis was carried out as published in literature.[87] To a mixture of 340 mL $H_2O$ and 90 mL $H_2SO_{4,conc}$ 41.0 g (379 mmol, 1.00 eq) 2-amino-5-methylpyridine were added and cooled down to 0 °C. Then, 34.7 g (502 mmol, 1.33 eq) $NaNO_2$ in 65 mL $H_2O$ were added within 45 min and the resulting solution heated to 95 °C for 50 min. After cooling down to room temperature, the pH was set to 6-7 by addition of about 80 mL NaOH (w = 50%). The warm solution was extracted five times with 150 mL ethyl acetate each, the combined organic layers dried with $Na_2SO_4$ and the solvents removed under vacuum to yield in 14.2 g, 35% product.

**$^1$H NMR:** δH [ppm] (400 MHz, $CDCl_3$) 13.35 (br, 1H, O*H*), 7.33 (d, J = 9.3 Hz, 1H, $H^4$), 7.14 (s, 1H, $H^6$), 6.52 (d, J = 9.4 Hz, 1H, $H^3$), 2.09 (s, 3H, C$H_3$).

***5-Methylpyridin-2-yl trifluoromethanesulfonate (6)***

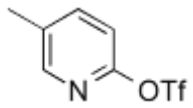


$C_7H_6F_3NO_3S$
241,18 g mol-1

The synthesis was carried out as published in literature.[87] Using Schlenk techniques, 4.85 g (44.4 mmol, 1.00 eq) 2-hydroxy-5-methylpyridine was dissolved in 140 mL dry pyridine and cooled down to -10 °C. After addition of 9.00 mL (15.1 g, 53.3 mmol, 1.20 eq) trifluoromethanesulfonic anhydride the solution was stirred at 0 °C for 35 min and then poured into 150 mL ice water. The solution was extracted three times with 100 mL $CH_2Cl_2$, the combined organic layers dried over $Na_2SO_4$ and the solvents removed under vacuum. For purification the raw product was distilled under reduced pressure (40°C, 2.5×10-2 mbar) to yield in 7.44 g product (69% yield) as colorless liquid.

**$^1$H NMR:** δH [ppm] (400 MHz, DMSO-$d_6$) 8.2-8.17 (m, 1H, $H^4$), 7.68 (dd, *J* = 8.3, 2.4 Hz, 1H, $H^3$), 7.08 (d, *J* = 8.3 Hz, 1H, $H^6$), 2.39 (s, 3H, $CH_3$).

***5-Methyl-2,2'-bipyridine (7)***

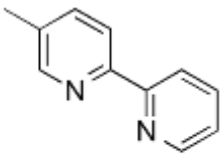

$C_{11}H_{10}N_2$
170,22 g $mol^{-1}$

The synthesis was carried out as published in literature.[87] Using Schlenk techniques, 30 mL dry THF were cooled down to -78 °C and 20.1 mL (34.2 mmol, 2.50 eq) *tert*-butyllithium (1.7M in pentane) added. Then, 1.59 mL (2.63 g, 16.7 mmol, 1.22 eq) 2-bromopyridine were added to the yellow solution within 10 min and stirred for 30 min at -78 °C. After addition of 35.8 mL (35.8 mmol, 2.62 eq) 1M $ZnCl_2$ solution in diethylether the mixture was stirred at room temperature for 2.5 h. 3.18 g (13.2 mmol, 1.00 eq) 5-methylpyridin-2-yl trifluoromethanesulfonate, 1.17 g (27.7 mmol, 2.10 eq) LiCl and 636 mg (550 µmol, 1.00 eq) $Pd(PPh_3)_4$ were added and the solution refluxed for 17 h. After cooling down to room temperature, 20.4 g (54.8 mmol, 4.15 eq) EDTA in 150 mL water were poured into the mixture, the pH set to 7-8 by addition of 50 mL saturated $NaHCO_3$ solution and stirred for 15 min. The solution was extracted three times with 100 mL $CH_2Cl_2$, the combined organic layers dried with $Na_2SO_4$ and the solvents removed under vacuum. The raw product was purified by flash chromatography (hexane:ethyl acetate = 100:0 → 80:20) to yield in 523 mg, (23% yield) as yellow, oily liquid.

**$^1$H NMR:** δH [ppm] (400 MHz, $CDCl_3$) 8.68-8.64 (m, 1H, $H^{6'}$), 8.50 (s, 1H, $H^6$), 8.35 (dd, *J* = 8.1, 1.2Hz, 1H, $H^{3'}$), 8.28 (d, *J* = 8.1Hz, 1H, $H^3$), 7.80 (td, *J* =7.7, 1.7 Hz, 1H, $H^4$), 7.62 (dd, *J* = 8.1, 2.2 Hz, 1H, $H^{4'}$), 7.28 (ddd, *J* = 7.5, 4.7, 1.1 Hz, 1H, $H^{5'}$), 2.39 (s, 3H, $CH_3$).

***5-Carboxyl-2,2'-bipyridine (8)***

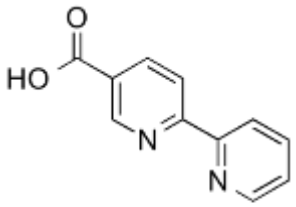

$C_{11}H_8N_2O_2$
200,20 g mol$^{-1}$

The synthesis was carried out as published in literature.[87] 523 mg (3.07 mmol, 1.00 eq) 5-methyl-2,2'-bipyridine were suspended in 15 mL $H_2O$ and 1.75 g (11.1 mmol, 3.60 eq) $KMnO_4$ in 20 mL $H_2O$ added within 5 h and the mixture stirred at 90 °C for 20 h. The brown suspension was filtered over celite, the filter cake washed three times with 10 mL water and the filtrates concentrated to a total volume of 15 mL. The pH was set to 4 with 1M HCl and the product precipitated by addition of acetone. The product is obtained by filtration to yield in 43 mg white solid (7% yield).

**$^1$H NMR** δH [ppm] (400 MHz, DMSO-$d_6$) 9.18 (d, *J* = 2.1 Hz, 1H, $H^6$), 8.76 (dd, *J* = 5.1, 1.7 Hz, 1H, $H^{6'}$), 8.53 (d, *J* = 8.3 Hz, 1H, $H^3$), 8.50 (d, *J* = 8.0 Hz, 1H, $H^{3'}$), 8.43 (dd, *J* = 8.3, 2.2 Hz, 1H, $H^4$), 8.12 8.00 (m, 1H, $H^{4'}$), 7.63 - 7.49 (m, 1H, $H^{5'}$).

## 13.2 Synthesis of Ruthenium Complexes

***[Ru(terpy)Cl$_3$] (2a)***

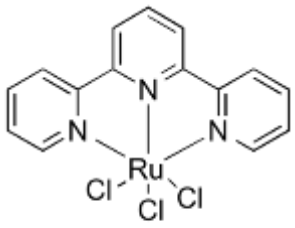


$C_{15}H_{11}Cl_3N_3Ru$
440,69 g mol$^{-1}$

The synthesis was carried out as published in literature.[85] 327 mg $RuCl_3 \cdot 3H_2O$ (1.25 mmol, 1.00 eq) was dissolved in 60 mL dry ethanol. 292 mg (1.25 mmol, 1.00 eq) 2,2':6',2''-terpyridine were added and the solution refluxed at 90°C under argon atmosphere for one hour. After cooling down, the precipitate was filtered and washed two times with 20 mL $H_2O$, ethanol and diethylether respectively to give a dark brown solid which was dried under vacuum to yield 490 mg (89% yield).

**Elemental Analysis:** Found: C, 40.02; H, 2.58; N, 9.77. Calc. for $C_{15}H_{11}Cl_3N_3Ru$: C, 40.88; H, 2.52; N, 9.54%.

***[Ru(terpy*)Cl$_3$] (2b)***

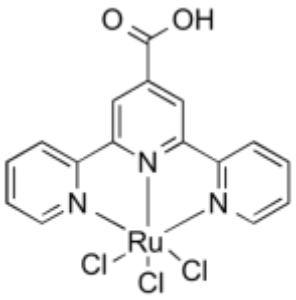


$C_{16}H_{11}Cl_3N_3O_2Ru$
484,70 g mol$^{-1}$

The synthesis was carried out as published in literature.[85] 327 mg $RuCl_3 \cdot 3H_2O$ (1.25 mmol, 1.00 eq) and 347 mg [2,2':6',2''-terpyridine]-4'-carboxylic acid (1.25 mmol, 1.00 eq) were dissolved in 60 mL dry ethanol and the solution heated to reflux at 90°C under argon atmosphere for one hour. The precipitate was filtered and washed two times with 20 mL water, ethanol and diethylether respectively. The dark brown solid was dried under vacuum to yield 375 mg (62% yield).

**Elemental Analysis:** Found: C, 39.50; H, 2.22; N, 8.73; Cl, 20.8. Calc. for $C_{16}H_{11}Cl_3N_3O_2Ru$: C, 39.65; H, 2.29; N, 8.67; Cl, 21.94%.

***[Ru(terpy)(terpy*)](PF$_6$)$_2$ (3a)***

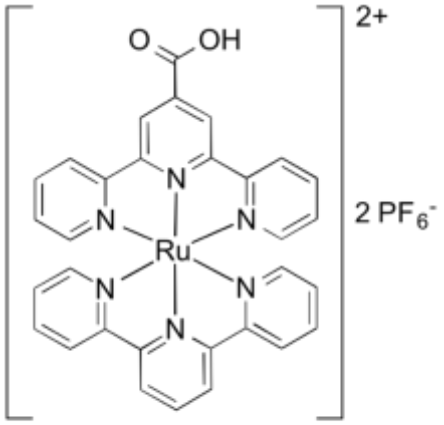


$C_{31}H_{22}N_6O_2Ru$
611,63 g mol$^{-1}$

The synthesis was carried out following a literature procedure.[84] To a mixture of [Ru(terpy)Cl$_3$] (304 mg, 0.70 mmol, 1.00 eq), 194 mg [2,2':6',2''-terpyridine]-4'-carboxylic acid (0.70 mmol, 1.00 eq) and LiCl (161 mg, 3.80 mmol, 5.00 eq) a mixture of ethanol and water (40 mL, 7:3) was added. Then, 0.6 mL triethylamine (4.30 mmol, 6.20 eq) were transferred to the solution and the mixture refluxed at 100°C for four hours. After cooling down to room temperature, the crude product was obtained by filtration. The resulting dark violet solid was dissolved in a mixture of acetonitrile and water and precipitated by addition of an aqueous 1M $KPF_6$ solution. The product was filtrated and dried under vacuum to yield 480 mg (76% yield).

**$^1$H NMR**: δH [ppm] (400 MHz; DMSO-d$_6$) 9.44 (s, 2H, $H_{terpy*}^{3',5'}$), 9.15 - 9.07 (m, 4H, $H_{terpy}^{3',5'}$, $H_{terpy*}^{3,3''}$), 8.84 (d, 2H, $H_{terpy}^{3,3''}$), 8.56 (dt, 1H, $H_{terpy}^{4}$), 8.10 - 7.97 (m, 4H, $H_{terpy*}^{4,4''}$, $H_{terpy}^{4,4''}$), 7.56 - 7.41 (m, 4H, $H_{terpy*}^{6,6''}$, $H_{terpy}^{6,6''}$) 7.34 - 7.14 (m, 4H, $H_{terpy*}^{5,5''}$, $H_{terpy}^{5,5''}$).

**$^{13}$C NMR**: δC [ppm] (101 MHz; DMSO-d$_6$) 165.79, 157.48, 157.39, 155.41, 154.32, 152.39, 151.89, 138.26, 138.19, 137.61, 127.97, 127.66, 125.06, 124.58, 124.07, 123.24, 120.88, 119.59.

**$^{31}$P NMR**: δP [ppm] (162 MHz; DMSO-d$_6$) −144.21 (sept, $PF_6^-$).

**ESI-MS**: *m/z* 757.05 $[M\text{-}PF_6]^+$, 306.04 $[M\text{-}2PF_6]^{2+}$.

***[Ru(terpy*)$_2$](PF$_6$)$_2$ (3b)***

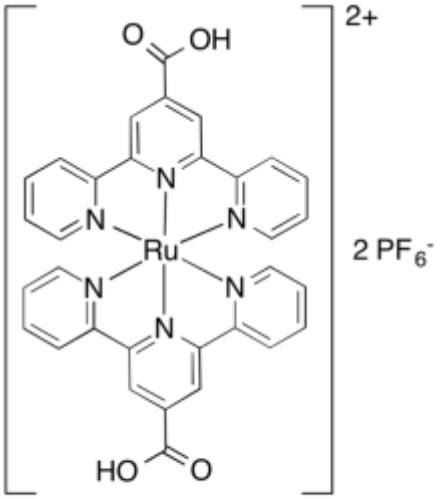


$C_{32}H_{22}N_6O_4Ru$
655,64 g mol$^{-1}$

The synthesis was carried out following a literature procedure.[84] 378 mg [Ru(terpy*)$Cl_3$] (0.78 mmol, 1.00 eq), 216 mg [2,2':6',2''-terpyridine]-4'-carboxylic acid (0.78 mmol, 1.00 eq) and LiCl (182 mg, 4.29 mmol, 5.50 eq) were diluted in 40 mL of a mixture of water: ethanol = 1:3. After addition of 0.65 mL triethylamine (4.68 mmol, 6.00 eq) the solution was refluxed for four hours at 100°C. Then, the mixture was reduced to a volume of 10 mL, acidified with 0.2 mL $HCl_{conc}$ and mixed with 3.20 mL of 1M $KPF_6$ solution (3.20 mmol, 4.00 eq) The resulting solid is filtrated over celite, washed with slight HCl-acidic water and recovered by diluting in acetone. After removal of the solvent the red brownish product yielded 306 mg (42% yield).

**$^1$H NMR**: δH [ppm] (400 MHz; DMSO-$d_6$) 14.49 (s, 2H, COO*H*), 9.45 (s, 4H, $H^{3',5'}$), 9.09 (d, 4H, $H^{3,3''}$), 8.02 (t, 4H, $H^{4,4''}$), 7.53 (d, 4H, $H^{6,6''}$), 7.26 (t, 4H, $H^{5,5''}$).

**$^{13}$C NMR**: δC [ppm] (101 MHz; DMSO-$d_6$) 165.63, 157.24, 155.16, 152.34, 138.44, 128.00, 125.25, 123.40.

**$^{31}$P NMR** δP [ppm] (162 MHz; DMSO-$d_6$) −144.21 (sept, $PF_6^-$).

**ESI-MS**: *m/z* 801.04 $[M\text{-}PF_6]^+$, 328.04 $[M\text{-}2PF_6]^{2+}$.

***[Ru(bipy)$_2$Cl$_2$] (4)***

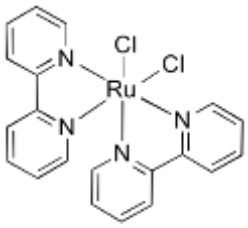


$C_{20}H_{16}Cl_2N_4Ru$
484,35 g mol$^{-1}$

This synthesis was carried out under inert atmosphere with argon as protection gas. 784 mg (3.00 mmol, 1.00 eq) $RuCl_3 \times 3H_2O$ and 936 mg (6.00 mmol, 2.00 eq) 2,2'-bipyridine were dissolved in 8 mL DMF and refluxed at 150°C for 15 h. After cooling down to room temperature, a brown solid was precipitated through addition of 30 mL acetone. The product was obtained by filtration, washed three times with 5 mL acetone and dried under vacuum to yield in 1.11 g (76% yield)

**$^1$H NMR**: δH [ppm] (400 MHz, DMSO-$d_6$) 9.97 (d, 1H), 8.64 (d, 1H), 8.49 (d, 1H), 8.06 (m, 1H), 7.77 (t, 1H), 7.68 (t, 1H), 7.51 (d, 1H), 7.10 (t, 1H).

**ESI-MS**: *m/z* 449.23 $[M\text{-}Cl]^+$, 489.79 $[M\text{-}Cl+CH_3CN]^+$.

**Elemental Analysis:** Found: C, 49.64; H, 3.39; N, 11.59; Cl, 13.5; Ru, n.d. Calc. for $C_{20}H_{16}Cl_2N_4Ru$: C, 49.60; H, 3.33; N, 11.57; Cl, 14.64; Ru, 20.87%.

***[Ru(bipy)$_2$(bipy*)](PF$_6$)$_2$ (9)***

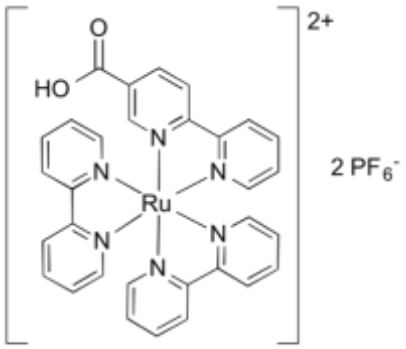


$C_{31}H_{24}F_{12}N_6O_2P_2Ru$
903,57 g mol$^{-1}$

Using Schlenk techniques, 48.4 mg of [Ru(bipy)$_2$Cl$_2$] (100 µmol, 1.00 eq) and 20.0 mg 5-carboxyl-2,2'-bipyridine (100 µmol, 1.00 eq) were combined and dissolved in 10 mL dry methanol. The solution was refluxed at 60 °C for 5 h. After removing the solvent under vacuum, a violet solid was precipitated by addition of 0.1M $KPF_6$ solution and filtered over celite. The product was obtained by dissolving the violet solid from the celite filter cake with acetone. After removing the solvent under vacuum, 4.8 mg, (6% yield) were obtained.

**$^1$H-NMR** δH [ppm] (400 MHz, DMSO-d$_6$) 13.94 (s, 1H), 9.67 (s, 1H), 8.90 (dt, *J* = 27.5, 8.7 Hz, 5H), 8.51 (d, *J* = 8.2 Hz, 1H), 8.20 (h, *J* = 7.3, 6.3 Hz, 4H), 7.97 (s, 1H), 7.85 (d, *J* = 5.6 Hz, 1H), 7.79 (t, *J* = 7.2 Hz, 2H), 7.73 (t, *J* = 7.0 Hz, 2H), 7.54 (tt, *J* = 20.3, 6.5 Hz, 4H).

**ESI-MS**: *m/z* 758.87 [M-PF$_6$]$^+$, 307.15 [M-2PF$_6$]$^{2+}$.

***[Ru(bipy)$_2$(bipy-AA)](PF$_6$)$_2$ (10)***

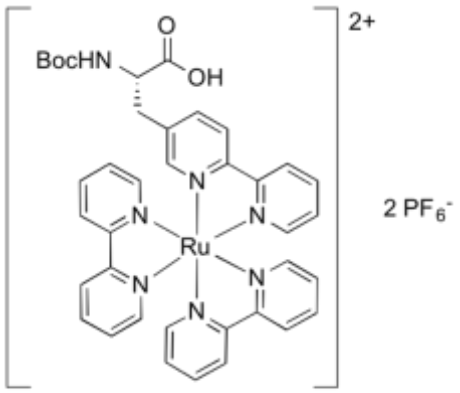


$C_{38}H_{37}F_{12}N_7O_4P_2Ru$
1046,76 g mol$^{-1}$

18.8 mg of [Ru(bipy)$_2$Cl$_2$] (39.0 µmol, 1.00 eq) and 10.0 mg bipy-AA (39.0 µmol, 1.00 eq) were combined in a J.Young NMR tube using Schlenk techniques and dissolved in 0.65 mL dry $CD_3OD$. The tube was heated to 60 °C and the reaction monitored with $^1$H NMR. After 6 h the solution was filtered and precipitated by addition of aqueous 0.1 M $KPF_6$ solution. The product is obtained after filtration as dark yellow solid yielding in 1.0 mg (2% yield).

**ESI-MS**: *m/z* 1085.44 $[M+K]^+$, 901.75 $[M-PF_6]^+$, 378.38 $[M-2PF_6]^{2+}$.

***[Ru(terpy)(bipy)Cl]$PF_6$ (11)***

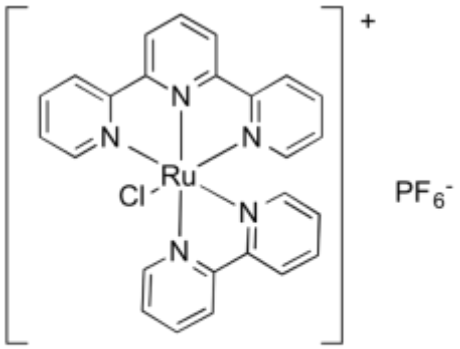

$C_{25}H_{19}ClF_6N_5PRu$
670,95 g $mol^{-1}$

The synthesis was carried out in analogy to a procedure published in literature.[85] 790 mg (1.79 mmol, 1.00 eq) [Ru(terpy)$Cl_3$], 290 mg 2,2'-bipyridine (1.88 mmol, 1.05 eq), 420 mg LiCl (9.90 mmol, 5.52 eq) and 1.57 mL triethylamine (11.5 mmol, 6.40 eq) were dissolved in 50 mL ethanol and 20 mL water and heated to reflux at 120 °C for 4 h. Then, the solution was concentrated to a total volume of 10 mL and a brown solid precipitated by addition of 1M $KPF_6$ solution. The crude product was obtained by filtration and purified with column chromatography with $CH_3CN$:$H_2O$:$KNO_{3,sat.}$ = 44:2:1 as eluent. The product ($R_f$ = 0.22) was collected, precipitated by addition of 1M $KPF_6$ solution, filtered over celite and the solid washed three times with water. The product was isolated from the celite filter cake by elution with $CH_3CN$. The solvent was removed under reduced pressure and the resulting solid dried under vacuum to result in 576 mg (48% yield).

**$^1$H NMR** δH [ppm] (400 MHz, acetone-$d_6$) 10.33 (d, 1H), 8.87 (d, 1H), 8.74 (d, 2H), 8.61 (t, 3H), 8.38 (td, 1.5 Hz, 1H), 8.20 (t, 1H), 8.07 (dd, 5.8 Hz, 1H), 7.99 (td, 1.4 Hz, 2H), 7.81 (dd, 3H), 7.58 (d, 1H), 7.40 (dd, 2H), 7.11 (dd, 1H).

**$^{13}$C NMR** δC [ppm] (101 MHz, acetone-$d_6$) 158.88, 158.11, 152.65, 152.17, 152.04, 136.90, 136.55, 135.47, 133.59, 127.23, 126.76, 126.27, 123.46, 123.28, 122.36.

***[Ru(terpy)(bipy)($CH_3CN$)]($PF_6$)$_2$ (12)***

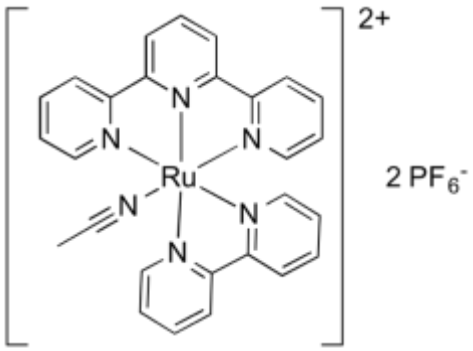


$C_{27}H_{22}F_{12}N_6P_2Ru$
821,51 g mol$^{-1}$

The synthesis was carried out in analogy to a procedure published in literature.[99] 205 mg [Ru(terpy)(bipy)Cl]$PF_6$ (0.31 mmol, 1.00 eq) and 99.3 mg (0.51 mmol, 1.67 eq) $AgBF_4$ were diluted in 200 mL solvents ($CH_3CN$:$H_2O$=4:1). The mixture was heated to reflux at 90°C for 3 hours and filtered hot over celite. The solvent was reduced to a total volume of 20 mL under vacuum and the raw product precipitated by addition of aqueous 1 M $KPF_6$ solution. After filtration, the product was purified with column chromatography using $CH_3CN$:$H_2O$:$KNO_{3,sat.}$ = 44:2:1 as eluent ($R_f$ = 0.9). The solvent of the combined product fractions was removed under reduced pressure and the dark red solid dissolved in a small amount of $CH_3CN$. Addition of 1 M $KPF_6$ solution and filtration yielded in 193 mg, 76% product.

**$^1$H NMR**: δH [ppm] (400 MHz; acetone-$d_6$) 9.90 (ddd, *J* = 5.5, 1.5, 0.8 Hz, 1H), 8.92 (dt, *J* = 8.2, 1.1 Hz, 1H), 8.87 (d, *J* = 8.1 Hz, 2H), 8.73 (ddd, *J* = 8.1, 1.4, 0.8 Hz, 2H), 8.66 (dt, *J* = 8.2, 1.1 Hz, 1H), 8.50-8.43 (m, 2H), 8.16 (td, *J* = 7.9, 1.5 Hz, 2H), 8.10 (ddd, *J* = 7.7, 5.6, 1.3 Hz, 1H), 8.01-7.93 (m, 3H), 7.63 (ddd, *J* = 5.7, 1.5, 0.7 Hz, 1H), 7.53 (ddd, *J* = 7.7, 5.5, 1.4 Hz, 2H), 7.25 (ddd, *J* = 7.3, 5.7, 1.4 Hz, 1H), 2.32 (s, 3H).

**$^{31}$P NMR**: δP [ppm] (162 MHz; acetone-$d_6$) −144.28 (sept, $PF_6^-$).

**ESI-MS**: *m/z* 265.6 $[M\text{-}2PF_6]^{2+}$, 242.2 $[M\text{-}2PF_6\text{-}CH_3CN]^{2+}$.

***[Ru(terpy)(bipy)(fampy)](PF$_6$)$_2$ (13)***

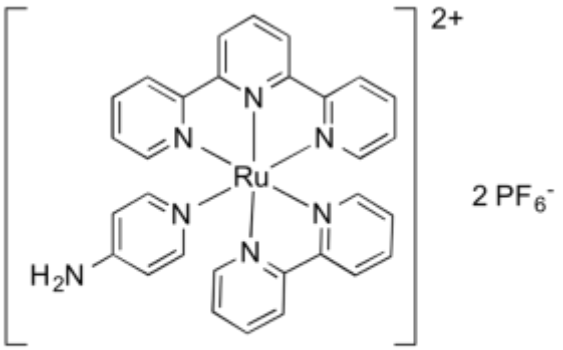


$C_{30}H_{25}F_{12}N_7P_2Ru$
874,58 g mol$^{-1}$

Under protection of light 250 mg (0.37 mmol, 1.00 eq) [Ru(terpy)(bipy)Cl]$PF_6$, 159 mg (1.68 mmol, 4.55 eq) 4-aminopyridine and 207 mg (0.82 mmol, 2.20 eq) $AgPF_6$ were dissolved in 32 mL of a mixture of water and acetone (5:3) and refluxed at 70°C for 16 h. The hot suspension was filtered over celite and washed three times with 10 mL acetone and water, respectively. The solution was concentrated to a total volume of 6 mL and the product precipitated by addition of diethylether. The dark red solid was obtained by filtration, washed with diethylether and dried under vacuum to yield in 176 mg, 54% product.

**$^1$H NMR**: δH [ppm] (400 MHz, acetone-$d_6$) 8.97 (d, *J* = 8.2 Hz, 1H), 8.86 (d, *J* = 8.2 Hz, 2H), 8.75 (d, *J* = 8.2 Hz, 2H), 8.71 (d, *J* = 5.3 Hz, 2H), 8.39 (t, *J* = 7.8 Hz, 1H), 8.30 (t, *J* = 8.0 Hz, 1H), 8.11 (t, *J* = 7.8 Hz, 2H), 8.02 (d, *J* = 6.5 Hz, 1H), 7.89 (t, *J* = 7.9 Hz, 1H), 7.79 (d, *J* = 5.4 Hz, 2H), 7.54-7.43 (m, 2H), 7.30 (d, *J* = 5.6Hz, 1H), 7.15 (t, *J* = 6.6 Hz, 1H), 6.94 (d, *J* = 6.3 Hz, 2H), 6.76 (s, 2H), 6.30 (d, *J* = 6.3 Hz, 2H).

**$^{13}$C NMR**: δH [ppm] (101 MHz, acetone-$d_6$) 209.13, 158.34, 157.77, 157.66, 156.35, 152.81, 151.76, 151.41, 150.49, 138.42, 137.63, 137.15, 135.57, 128.72, 127.83, 126.80, 124.76, 124.46, 123.69, 111.01, 68.33.

**ESI-MS**: *m/z* 729.92 $[M\text{-}PF_6]^+$, 292.45 $[M\text{-}2PF_6]^{2+}$.

**Elemental Analysis:** Found: C, 41.13; H, 2.82; N, 10.95; P, 6.98; F, 26.00; Ru, 11.56. Calc. for $C_{30}H_{25}F_{12}N_7P_2Ru$: C, 41.20; H, 2.88; N, 11.21; P, 7.08; F, 26.07; Ru, 11.56%.

## 13.3 Peptide Synthesis

***Preparation of the cyclic pentapeptide cyc(RGDfK)***

**Preloading of the resin**

First, 375 mg (0.50 mmol) 2-chlorotrityl chloride resin (100-200 mesh, 1.33 mmol/g) was washed two times with DMF and was then swollen in 20 mL DMF for 10 min under nitrogen counterflow. 1.10 eq of the first amino acid, Fmoc-Gly-OH (164 mg, 0.55 mmol) were dissolved in 1.5 mL DMF, transferred to the resin and mixed with 0.43 mL DIPEA (2.50 mmol, 5.00 eq). After stirring at room temperature for 30 min, the resin was washed three times with a mixture of DCM, methanol and DIPEA (17:2:1), then three times with DCM, two times with DMF and finally again two times with DCM. The resin was dried under vacuum.

**Synthesis of linear peptide**

The protected linear pentapeptide D(*t*Bu)fK(ivDde)R(Pbf)G (sequence Asp(*t*Bu)-Phe-Lys(ivDde)-Arg(Pbf)-Gly) was prepared manually by Fmoc-based Solid Phase Peptide Synthesis in a glass frit using glycine-preloaded 2-chlorotrityl chloride resin and PyBop and HOBt as coupling agents. In order to obtain complete reaction of the amino acids, double coupling was performed. After swelling of the preloaded resin in 5 mL DMF for 1 h, the following steps were performed:

1. Cleavage of Fmoc protection group with 4 mL 20% piperidine in DMF.
2. Wash of the resin, three times with DCM and DMF respectively.
3. Addition of a solution containing 3.00 eq (1.50 mmol) of the appropriate amino acid, 3.00 eq (1.50 mmol) of PyBop and HOBt each and 6.00 eq of DIPEA (3.00 mmol) and reaction for 2 h in nitrogen counterflow.
4. Wash of the resin, three times with DCM and DMF respectively.
5. Double coupling: Addition of a solution containing 3.00 eq (1.50 mmol) of the appropriate amino acid, 3.00 eq (1.50 mmol) of PyBop and HOBt each and 6.00 eq of DIPEA (3.00 mmol) and reaction for 2 h in nitrogen counterflow.
6. Wash of the resin, three times with DCM and DMF respectively.

These steps were repeated until the sequence of the pentapeptide was attached to the resin. Finally, the remaining Fmoc protection group at the last amino acid was cleaved by addition of 4 mL 20% piperidine in DMF and the resin washed three times with DCM and DMF each.

**Cleavage of linear pentapeptide from resin**

First, 100 g of the resin-attached linear D(*t*Bu)fK(ivDde)R(Pbf)G peptide was swollen in DCM for 15 min under nitrogen counterflows in a glass frit. The cleavage of the peptide from the resin was carried out with 10 portions of 1 % TFA in DCM whereas each portion was reacted in nitrogen counterflows for 5 min and then collected in 10 flasks, each containing a solution of 10% pyridine in methanol (0.5 mL). The factions were analyzed with RP-HPLC and the solvents of the combined product fractions evaporated. The obtained solid was dissolved in DCM and precipitated by addition of diethylether. RP-HPLC analysis (method B) showed pure product at $R_t$ = 20.6 min.

**Cyclization of the linear peptide**

A 5 mM solution of 23.7 mg (23.0 µmol, 1.00 eq) linear D(*t*Bu)fK(ivDde)R(Pbf)G in a mixture of DCM:DMF = 11:1 (4.6 mL) was prepared and then 29.9 mg (57.5 µmol, 2.50 eq) PyBop and 7.78 mg (57.5 µmol, 2.50 eq) HOBt added. This solution was dropped slowly into a solution of 39.1 µL DIPEA (29.7 mg, 230 µmol, 10.0 eq) in 0.4 mL DCM. The formation of product (cyc(R(Pbf)GD(*t*Bu)fK(ivDde)) was analyzed with RP-HPLC ($R_t$ = 10.4 min, method A). Purification was carried out with semi-preparative RP-HPLC ($R_t$ = 25.7 min, method A).

**Cleavage of ivDde protection group:**

The ivDde protection group was cleaved with 2 mL of a 2% $N_2H_4 \cdot H_2O$ solution in DMF. After 1.5 h of stirring at room temperature, the peptide was precipitated by addition of cold water, filtered and washed three times with cold diethylether to yield in cyc(R(Pbf)GD(*t*Bu)fK)

**ESI-MS**: *m/z* 912.21 $[M]^+$ (calcd for $C_{44}H_{65}N_9O_{10}S$: 912.12), 456.68 $[M]^{2+}$.

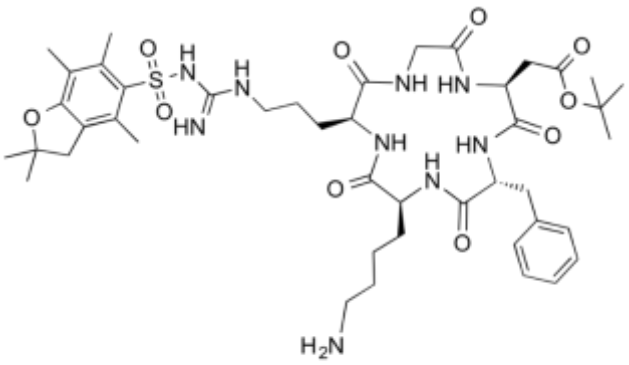

$C_{44}H_{65}N_9O_{10}S$
912,12 g mol$^{-1}$

**Cleavage of Pbf and *t*Bu protection groups:**

For deprotection of the remaining protection groups (Pbf and *t*Bu) a mixture of 500 µL DCM, 250 µL $H_2O$, 250 µL TIPS and 4 mL TFA was added. After one hour stirring at room temperature, volatiles were evaporated under reduced pressure. The product washed twice with DMF and precipitated by addition of diethylether. The pure product (cyc(RGDfK) was analyzed by analytical RP-HPLC ($R_t$ = 17.0 min, method A) and lyophilized prior to use.

**ESI-MS**: *m/z* 604.3 $[M+H]^+$.

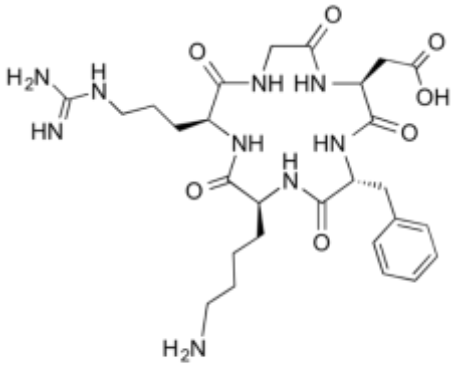

$C_{27}H_{41}N_9O_7$
603,68 g mol$^{-1}$

## 13.4 Coupling of Ruthenium Complexes to the RGD Peptide

***cyc(RGDfK(bipy-AA)) (14)***

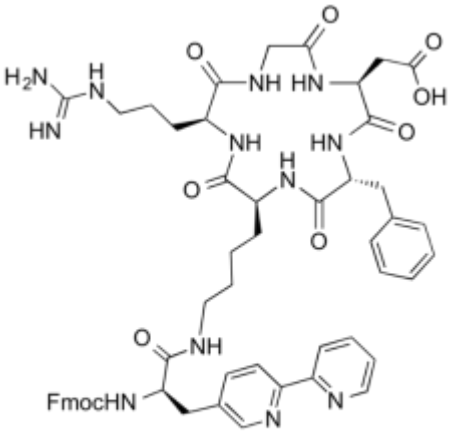

$C_{55}H_{62}N_{12}O_{10}$
1051,18 g mol$^{-1}$

The unnatural amino acid Fmoc-bipy-AA (1.85 mg, 3.98 µmol, 1.20 eq) was preincubated with 1.51 mg HBTU (3.98 µmol, 1.20 eq) in 1 mL DMF for 30 min at room temperature. Then, the unprotected peptide cyc(RGDfK) (2.0 mg, 3.31 µmol, 1.00 eq), 2.80 µL DIPEA (2.14 mg, 16.6 µmol, 5.00 eq) and 1 mL DMF were added. After 40 h stirring under nitrogen at room temperature the formation of product was verified with analytical RP-HPLC ($R_t$ = 12.5 min, method B), then purification was carried out with semi-preparative RP-HPLC ($R_t$ = 22.6 min, method B) to yield in 1.00 mg, 29% white powder as product.

**ESI-MS**: *m/z* 1051.4 $[M+H]^+$, 526.4 $[M+H]^{2+}$.

***cyc(RGDfK(terpy)) (15)***

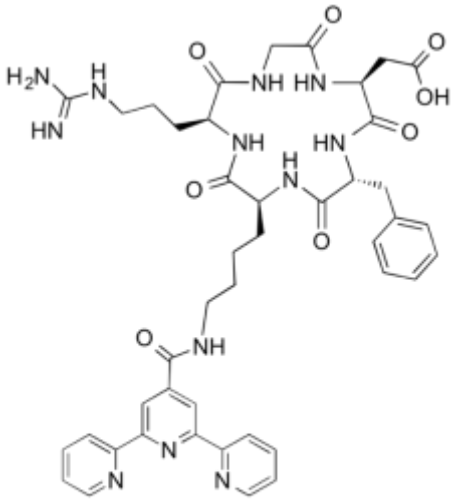

$C_{43}H_{50}N_{12}O_8$
862,95 g mol$^{-1}$

[2,2':6',2''-Terpyridine]-4'-carboxylic acid (1.11 mg, 3.98 µmol, 1.20 eq) was preincubated with 1.51 mg HBTU (3.98 µmol, 1.20 eq) in 1 mL DMF for 30 min at room temperature. Then, the unprotected peptide cyc(RGDfK) (2.0 mg, 3.31 µmol, 1.00 eq), 2.80 µL DIPEA (2.14 mg, 16.6 µmol, 5.00 eq) and 1 mL DMF were added. After 24 h stirring under nitrogen at room temperature the formation of product was verified with analytical RP-HPLC ($R_t$ = 13.5 min, method A). Purification is carried out with semi-preparative RP-HPLC ($R_t$ = 22.5 min, method A) to yield in 0.1 mg, 3 % white powder as product.

**ESI-MS**: *m/z* 863.0 $[M+H]^+$.

***[cyc(RGDfK)[Ru(terpy)(terpy*)](PF$_6$)$_2$] (16a)***

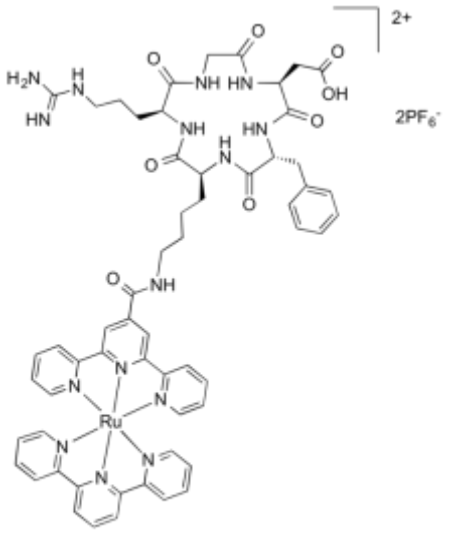


$C_{58}H_{61}F_{12}N_{15}O_8P_2Ru$
1487,22 g mol$^{-1}$

The peptide cyc(R(Pbf)GD(*t*Bu)fK) (11.4 mg, 12.5 µmol) and [Ru(terpy)(terpy*)](PF$_6$)$_2$] (11.8 mg, 13.1 µmol, 1.05 eq) were dissolved in 0.7 mL of DMF. To the solution, the coupling agents HATU (7.1 mg, 18.7 µmol, 1.50 eq), HOAt (2.5 mg, 18.7 µmol, 1.50 eq) and DIPEA (4.8 mg, 37.5 µmol, 3.00 eq) were added. After 24 h the product was dried under vacuum and dissolved in a mixture of 500 µL DCM, 250 µL $H_2O$, 250 µL TIPS and 4 mL TFA. After one hour, the cleavage of protection groups was complete and the product was dried under vacuum and washed twice with DMF. For purification the red solid was dissolved in PBS buffer (pH = 7.4) and purified by Size Exclusion Chromatography with Sephadex G-15. The pure product was obtained via addition of solid $KPF_6$ and filtered to result in 7.0 mg, 42 % product.

**ESI-MS**: *m/z* 671.68 $[M\text{-}PF_6+H]^{2+}$, 399.46 $[M\text{-}2PF_6+H]^{3+}$.

***[(cyc(RGDfK))$_2$Ru(terpy*)$_2$](PF$_6$)$_2$] (16b)***

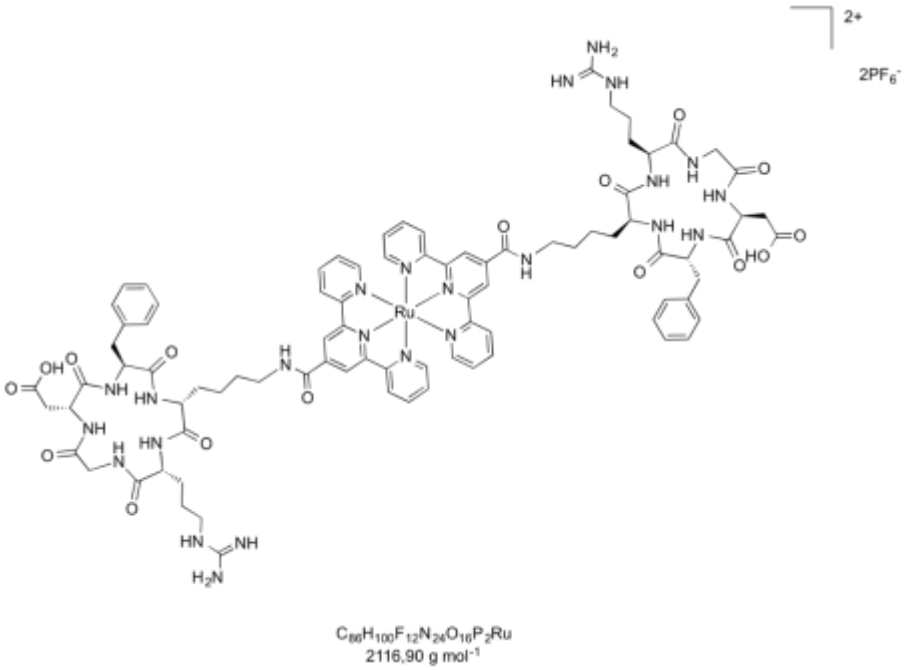


The peptide cyc(R(Pbf)GD(*t*Bu)fK) (12.0 mg, 13.2 µmol, 1.00 eq) and [Ru(terpy*)$_2$](PF$_6$)$_2$] (6.2 mg, 6.6 µmol, 1.0 eq) were dissolved in 0.7 mL of DMF. To the solution, the coupling agents HATU (7.5 mg, 19.7 µmol, 3.00 eq), HOAt (2.7 mg, 19.7 µmol, 3.00 eq) and DIPEA (5.1 mg, 39.5 µmol, 6.00 eq) were added. After 24 h the product was dried under vacuum and dissolved in a mixture of 500 µL DCM, 250 µL $H_2O$, 250 µL TIPS and 4 mL TFA. After one hour, the cleavage of protection groups was complete and the product was dried under vacuum and washed twice with DMF. For purification the red solid was dissolved in PBS buffer (pH = 7.4) and purified by Size Exclusion Chromatography with Sephadex G-15. The pure product was obtained via addition of solid $KPF_6$ and filtered to result in 4.5 mg, 33% product.

**ESI-MS**: *m/z* 913.34 $[M\text{-}2PF_6]^{2+}$, 609.23 $[M\text{-}2PF_6+H]^{3+}$, 457.17 $[M\text{-}2PF_6+2H]^{4+}$.

# 14 Gold Complexes

## 14.1 Synthesis of ligands

***Boc-His-Me (17a)***

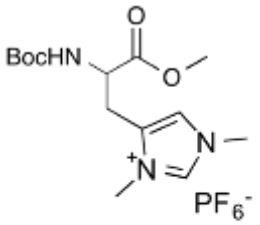


$C_{14}H_{24}F_6N_3O_4P$
443,33 g mol$^{-1}$

The synthesis of the ligands was carried out based on a published procedure.[90] 600 mg Boc-His-OH (2.35 mmol, 1.00 eq) and 987 mg $NaHCO_3$ (11.8 mmol, 5.00 equiv.) were dissolved in 40 mL $CH_3CN$ and stirred at room temperature. After 1 h methyl iodide (11.8 mmol, 5.00 equiv.) was added and the suspension refluxed at 100°C for 24 h. The hot mixture was filtered over celite and washed three times with 10 mL $CH_3CN$. After evaporation of the solvent the solid was dissolved in water and precipitated by adding solid $KPF_6$ (0.79 g, 2.60 mmol, 1.10 equiv.). The product is obtained by filtration, washed with water and diethylether and dried under vacuum to yield in 469 mg, 45% white powder.

**$^1$H-NMR** (400 MHz, $CD_3CN$): 8.30 (s, 1H, NC*H*N), 7.13 (s, 1H, NC*H*C), 5.73 (d, *J* = 8.6 Hz, 1H, N*H*), 4.45 (d, *J* = 3.9 Hz, 1H, C$H_{AA}$), 3.86 – 3.65 (m, 9H, OC$H_3$, NC$H_3$), 3.27 – 2.94 (m, 2H, C$H_{2AA}$), 1.37 (s, 9H, C(C$H_3$)$_3$).

**$^{13}$C-NMR**: δC [ppm] (101 MHz, $CD_3CN$) 171.94, 137.17, 132.72, 122.75, 122.43, 118.42, 80.76, 53.50, 53.24, 36.86, 36.60, 34.49, 34.24, 28.46, 28.32, 28.19, 26.59.

**$^{31}$P-NMR**: δP [ppm] (162 MHz; $CD_3CN$) 144.65 (sept, *P*$F_6^-$).

**ESI-MS**: *m*/*z* 298.04 $[M - PF_6]^+$.

***Boc-His-Et (17b)***

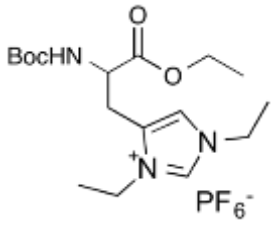


$C_{17}H_{30}F_6N_3O_4P$
485,41 g mol$^{-1}$

The synthesis of the ligands was carried out based on a published procedure.[90] Boc-His-OH (600 mg, 2.35 mmol, 1.00 eq) and $NaHCO_3$ (987 mg, 11.8 mmol, 5.00 eq) were dissolved in 40 mL $CH_3CN$ and stirred at room temperature. After 1 h 1.84 g ethyl iodide (11.8 mmol, 5.00 eq) were added and the suspension refluxed at 100°C for 24 h. The hot mixture was filtered over celite and washed three times with 10 mL $CH_3CN$. After evaporation of the solvent the white solid was dissolved in water and precipitated by adding solid $KPF_6$ (0.79 g, 2.60 mmol, 1.10 eq). The product was obtained by filtration, washed with water and diethylether and dried under vacuum to yield in 352 mg, 31% white powder.

**$^1$H-NMR** (400 MHz, $CD_3CN$) 8.41 (d, *J* = 1.8 Hz, 1H, NC*H*N), 7.21 (d, *J* = 1.7 Hz, 1H, NC*H*C), 5.77 (d, *J* = 8.4 Hz, 1H, N*H*), 4.43 (d, *J* = 5.5 Hz, 1H, C$H_{AA}$), 4.28 – 3.98 (m, 6H, OC$H_2$CH$_3$, NC$H_2$ CH$_3$), 3.09 (dd, *J* = 16.0, 5.1 Hz, 2H, C$H_{2AA}$), 1.45 (dt, *J* = 10.1, 7.3 Hz, 6H, OCH$_2$C$H_3$), 1.38 (s, 9H, C(C$H_3$)$_3$), 1.24 (t, *J* = 7.1 Hz, 3H, NCH$_2$C$H_3$).

**$^{13}$C-NMR** (101MHz, $CD_3CN$) 171.44, 135.33, 132.48, 121.08, 80.62, 62.68, 45.88, 43.29, 28.46, 28.40, 26.75, 15.44, 15.39, 15.11, 15.07, 14.47.

**$^{31}$P-NMR**: δP [ppm] (162 MHz; $CD_3CN$) 144.42 (sept, *P*$F_6^-$).

**ESI-MS**: *m/z* 340.13 $[M - PF_6]^+$.

***Boc-His-Bz (17c)***

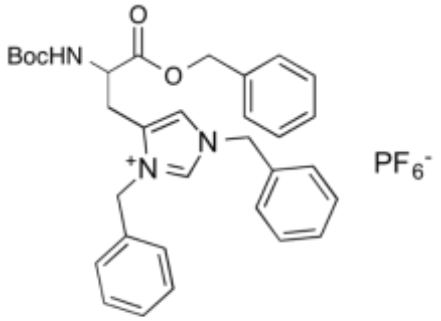


$C_{32}H_{36}F_6N_3O_4P$
671,62 g $mol^{-1}$

The synthesis of the ligands was carried out based on a published procedure.[90] 987 mg (11.8 mmol, 5.00 eq) $NaHCO_3$ were added to a solution of 600 mg Boc-His-OH (2.35 mmol, 1.00 eq) in 50 mL $CH_3CN$ and stirred at room temperature for one hour. Then, 2.00 g (11.8 mmol, 5.00 eq) benzyl bromide were transferred into the suspension and the mixture heated to reflux at 110 °C for 22 h. After filtration of the suspension the volatiles were removed under reduced pressure. The resulting yellow oil was precipitated by addition of diethylether to give a colorless solid. The crude product was filtered off and dissolved in $H_2O$, precipitated by addition of solid $KPF_6$ (790 mg, 2.60 mmol, 1.10 eq). The white solid was filtered, washed three times with 10 mL $H_2O$ and diethylether to yield in 1.18 g, 67% product.

**$^1$H-NMR** δH [ppm] (400 MHz, $CD_3CN$) 8.46 (s, 1H, NC*H*N), 7.50 – 7.23 (m, 15H, $H_{er}$), 7.18 (s, 1H, NC*H*C), 5.82 (d, *J* = 8.3 Hz, 1H, N*H*), 5.26 (d, *J* = 15.3 Hz, 4H, NC$H_2$Ph), 5.10 (s, 2H, OC$H_2$Ph), 4.35 (s, 1H, C$H_{AA}$), 3.18 – 2.87 (m, 2H, C$H_{2AA}$), 1.33 (s, 9H, C(C$H_3$)$_3$).

**$^{13}$C-NMR**: δC [ppm] (101 MHz, $CD_3CN$) 170.25, 135.74, 135.64, 135.64, 133.58, 132.86, 132.18, 129.34, 129.25, 129.16, 128.59, 128.49, 128.41, 128.20, 128.13, 98.74, 67.12, 50.69, 27.44, 25.79, 23.01.

**$^{31}$P-NMR**: δP [ppm] (162 MHz; $CD_3CN$) 144.65 (sept, $PF_6^-$).

**ESI-MS**: *m*/*z* 526.27 $[M - PF_6]^+$.

## 14.2 Synthesis of Complexes

***[Au(Boc-His-Me)$_2$]PF$_6$ (18a)***

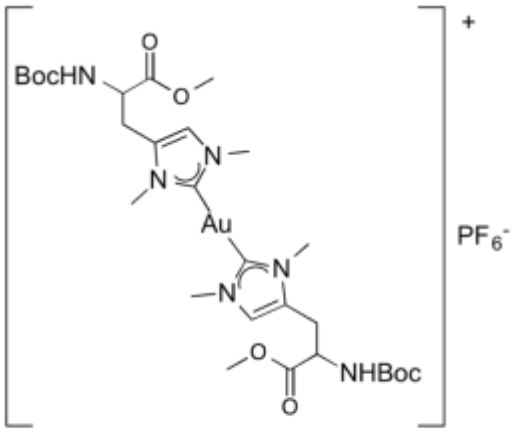


$C_{28}H_{46}AuF_6N_6O_8P$
936,64 g mol$^{-1}$

Boc-His-Me (133 mg, 0.30 mmol, 2.00 eq) was dissolved in 20 mL DCM with 1.60 eq silver oxide (55.2 mg, 0.24 mmol) and stirred for 72 h at room temperature by exclusion of light. Chloro(dimethylsulfide)gold(I) (44.2 mg, 0.15 mmol, 1.00 eq) was added and the solution stirred at room temperature until the reaction was complete, which was monitored by ESI-MS. The resulting suspension was filtered through celite and active coal, washed four times with 20 mL DCM and the filtrate evaporated under reduced pressure to a total volume of 5 mL. The product is precipitated by addition of pentane and filtered to yield 28 mg, 20% of white powder.

**$^1$H NMR:** δH [ppm] (400 MHz, $CD_2Cl_2$) 6.73 (s, 2H, $H_{im}$), 5.19 (d, 2H, N-*H*), 4.56 (t, 4H, C$H_{AA}$), 3.75 (s, 12H, N-C$H_3$), 3.00 (dd, 4H, C$H_{2AA}$), 1.54 (d, 6H, O-C$H_3$), 1.40 (s, 18H, C(C$H_3$)$_3$.

**ESI-MS:** *m/z* 791.20 [M-$PF_6$]$^+$.

***[Au(Boc-His-Et)$_2$]PF$_6$ (18b)***

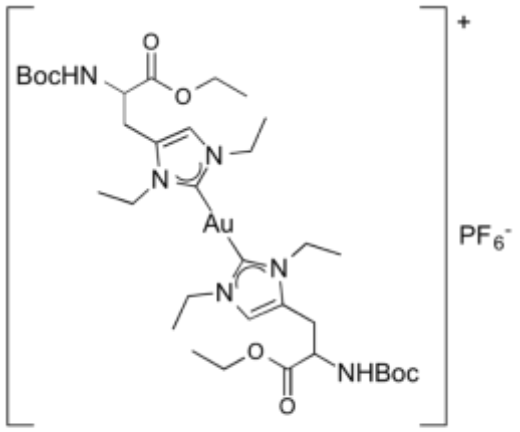


$C_{34}H_{58}AuF_6N_6O_8P$
1029,80 g mol$^{-1}$

Boc-His-Et (146 mg, 0.30 mmol, 2.00 eq) was dissolved in 20 mL DCM with 1.60 eq silver oxide (55.2 mg, 0.24 mmol) and stirred for 72 h at room temperature by exclusion of light. Chloro(dimethylsulfide)gold(I) (44.2 mg, 0.15 mmol, 1.00 eq) was added and the solution stirred at room temperature until the reaction was complete, which was monitored by ESI-MS. The resulting suspension was filtered through celite and active coal, washed four times with 20 mL DCM and the filtrate evaporated under reduced pressure to a total volume of 5 mL. The product is precipitated by addition of pentane and filtered to yield 48 mg, 31% of white powder.

**$^1$H NMR:** δH [ppm] (400 MHz, $CD_3CN$) 7.02 (s, 2H, $H_{im}$), 5.80 (s, 2H, N-*H*), 4.41 (s, 4H, C$H_{AA}$), 4.27 – 4.09 (m, 6H, C$H_2$-$CH_3$), 3.00 (dd, 4H, C$H_{2AA}$), 1.48 – 1.40 (m, 6H, N-$CH_2$-C$H_3$), 1.39 (s, 18H, C(C$H_3$)$_3$), 1.23 (t, 3H, O-$CH_2$-C$H_3$).

**ESI-MS:** *m/z* 875.29 [M-$PF_6$]$^+$.

***[Au(Boc-His-Bz)$_2$]PF$_6$ (18c)***

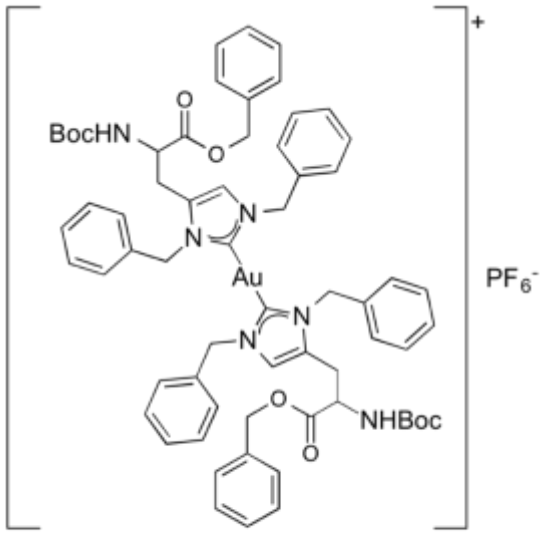


$C_{64}H_{70}AuF_6N_6O_8P^-$
1393,23 g mol$^{-1}$

Boc-His-Bz (200 mg, 0.30 mmol, 2.00 eq) was dissolved in 20 mL DCM with 1.60 eq silver oxide (55.2 mg, 0.24 mmol) and stirred for 72 h at room temperature by exclusion of light. Chloro(dimethylsulfide)gold(I) (44.2 mg, 0.15 mmol, 1.00 eq) was added and the solution stirred at room temperature until the reaction was complete, which was monitored by ESI-MS. The resulting suspension was filtered through celite and active coal, washed four times with 20 mL DCM and the filtrate evaporated under reduced pressure to a total volume of 5 mL. The product is precipitated by addition of pentane and filtered to yield 50 mg, 24% of white powder.

**$^1$H NMR:** δH [ppm] (400 MHz, $CD_2Cl_2$) 7.41-7.14 (m, 30H, $H_{ar}$), 6.54 (s, 2H, $H_{im}$), 4.42 (t, 2H, C$H_{AA}$), 2.97-2.73 (dd, 4H, C$H_{2AA}$), 1.54 (s, 12H, C$H_2$-Bz), 1.38 (s, 18H, C(C$H_3$)$_3$), 1.26 (d, 2H, N-*H*).

**ESI-MS:** *m/z* 1247.43 [M-$PF_6$]$^+$.

# VI. REPRINT PERMISSIONS

# 15 Reprint Permissions

Figure 3: Direct Cellular Responses to Platinum-Induced DNA Damage

Reprinted with permission from Chemical Reviews, 2007, 107, 1387-1407.

Copyright 2007, American Chemical Society.

Figure 18: Ligands for Mapping $\alpha_v\beta_3$- Integrin Expression in Vivo

Reprinted with permission from Accounts of Chemical Research, 2009, 42, 969-980.

Copyright 2009, American Chemical Society.

Figure 19: Crystal Structure of the Extracellular Segment of Integrin $\alpha_v\beta_3$ in Complex with an Arg-Gly-Asp Ligand

Reprinted with permission from Science, 2002, 296, 151-155.

American Association for the Advancement of Science TERMS AND CONDITIONS
Regarding your request, we are pleased to grant you non-exclusive, non-transferable permission, to republish the AAAS material identified above in your work identified above, subject to the terms and conditions herein. We must be contacted for permission for any uses other than those specifically identified in your request above.
The following credit line must be printed along with the AAAS material: "From [Full Reference Citation]. Reprinted with permission from AAAS."
All required credit lines and notices must be visible any time a user accesses any part of the AAAS material and must appear on any printed copies and authorized user might make.
This permission does not apply to figures / photos / artwork or any other content or materials included in your work that are credited to non-AAAS sources. If the requested material is sourced to or references non-AAAS sources, you must obtain authorization from that source as well before using that material. You agree to hold harmless and indemnify AAAS against any claims arising from your use of any content in your work that is credited to non-AAAS sources.
If the AAAS material covered by this permission was published in Science during the years 1974 - 1994, you must also obtain permission from the author, who may grant or withhold permission, and who may or may not charge a fee if permission is granted. See original article for author's address. This condition does not apply to news articles.
The AAAS material may not be modified or altered except that figures and tables may be modified with permission from the author. Author permission for any such changes must be secured prior to your use.
Whenever possible, we ask that electronic uses of the AAAS material permitted herein include a hyperlink to the original work on AAAS's website (hyperlink may be embedded in the reference citation).
AAAS material reproduced in your work identified herein must not account for more than 30% of the total contents of that work.
AAAS must publish the full paper prior to use of any text.
AAAS material must not imply any endorsement by the American Association for the Advancement of Science.
This permission is not valid for the use of the AAAS and/or Science logos.
AAAS makes no representations or warranties as to the accuracy of any information contained in the AAAS material covered by this permission, including any warranties of
merchantability or fitness for a particular purpose.
If permission fees for this use are waived, please note that AAAS reserves the right to charge for reproduction of this material in the future.
Permission is not valid unless payment is received within sixty (60) days of the issuance of this permission. If payment is not received within this time period then all rights granted herein shall be revoked and this permission will be considered null and void.
In the event of breach of any of the terms and conditions herein or any of CCC's Billing and Payment terms and conditions, all rights granted herein shall be revoked and this permission will be considered null and void.
AAAS reserves the right to terminate this permission and all rights granted herein at its discretion, for any purpose, at any time. In the event that AAAS elects to terminate this permission, you will have no further right to publish, publicly perform, publicly display, distribute or otherwise use any matter in which the AAAS content had been included, and all fees paid hereunder shall be fully refunded to you. Notification of termination will be sent to the contact information as supplied by you during the request process and termination shall be immediate upon sending the notice. Neither AAAS nor CCC shall be liable for any costs, expenses, or damages you may incur as a result of the termination of this permission, beyond the refund noted above.
This Permission may not be amended except by written document signed by both parties.
The terms above are applicable to all permissions granted for the use of AAAS material. Below you will find additional conditions that apply to your particular type of use.

**FOR A THESIS OR DISSERTATION**

If you are using figure(s)/table(s), permission is granted for use in print and electronic versions of your dissertation or thesis. A full text article may be used in print versions only of a dissertation or thesis.
Permission covers the distribution of your dissertation or thesis on demand by ProQuest / UMI, provided the AAAS material covered by this permission remains in situ.
If you are an Original Author on the AAAS article being reproduced, please refer to your License to Publish for rules on reproducing your paper in a dissertation or thesis.

**FOR JOURNALS:**

Permission covers both print and electronic versions of your journal article, however the AAAS material may not be used in any manner other than within the context of your article.

**FOR BOOKS/TEXTBOOKS:**

If this license is to reuse figures/tables, then permission is granted for non-exclusive world rights in all languages in both print and electronic formats (electronic formats are defined below).
If this license is to reuse a text excerpt or a full text article, then permission is granted for non-exclusive world rights in English only. You have the option of securing either print or electronic rights or both, but electronic rights are not automatically granted and do garner additional fees. Permission for translations of text excerpts or full text articles into other languages must be obtained separately.
Licenses granted for use of AAAS material in electronic format books/textbooks are valid only in cases where the electronic version is equivalent to or substitutes for the print version of the book/textbook. The AAAS material reproduced as permitted herein must remain in situ and must not be exploited separately (for example, if permission covers the use of a full text article, the article may not be offered for access or for purchase as a stand-alone unit), except in the case of permitted textbook companions as noted below.
You must include the following notice in any electronic versions, either adjacent to the reprinted AAAS material or in the terms and conditions for use of your electronic products: "Readers may view, browse, and/or download material for temporary copying purposes only, provided these uses are for noncommercial personal purposes. Except as provided by law, this material may not be further reproduced, distributed, transmitted, modified, adapted, performed, displayed, published, or sold in whole or in part, without prior written permission from the publisher."
If your book is an academic textbook, permission covers the following companions to your textbook, provided such companions are distributed only in conjunction with your textbook at no additional cost to the user:

- Password-protected website
- Instructor's image CD/DVD and/or PowerPoint resource
- Student CD/DVD

All companions must contain instructions to users that the AAAS material may be used for non-commercial, classroom purposes only. Any other uses require the prior written permission from AAAS.

If your license is for the use of AAAS Figures/Tables, then the electronic rights granted herein permit use of the Licensed Material in any Custom Databases that you distribute the electronic versions of your textbook through, so long as the Licensed Material remains within the context of a chapter of the title identified in your request and cannot be downloaded by a user as an independent image file.

Rights also extend to copies/files of your Work (as described above) that you are required to provide for use by the visually and/or print disabled in compliance with state and federal laws.

This permission only covers a single edition of your work as identified in your request.

**FOR NEWSLETTERS:**

Permission covers print and/or electronic versions, provided the AAAS material reproduced as permitted herein remains in situ and is not exploited separately (for example, if permission covers the use of a full text article, the article may not be offered for access or for purchase as a stand-alone unit)

**FOR ANNUAL REPORTS:**

Permission covers print and electronic versions provided the AAAS material reproduced as permitted herein remains in situ and is not exploited separately (for example, if permission covers the use of a full text article, the article may not be offered for access or for purchase as a stand-alone unit)

**FOR PROMOTIONAL/MARKETING USES:**

Permission covers the use of AAAS material in promotional or marketing pieces such as information packets, media kits, product slide kits, brochures, or flyers limited to a single print run. The AAAS Material may not be used in any manner which implies endorsement or promotion by the American Association for the Advancement of Science (AAAS) or Science of any product or service. AAAS does not permit the reproduction of its name, logo or text on promotional literature.

If permission to use a full text article is permitted, The Science article covered by this permission must not be altered in any way. No additional printing may be set onto an article copy other than the copyright credit line required above. Any alterations must be approved in advance and in writing by AAAS. This includes, but is not limited to, the placement of sponsorship identifiers, trademarks, logos, rubber stamping or self-adhesive stickers onto the article copies.

Additionally, article copies must be a freestanding part of any information package (i.e. media kit) into which they are inserted. They may not be physically attached to anything, such as an advertising insert, or have anything attached to them, such as a sample product. Article copies must be easily removable from any kits or informational packages in which they are used. The only exception is that article copies may be inserted into three-ring binders.

**FOR CORPORATE INTERNAL USE:**

The AAAS material covered by this permission may not be altered in any way. No additional printing may be set onto an article copy other than the required credit line. Any alterations must be approved in advance and in writing by AAAS. This includes, but is not limited to the placement of sponsorship identifiers, trademarks, logos, rubber stamping or self-adhesive stickers onto article copies.

If you are making article copies, copies are restricted to the number indicated in your request and must be distributed only to internal employees for internal use.

If you are using AAAS Material in Presentation Slides, the required credit line must be visible on the slide where the AAAS material will be reprinted

If you are using AAAS Material on a CD, DVD, Flash Drive, or the World Wide Web, you must include the following notice in any electronic versions, either adjacent to the reprinted AAAS material or in the terms and conditions for use of your electronic products: "Readers may view, browse, and/or download material for temporary copying purposes only, provided these uses are for noncommercial personal purposes. Except as provided by law, this material may not be further reproduced, distributed, transmitted, modified, adapted, performed, displayed, published, or sold in whole or in part, without prior written permission from the publisher." Access to any such CD, DVD, Flash Drive or Web page must be restricted to your organization's employees only.

**FOR CME COURSE and SCIENTIFIC SOCIETY MEETINGS:**

Permission is restricted to the particular Course, Seminar, Conference, or Meeting indicated in your request. If this license covers a text excerpt or a Full Text Article, access to the reprinted AAAS material must be restricted to attendees of your event only (if you have been granted electronic rights for use of a full text article on your website, your website must be password protected, or access restricted so that only attendees can access the content on your site).

If you are using AAAS Material on a CD, DVD, Flash Drive, or the World Wide Web, you must include the following notice in any electronic versions, either adjacent to the reprinted AAAS material or in the terms and conditions for use of your electronic products: "Readers may view, browse, and/or download material for temporary copying purposes only, provided these uses are for noncommercial personal purposes. Except as provided by law, this material may not be further reproduced, distributed, transmitted, modified, adapted, performed, displayed, published, or sold in whole or in part, without prior written permission from the publisher."

**FOR POLICY REPORTS:**

These rights are granted only to non-profit organizations and/or government agencies. Permission covers print and electronic versions of a report, provided the required credit line appears in both versions and provided the AAAS material reproduced as permitted herein remains in situ and is not exploited separately.

**FOR CLASSROOM PHOTOCOPIES:**

Permission covers distribution in print copy format only. Article copies must be freestanding and not part of a course pack. They may not be physically attached to anything or have anything attached to them.

**FOR COURSEPACKS OR COURSE WEBSITES:**

These rights cover use of the AAAS material in one class at one institution. Permission is valid only for a single semester after which the AAAS material must be removed from the Electronic Course website, unless new permission is obtained for an additional semester. If the material is to be distributed online, access must be restricted to students and instructors enrolled in that particular course by some means of password or access control.

**FOR WEBSITES:**

You must include the following notice in any electronic versions, either adjacent to the reprinted AAAS material or in the terms and conditions for use of your electronic products: "Readers may view, browse, and/or download material for

Figure 19: Structure-Based Design of Inhibitors of Protein–Protein Interactions: Mimicking Peptide Binding Epitopes

Reprinted with permission from Angewandte Chemie International Edition, 2015, 54, 8896 – 8927.



**JOHN WILEY AND SONS LICENSE TERMS AND CONDITIONS**

Oct 05, 2016

This Agreement between Eva M Hahn ("You") and John Wiley and Sons ("John Wiley and Sons") consists of your license details and the terms and conditions provided by John Wiley and Sons and Copyright Clearance Center.

| | |
|---|---|
| License Number | 3962420802188 |
| License date | Oct 05, 2016 |
| Licensed Content Publisher | John Wiley and Sons |
| Licensed Content Publication | Angewandte Chemie International Edition |
| Licensed Content Title | Structure-Based Design of Inhibitors of Protein–Protein Interactions: Mimicking Peptide Binding Epitopes |
| Licensed Content Author | Marta Pelay-Gimeno,Adrian Glas,Oliver Koch,Tom N. Grossmann |
| Licensed Content Date | Jun 26, 2015 |
| Licensed Content Pages | 32 |
| Type of use | Dissertation/Thesis |
| Requestor type | University/Academic |
| Format | Print and electronic |
| Portion | Figure/table |
| Number of figures/tables | 1 |
| Original Wiley figure/table number(s) | Figure 15a |
| Will you be translating? | No |
| Title of your thesis / dissertation | Ruthenium and Gold Complexes as Targeted Anticancer Agents |
| Expected completion date | Sep 2016 |
| Expected size (number of pages) | 160 |
| Requestor Location | Eva M Hahn<br>bei Korehnke<br>Motorstr. 38<br><br>München, 80809<br>Germany<br>Attn: Eva M Hahn |
| Publisher Tax ID | EU826007151 |
| Billing Type | Invoice |
| Billing Address | Eva M Hahn<br>bei Korehnke<br>Motorstr. 38<br><br>München, Germany 80809<br>Attn: Eva M Hahn |
| Total | 0.00 EUR |
| Terms and Conditions | |

**TERMS AND CONDITIONS**

This copyrighted material is owned by or exclusively licensed to John Wiley & Sons, Inc. or one of its group companies (each a "Wiley Company") or handled on behalf of a society with which a Wiley Company has exclusive publishing rights in relation to a particular work (collectively "WILEY"). By clicking "accept" in connection with completing this licensing transaction, you agree that the following terms and conditions apply to this transaction (along with the billing and payment terms and conditions established by the Copyright Clearance Center Inc., ("CCC's Billing and Payment terms and conditions"), at the time that you opened your RightsLink account (these are available at any time at http://myaccount.copyright.com).

**Terms and Conditions**

- The materials you have requested permission to reproduce or reuse (the "Wiley Materials") are protected by copyright.
- You are hereby granted a personal, non-exclusive, non-sublicensable (on a stand-alone basis), non-transferable, worldwide, limited license to reproduce the Wiley Materials for the purpose specified in the licensing process. This license, **and any CONTENT (PDF or image file) purchased as part of your order,** is for a one-time use only and limited to any maximum distribution number specified in the license. The first instance of republication or reuse granted by this license must be completed within two years of the date of the grant of this license (although copies prepared before the end date may be distributed thereafter). The Wiley Materials shall not be used in any other manner or for any other purpose, beyond what is granted in the license. Permission is granted subject to an appropriate acknowledgement given to the author, title of the material/book/journal and the publisher. You shall also duplicate the copyright notice that appears in the Wiley publication in your use of the Wiley Material. Permission is also granted on the understanding that nowhere in the text is a previously published source acknowledged for all or part of this Wiley Material. Any third party content is expressly excluded from this permission.
- With respect to the Wiley Materials, all rights are reserved. Except as expressly granted by the terms of the license, no part of the Wiley Materials may be copied, modified, adapted (except for minor reformatting required by the new Publication), translated, reproduced, transferred or distributed, in any form or by any means, and no derivative works may be made based on the Wiley Materials without the prior permission of the respective copyright owner. **For STM Signatory Publishers clearing permission under the terms of the STM Permissions Guidelines only, the terms of the license are extended to include subsequent editions and for editions in other languages, provided such editions are for the work as a whole in situ and does not involve the separate exploitation of the permitted figures or extracts,** You may not alter, remove or suppress in any manner any copyright, trademark or other notices displayed by the Wiley Materials. You may not license, rent, sell, loan, lease, pledge, offer as security, transfer or assign the Wiley Materials on a stand-alone basis, or any of the rights granted to you hereunder to any other person.
- The Wiley Materials and all of the intellectual property rights therein shall at all times remain the exclusive property of John Wiley & Sons Inc, the Wiley Companies, or their respective licensors, and your interest therein is only that of having possession of and the right to reproduce the Wiley Materials pursuant to Section 2 herein during the continuance of this Agreement. You agree that you own no right, title or interest in or to the Wiley Materials or any of the intellectual property rights therein. You shall have no rights hereunder other than the license as provided for above in Section 2. No right, license or interest to any trademark, trade name, service mark or other branding ("Marks") of WILEY or its licensors is granted hereunder, and you agree that you shall not assert any such right, license or interest with respect thereto
- NEITHER WILEY NOR ITS LICENSORS MAKES ANY WARRANTY OR REPRESENTATION OF ANY KIND TO YOU OR ANY THIRD PARTY, EXPRESS, IMPLIED OR STATUTORY, WITH RESPECT TO THE MATERIALS OR THE ACCURACY OF ANY INFORMATION CONTAINED IN THE MATERIALS, INCLUDING, WITHOUT LIMITATION, ANY IMPLIED WARRANTY OF MERCHANTABILITY, ACCURACY, SATISFACTORY QUALITY, FITNESS FOR A PARTICULAR PURPOSE, USABILITY, INTEGRATION OR NON-INFRINGEMENT AND ALL SUCH WARRANTIES ARE HEREBY EXCLUDED BY WILEY AND ITS LICENSORS AND WAIVED BY YOU.
- WILEY shall have the right to terminate this Agreement immediately upon breach of this Agreement by you.
- You shall indemnify, defend and hold harmless WILEY, its Licensors and their respective directors, officers, agents and employees, from and against any actual or threatened claims, demands, causes of action or proceedings arising from any breach of this Agreement by you.
- IN NO EVENT SHALL WILEY OR ITS LICENSORS BE LIABLE TO YOU OR ANY OTHER PARTY OR ANY OTHER PERSON OR ENTITY FOR ANY SPECIAL, CONSEQUENTIAL, INCIDENTAL, INDIRECT, EXEMPLARY OR PUNITIVE DAMAGES, HOWEVER CAUSED, ARISING OUT OF OR IN CONNECTION WITH THE DOWNLOADING, PROVISIONING, VIEWING OR USE OF THE MATERIALS REGARDLESS OF THE FORM OF ACTION, WHETHER FOR BREACH OF CONTRACT, BREACH OF WARRANTY, TORT, NEGLIGENCE, INFRINGEMENT OR OTHERWISE (INCLUDING, WITHOUT LIMITATION, DAMAGES BASED ON LOSS OF PROFITS, DATA, FILES, USE, BUSINESS OPPORTUNITY OR CLAIMS OF THIRD PARTIES), AND WHETHER OR NOT THE PARTY HAS BEEN ADVISED OF THE POSSIBILITY OF SUCH DAMAGES. THIS LIMITATION SHALL APPLY NOTWITHSTANDING ANY FAILURE OF ESSENTIAL PURPOSE OF ANY LIMITED REMEDY PROVIDED HEREIN.
- Should any provision of this Agreement be held by a court of competent jurisdiction to be illegal, invalid, or unenforceable, that provision shall be deemed amended to achieve as nearly as possible the same economic effect as the original provision, and the legality, validity and enforceability of the remaining provisions of this Agreement shall not be affected or impaired thereby.
- The failure of either party to enforce any term or condition of this Agreement shall not constitute a waiver of either party's right to enforce each and every term and condition of this Agreement. No breach under this agreement shall be deemed waived or excused by either party unless such waiver or consent is in writing signed by the party granting such waiver or consent. The waiver by or consent of a party to a breach of any provision of this Agreement shall not operate or be construed as a waiver of or consent to any other or subsequent breach by such other party.

- This Agreement may not be assigned (including by operation of law or otherwise) by you without WILEY's prior written consent.
- Any fee required for this permission shall be non-refundable after thirty (30) days from receipt by the CCC.
- These terms and conditions together with CCC's Billing and Payment terms and conditions (which are incorporated herein) form the entire agreement between you and WILEY concerning this licensing transaction and (in the absence of fraud) supersedes all prior agreements and representations of the parties, oral or written. This Agreement may not be amended except in writing signed by both parties. This Agreement shall be binding upon and inure to the benefit of the parties' successors, legal representatives, and authorized assigns.
- In the event of any conflict between your obligations established by these terms and conditions and those established by CCC's Billing and Payment terms and conditions, these terms and conditions shall prevail.
- WILEY expressly reserves all rights not specifically granted in the combination of (i) the license details provided by you and accepted in the course of this licensing transaction, (ii) these terms and conditions and (iii) CCC's Billing and Payment terms and conditions.
- This Agreement will be void if the Type of Use, Format, Circulation, or Requestor Type was misrepresented during the licensing process.
- This Agreement shall be governed by and construed in accordance with the laws of the State of New York, USA, without regards to such state's conflict of law rules. Any legal action, suit or proceeding arising out of or relating to these Terms and Conditions or the breach thereof shall be instituted in a court of competent jurisdiction in New York County in the State of New York in the United States of America and each party hereby consents and submits to the personal jurisdiction of such court, waives any objection to venue in such court and consents to service of process by registered or certified mail, return receipt requested, at the last known address of such party.

**WILEY OPEN ACCESS TERMS AND CONDITIONS**

Wiley Publishes Open Access Articles in fully Open Access Journals and in Subscription journals offering Online Open. Although most of the fully Open Access journals publish open access articles under the terms of the Creative Commons Attribution (CC BY) License only, the subscription journals and a few of the Open Access Journals offer a choice of Creative Commons Licenses. The license type is clearly identified on the article.

**The Creative Commons Attribution License**

The Creative Commons Attribution License (CC-BY) allows users to copy, distribute and transmit an article, adapt the article and make commercial use of the article. The CC-BY license permits commercial and non-

**Creative Commons Attribution Non-Commercial License**

The Creative Commons Attribution Non-Commercial (CC-BY-NC)License permits use, distribution and reproduction in any medium, provided the original work is properly cited and is not used for commercial purposes.(see below)

**Creative Commons Attribution-Non-Commercial-NoDerivs License**

The Creative Commons Attribution Non-Commercial-NoDerivs License (CC-BY-NC-ND) permits use, distribution and reproduction in any medium, provided the original work is properly cited, is not used for commercial purposes and no modifications or adaptations are made. (see below)

**Use by commercial "for-profit" organizations**

Use of Wiley Open Access articles for commercial, promotional, or marketing purposes requires further explicit permission from Wiley and will be subject to a fee.

Further details can be found on Wiley Online Library http://olabout.wiley.com/WileyCDA/Section/id-410895.html

**Other Terms and Conditions:**

**v1.10 Last updated September 2015**

**Questions? customercare@copyright.com or +1-855-239-3415 (toll free in the US) or +1-978-646-2777.**

**JOHN WILEY AND SONS LICENSE**
**TERMS AND CONDITIONS**
Jun 23, 2016

# VII. REFERENCES

**REFERENCES**


[1] B. W. Stewart, C. P. Wild, *World Cancer Report 2014*, IARC Nonserial Publication, **2014**.

[2] E. Bianconi, A. Piovesan, F. Facchin, A. Beraudi, R. Casadei, F. Frabetti, L. Vitale, M. C. Pelleri, S. Tassani, F. Piva, S. Perez-Amodio, P. Strippoli, S. Canaider, *Annals of Human Biology* **2013**, *40*, 463-471.

[3] V. T. Devita, S. Hellman, S. A. Rosenberg, *Cancer: Principles and Practice of Oncology*, 6th edition ed., Lippincott Williams & Wilkins, Philadelphia, PA London, **2001**.

[4] B. Rosenberg, L. Vancamp, J. E. Trosko, V. H. Mansour, *Nature* **1969**, *222*, 385-386.

[5] Y. Jung, S. J. Lippard, *Chemical Reviews* **2007**, *107*, 1387-1407.

[6] P. C. A. Bruijnincx, P. J. Sadler, *Current Opinion in Chemical Biology* **2008**, *12*, 197-206.

[7] C. S. Allardyce, P. J. Dyson, *Dalton Transactions* **2016**, *45*, 3201-3209.

[8] K. D. Mjos, C. Orvig, *Chemical Reviews* **2014**, *114*, 4540-4563.

[9] S. Medici, M. Peana, V. M. Nurchi, J. I. Lachowicz, G. Crisponi, M. A. Zoroddu, *Coordination Chemistry Reviews* **2015**, *284*, 329-350.

[10] S. Spreckelmeyer, C. Orvig, A. Casini, *Molecules* **2014**, *19*, 15584.

[11] L. Oehninger, R. Rubbiani, I. Ott, *Dalton Transactions* **2013**, *42*, 3269-3284.

[12] W. Liu, K. Bensdorf, M. Proetto, A. Hagenbach, U. Abram, R. Gust, *Journal of Medicinal Chemistry* **2012**, *55*, 3713-3724.

[13] B. Bertrand, L. Stefan, M. Pirrotta, D. Monchaud, E. Bodio, P. Richard, P. Le Gendre, E. Warmerdam, M. H. de Jager, G. M. M. Groothuis, M. Picquet, A. Casini, *Inorganic Chemistry* **2014**, *53*, 2296-2303.

[14] M. Zaki, F. Arjmand, S. Tabassum, *Inorganica Chimica Acta* **2016**, *444*, 1-22.

[15] L. Maiore, M. A. Cinellu, S. Nobili, I. Landini, E. Mini, C. Gabbiani, L. Messori, *Journal of Inorganic Biochemistry* **2012**, *108*, 123-127.

[16] R. W.-Y. Sun, C.-N. Lok, T. T.-H. Fong, C. K.-L. Li, Z. F. Yang, T. Zou, A. F.-M. Siu, C.-M. Che, *Chemical Science* **2013**, *4*, 1979-1988.

[17] M. Serratrice, F. Edafe, F. Mendes, R. Scopelliti, S. M. Zakeeruddin, M. Gratzel, I. Santos, M. A. Cinellu, A. Casini, *Dalton Transactions* **2012**, *41*, 3287-3293.

[18] A. de Almeida, B. L. Oliveira, J. D. G. Correia, G. Soveral, A. Casini, *Coordination Chemistry Reviews* **2013**, *257*, 2689-2704.

[19] G. Palermo, A. Magistrato, T. Riedel, T. von Erlach, C. A. Davey, P. J. Dyson, U. Rothlisberger, *ChemMedChem* **2015**, 1199–1210.

[20] J. M. Rademaker-Lakhai, D. van den Bongard, D. Pluim, J. H. Beijnen, J. H. M. Schellens, *Clinical Cancer Research* **2004**, *10*, 3717-3727.

[21] M. J. Clarke, *Coordination Chemistry Reviews* **2002**, *232*, 69-93.

[22] S. Leijen, S. A. Burgers, P. Baas, D. Pluim, M. Tibben, E. Werkhoven, E. Alessio, G. Sava, J. H. Beijnen, J. H. M. Schellens, *Investigational New Drugs* **2014**, *33*, 201-214.

[23] R. Trondl, P. Heffeter, C. R. Kowol, M. A. Jakupec, W. Berger, B. K. Keppler, *Chemical Science* **2014**, *5*, 2925-2932.

[24] B. K. Keppler, M. Henn, U. M. Juhl, M. R. Berger, R. Niebl, F. E. Wagner, in *Ruthenium and Other Non-Platinum Metal Complexes in Cancer Chemotherapy* (Eds.: E. Baulieu, D. T. Forman, M. Ingelman-Sundberg, L. Jaenicke, J. A. Kellen, Y. Nagai, G. F. Springer, L. Träger, L. Will-Shahab, J. L. Wittliff), Springer Berlin Heidelberg, Berlin, Heidelberg, **1989**, pp. 41-69.

[25] C. Mari, V. Pierroz, S. Ferrari, G. Gasser, *Chemical Science* **2015**, *6*, 2660-2686.

[26] S. L. H. Higgins, K. J. Brewer, *Angewandte Chemie International Edition* **2012**, *51*, 11420-11422.

[27] M. Broekgaarden, R. Weijer, T. M. Gulik, M. R. Hamblin, M. Heger, *Cancer and Metastasis Reviews* **2015**, *34*, 643-690.

[28] Z. Huang, *Technology in cancer research & treatment* **2005**, *4*, 283-293.

[29] C. Lottner, K.-C. Bart, G. Bernhardt, H. Brunner, *Journal of Medicinal Chemistry* **2002**, *45*, 2064-2078.

[30] F. Schmitt, P. Govindaswamy, G. Süss-Fink, W. H. Ang, P. J. Dyson, L. Juillerat-Jeanneret, B. Therrien, *Journal of Medicinal Chemistry* **2008**, *51*, 1811-1816.

[31] N. J. Farrer, L. Salassa, P. J. Sadler, *Dalton Transactions* **2009**, 10690-10701.

[32] O. Jacobson, G. Abourbeh, D. Tsvirkun, E. Mishani, *Nuclear Medicine and Biology* **2013**, *40*, 967-973.

[33] I. Buchmann, A. T. J. Vogg, G. Glatting, S. Schultheiß, P. Möller, F. Leithäuser, M. Schulte, W. Gfrörer, J. Kotzerke, S. N. Reske, *Cancer Biotherpay & Radiopharmaceuticals* **2003**, *18*, 327-337.

[34] J. Notni, K. Pohle, H.-J. r. Wester, *EJNMMI Research* **2012**, *2*, 1-5.

[35] I. Velikyan, *Theranostics* **2014**, *4*, 47-80.

[36] O. Gardelle, U. Roelcke, P. Vontobel, N. E. A. Crompton, I. Guenther, P. Bläuenstein, A. P. Schubiger, H. Blattmann, J. E. Ryser, K. L. Leenders, B. Kaser-Hotz, *Nuclear Medicine and Biology*, *28*, 51-57.

[37] S. Jakobson Mo, J. Linder, L. Forsgren, H. Holmberg, A. Larsson, K. Riklund, *BioMed Research International* **2013**, *2013*, 14.

[38] U. Abram, R. Alberto, *Journal of the Brazilian Chemical Society* **2006**, *17*, 1486-1500.

[39] R. Alberto, *COSMOS* **2012**, *08*, 83-101.

[40] T. Mindt, H. Struthers, E. Garcia-Garayoa, D. Desbouis, R. Schibli, *CHIMIA International Journal for Chemistry* **2007**, *61*, 725-731.

[41] S. Jürgens, W. A. Herrmann, F. E. Kühn, *Journal of Organometallic Chemistry* **2013**.

[42] E. W. Price, C. Orvig, *Chemical Society Reviews* **2014**, *43*, 260-290.

[43] S. Dizdarevic, A. M. Peters, *Cancer Imaging* **2011**, *11*, 1-8.

[44] W. Luboldt, B. Wiedemann, S. Fischer, B. Bodelle, H. J. Luboldt, F. Grünwald, T. J. Vogl, *European Journal of Medical Research* **2016**, *21*, 2.

[45] E. M. Hahn, A. Casini, F. E. Kühn, *Coordination Chemistry Reviews* **2014**, *276*, 97-111.

[46] R. E. Mewis, S. J. Archibald, *Coordination Chemistry Reviews* **2010**, *254*, 1686-1712.

[47] R. Schibli, R. La Bella, R. Alberto, E. Garcia-Garayoa, K. Ortner, U. Abram, P. A. Schubiger, *Bioconjugate Chemistry* **2000**, *11*, 345-351.

[48] P. Nunes, G. R. Morais, E. Palma, F. Silva, M. C. Oliveira, V. F. C. Ferreira, F. Mendes, L. Gano, H. V. Miranda, T. F. Outeiro, I. Santos, A. Paulo, *Organic & Biomolecular Chemistry* **2015**, *13*, 5182-5194.

[49] T. D. Bradshaw, M. C. Bibby, J. A. Double, I. Fichtner, P. A. Cooper, M. C. Alley, S. Donohue, S. F. Stinson, J. E. Tomaszewjski, E. A. Sausville, M. F. G. Stevens, *Molecular Cancer Therapeutics* **2002**, *1*, 239-246.

[50] I. Fichtner, A. Monks, C. Hose, M. F. G. Stevens, T. D. Bradshaw, *Breast Cancer Research and Treatment* **2004**, *87*, 97-107.

[51] Y. Tooyama, H. Braband, B. Spingler, U. Abram, R. Alberto, *Inorganic Chemistry* **2008**, *47*, 257-264.

[52] H. Braband, *Chimia* **2011**, *65*, 776-781.

[53] X. Wang, Z. Guo, *Chemical Society Reviews* **2013**, *42*, 202-224.

[54] E. Kim, P. T. Rye, J. M. Essigmann, R. G. Croy, *Journal of Inorganic Biochemistry* **2009**, *103*, 256-261.

[55] O. Ingo, G. Ronald, *Anti-Cancer Agents in Medicinal Chemistry* **2007**, *7*, 95-110.

[56] S. Ding, X. Qiao, G. L. Kucera, U. Bierbach, *Chemical communications (Cambridge, England)* **2013**, *49*, 2415-2417.

[57] R. Wai-Yin Sun, D.-L. Ma, E. L.-M. Wong, C.-M. Che, *Dalton Transactions* **2007**, 4884-4892.

[58] Z. Xue, M. Lin, J. Zhu, J. Zhang, Y. Li, Z. Guo, *Chemical Communications* **2010**, *46*, 1212-1214.

[59] X. Wang, X. Wang, Z. Guo, *Accounts of Chemical Research* **2015**, *48*, 2622-2631.

[60] Z. Yang, X. Wang, H. Diao, J. Zhang, H. Li, H. Sun, Z. Guo, *Chemical Communications* **2007**, 3453-3455.

[61] R. Cescato, T. Maina, B. Nock, A. Nikolopoulou, D. Charalambidis, V. Piccand, J. C. Reubi, *Journal of Nuclear Medicine* **2008**, *49*, 318-326.

[62] A. C. Kluba, L. T. Mindt, *Molecules* **2013**, *18*.

[63] Y. Shen, M. Schottelius, K. Zelenka, M. De Simone, K. Pohle, H. Kessler, H.-J. Wester, P. Schmutz, R. Alberto, *Bioconjugate Chemistry* **2013**, *24*, 26-35.

[64] N. Graf, T. E. Mokhtari, I. A. Papayannopoulos, S. J. Lippard, *Journal of Inorganic Biochemistry* **2012**, *110*, 58-63.

[65] R. Haubner, D. Finsinger, H. Kessler, *Angewandte Chemie International Edition in English* **1997**, *36*, 1374-1389.

[66] J. Thundimadathil, *Journal of Amino Acids* **2012**, *2012*, 13.

[67] M. Schottelius, B. Laufer, H. Kessler, H.-J. Wester, *Accounts of Chemical Research* **2009**, *42*, 969-980.

[68] J. Cao, S. Wan, J. Tian, S. Li, D. Deng, Z. Qian, Y. Gu, *Contrast Media & Molecular Imaging* **2012**, *7*, 390-402.

[69] M. D. Pierschbacher, E. Ruoslahti, *Nature* **1984**, *309*, 30-33.

[70] R. Haubner, R. Gratias, B. Diefenbach, S. L. Goodman, A. Jonczyk, H. Kessler, *Journal of the American Chemical Society* **1996**, *118*, 7461-7472.

[71] J.-P. Xiong, T. Stehle, R. Zhang, A. Joachimiak, M. Frech, S. L. Goodman, M. A. Arnaout, *Science* **2002**, *296*, 151-155.

[72] M. Pelay-Gimeno, A. Glas, O. Koch, T. N. Grossmann, *Angewandte Chemie International Edition* **2015**, *54*, 8896-8927.

[73] M. Kantlehner, P. Schaffner, D. Finsinger, J. Meyer, A. Jonczyk, B. Diefenbach, B. Nies, G. Hölzemann, S. L. Goodman, H. Kessler, *ChemBioChem* **2000**, *1*, 107-114.

[74] Y. Yuan, R. T. K. Kwok, B. Z. Tang, B. Liu, *Journal of the American Chemical Society* **2014**, *136*, 2546-2554.

[75] A. Massaguer, A. Gonzalez-Canto, E. Escribano, S. Barrabes, G. Artigas, V. Moreno, V. Marchan, *Dalton Transactions* **2015**, *44*, 202-212.

[76] N. Graf, D. R. Bielenberg, N. Kolishetti, C. Muus, J. Banyard, O. C. Farokhzad, S. J. Lippard, *ACS Nano* **2012**, *6*, 4530-4539.

[77] Y. Miura, T. Takenaka, K. Toh, S. Wu, H. Nishihara, M. R. Kano, Y. Ino, T. Nomoto, Y. Matsumoto, H. Koyama, H. Cabral, N. Nishiyama, K. Kataoka, *ACS Nano* **2013**, *7*, 8583-8592.

[78] W.-H. Chen, Q. Lei, G.-F. Luo, H.-Z. Jia, S. Hong, Y.-X. Liu, Y.-J. Cheng, X.-Z. Zhang, *ACS Applied Materials & Interfaces* **2015**, *7*, 17171-17180.

[79] J. Zhu, F. Fu, Z. Xiong, M. Shen, X. Shi, *Colloids and Surfaces B: Biointerfaces* **2015**, *133*, 36-42.

[80] J. Conde, F. Tian, Y. Hernández, C. Bao, D. Cui, K.-P. Janssen, M. R. Ibarra, P. V. Baptista, T. Stoeger, J. M. de la Fuente, *Biomaterials* **2013**, *34*, 7744-7753.

[81] F. Barragán, P. López-Senín, L. Salassa, S. Betanzos-Lara, A. Habtemariam, V. Moreno, P. J. Sadler, V. Marchán, *Journal of the American Chemical Society* **2011**, *133*, 14098-14108.

[82] K. Adamson, C. Dolan, N. Moran, R. J. Forster, T. E. Keyes, *Bioconjugate Chemistry* **2014**, *25*, 928-944.

[83] L. He, Y. Huang, H. Zhu, G. Pang, W. Zheng, Y.-S. Wong, T. Chen, *Advanced Functional Materials* **2014**, *24*, 2754-2763.

[84] J. Husson, J. Dehaudt, L. Guyard, *Nat. Protocols* **2014**, *9*, 21-26.

[85] S. Bonnet, J.-P. Collin, N. Gruber, J.-P. Sauvage, E. R. Schofield, *Dalton Transactions* **2003**, 4654-4662.

[86] E. Terpetschnig, H. Szmacinski, H. Malak, J. R. Lakowicz, *Biophysical Journal* **1995**, *68*, 342-350.

[87] A. P. Smith, S. A. Savage, J. C. Love, C. L. Fraser, *Organic Synthesis* **2002**, *78*, 51.

[88] S. Adam, *Bioorganic & Medicinal Chemistry Letters* **1992**, *2*, 571-574.

[89] T. G. Kapp, M. Fottner, O. V. Maltsev, H. Kessler, *Angewandte Chemie International Edition* **2016**, *55*, 1540-1543.

[90] A. Monney, G. Venkatachalam, M. Albrecht, *Dalton Transactions* **2011**, *40*, 2716-2719.

[91] APEX suite of crystallographic software. APEX 2 Version 2014.9-0. Bruker AXS Inc, Madison, Wisconsin, USA (**2014**).

[92] SAINT, Version 7.56a and SADABS Version 2008/1. Bruker AXS Inc., Madison, Wisconsin, USA (**2008**).

[93] Sheldrick, G. M. "SHELXS-97" Program for Crystal Structure Solution, Göttingen (**1997**).

[94] G. M. Sheldrick, "SHELXL-97", University of Göttingen, Göttingen, Germany, (1998) or G. M. Sheldrick, "SHELXL-2014", University of Göttingen, Göttingen, Germany, (2014).

[95] C. B. Huebschle, G. M. Sheldrick, B. Dittrich, **"SHELXLE"**, *J. A. Cryst.* **2011**, *44*, 1281-1284.

[96] International Tables for Crystallography, Vol. C, Tables 6.1.1.4 (pp. 500-502), 4.2.6.8 (pp. 219-222), and 4.2.4.2 (pp. 193-199), Dordrecht, The Netherlands, **1992**.

[97] A. L. Spek, "PLATON", A Multipurpose Crystallographic Tool, Utrecht University, Utrecht, The Netherlands (**2010**).

[98] A. O. Frank, E. Otto, C. Mas-Moruno, H. B. Schiller, L. Marinelli, S. Cosconati, A. Bochen, D. Vossmeyer, G. Zahn, R. Stragies, E. Novellino, H. Kessler, *Angewandte Chemie International Edition* **2010**, *49*, 9278-9281.

[99] S. Bonnet, J.-P. Collin, J.-P. Sauvage, E. Schofield, *Inorganic Chemistry* **2004**, *43*, 8346-8354.